The immune system dependency
of the protein corona

Dissertation

zur Erlangung des Grades
„Doktor der Naturwissenschaften" (Dr. rer. nat.)
im Promotionsfach Chemie

am Fachbereich Chemie, Pharmazie, Geographie und Geowissenschaften
der Johannes-Gutenberg Universität in Mainz
D77 - Mainzer Dissertation

Domenik Prozeller

geb. in Mannheim

Mainz, 2019

Dekan:

1. Gutachterin:
2. Gutachter:

Tag der mündlichen Prüfung:

Abstract

Biomedical applications of nanocarriers are a research field with increasing focus within the scientific community. Through the blood stream, nanocarriers may transport drugs or reporter molecules to specific cells or tissues without exposing them to other parts of the organism. Upon interactions of nanocarriers with blood proteins, a protein corona is formed. These interactions with proteins tremendously influence the properties and behavior of nanocarriers in biological media. In order to achieve applicable nanomedicines, control over the protein corona is required. The blood composition of individuals varies vastly based on constitution, environmental conditions and nutrition. Immunoglobulins are a protein class that is particularly affected by the individual state of the immune system. Therefore, the aim of this work is to investigate the interactions nanocarriers undergo with different immunoglobulins and how varrying immunoglobulin concentrations in blood plasma affect the protein corona.

First, the interactions, which differently charged polymeric nanoparticles undergo with different immunoglobulins in the form of IgG, IgA, and IgM were investigated. Each immunoglobulin class showed different binding parameters to the different nanoparticles and in some cases induced aggregation processes. All immunoglobulins appeared denatured on the surface of nanoparticles with the possible consequence of unwanted reactions of the immune system.

Afterwards, the protein corona of different nanocarriers was compared after incubation in pooled blood plasma and blood plasma of varied, physiologically relevant immunoglobulin concentrations. For this, averaged plasma was modified by increasing IgG, IgA, or IgM or by decreasing the IgG concentration. In all four cases, a significant alteration of the protein corona was observed. The promoted adsorption of IgG in IgG-enriched plasma was further analyzed and resulted in a promoted uptake in macrophages. The effects of IgG-enriched plasma on the protein corona could be prevented successfully by pre-incubation of nanocarriers with the protein clusterin.

Finally, poly(ethylene glycol)-binding IgG was quantified in blood plasma and the protein corona of different nanocarriers. It could be observed, that the concentration of these antibodies was relatively high on nanocarriers containing poly(ethylene glycol)-chains on their surface.

In conclusion, further understanding of the complex interactions nanocarriers undergo with blood proteins with special regards to immunoglobulins was gained. By pre-incubation with clusterin, nanocarriers behave more independent on the individual blood composition.

Kurzfassung

Biomedizinische Anwendungen von Nanoträgern gewinnen in der Forschung zunehmend an Bedeutung. Durch den Blutstrom können Nanoträger Wirkstoffe und Reportermoleküle zu spezifischen Zellen und Geweben transportieren, ohne sie anderen Teilen des Organismus zu präsentieren. Bei Interaktionen zwischen Nanoträgern und Blutproteinen bildet sich eine Korona aus Proteinen, die die Eigenschaften von Nanoträgern drastisch beeinflusst. Um anwendbare Nanomedizin zu realisieren, muss die Proteinkorona zwingend kontrolliert werden. Die individuelle Blutzusammensetzung variiert deutlich basierend auf der Konstitution, Umweltbedingungen und der Ernährung. Immunglobuline sind eine Proteinklasse, die besonders vom individuellen Zustand des Immunsystems abhängig ist. Daher ist es das Ziel dieser Arbeit, die Interaktionen zwischen Nanoträgern und unterschiedlichen Immunglobulinen, sowie den Einfluss variierender Immunglobulinkonzentrationen in Blutplasma auf die Proteinkorona zu untersuchen.

Zunächst wurden die Interaktionen unterschiedlich geladener, polymerischer Nanopartikel mit verschiedenen Immunglobulinen in Form von IgG, IgA und IgM untersucht. Diese Immunglobulinklassen zeigten unterschiedliche Interaktionsparameter zu den unterschiedlichen Nanopartikeln und verursachten in manchen Fällen Aggregationsprozesse. Alle untersuchten Immunglobuline lagen denaturiert auf den Partikeloberflächen vor.

Anschließend wurde die Proteinkorona unterschiedlicher Nanoträger nach der Inkubation in Blutplasma mit variierten, physiologisch relevanten Immunglobulinkonzentrationen verglichen. Hierfür wurde gepooltes Plasma durch Erhöhen der IgG-, IgA- oder IgM-Konzentration oder durch Verringern der IgG-Konzentration modifiziert. In allen vier Fällen resultierte eine signifikant veränderte Proteinkorona. Die geförderte Adsorption von IgG in IgG-erhöhtem Plasma wurde weiter analysiert und resultierte in erhöhter Aufnahme in Makrophagen. Die Effekte des IgG-erhöhten Plasmas auf die Proteinkorona konnten erfolgreich durch Vorinkubation der Nanoträger mit dem Protein Clusterin verhindert werden.

Schließlich wurde Polyethylenglykol-bindendes IgG in Blutplasma und der Proteinkorona quantifiziert. Die Konzentration dieser Antikörper war besonders hoch in der Korona von Nanoträgern, die Polyethylenglycol-Ketten auf ihrer Oberfläche beinhalten.

Zusammenfassend wurden wichtige Erkenntnisse über die komplexen Interaktionen von Nanoträgern mit Proteinen, mit besonderem Augenmerk auf Immunglobuline, gewonnen. Durch Vorinkubation von Nanoträgern mit Clusterin konnte ihr biologisches Verhalten unabhängiger von der individuellen Blutkomposition gemacht werden.

Table of Contents

1.   Introduction

In Richard Fleischer's classic science-fiction movie "Fantastic Voyage" from 1966, scientists miniaturize a navy submarine to the size of a microbe in order to save the life of a comatose person with a blood clot in his brain, which cannot be removed from the outside. Through the blood stream, the crew inside this submarine could reach the site of the blood clot and perform precision surgery from within. This futuristic idea is not distant science-fiction anymore, as small carrier systems in the nanometer range are in development to transport medical substances to specific sites of the body. The use of spherical nanomaterials as drug carrier systems is being investigated with continuously rising interest, as nanocarriers are considered as promising candidates for therapeutic and diagnostic medical applications. Nanocarriers may be loaded with drugs or reporter molecules in order to transport those to specific cells or tissues without exposing them to other parts of the organism.[1] The success of these nanocarrier systems in medical applications strongly depends on the interactions they undergo in the body. If nanocarriers are administered *via* intravenous injection, proteins in the blood will inevitably interact with the surface of nanomaterials.[2-4] These nanocarrier-protein interactions in biological fluids, such as blood or blood plasma, lead to the formation of a protein corona around the nanocarriers. This protein corona heavily influences the physicochemical properties and thus the behavior of nanocarriers, as it is an important factor concerning the circulation time of the nanocarriers in the blood stream.[5]

Long circulations times are required necessarily, in order to ensure that higher doses of the active substance reach the destined target. Therefore, the protein corona is of utmost importance to the success of nanocarriers in medicine and the adsorption process of proteins to nanocarriers must be understood and controlled before applicable nanomedicines can be achieved. It is well established, that the design of nanocarriers is crucial for the interactions they undergo with proteins and consequently with cells.[4,6-10] Some proteins, such as immunoglobulins (Igs), were reported to act as opsonins in the protein corona, marking nanocarriers for digestion by phagocyte cells and removal from the blood stream.[6,10] Other proteins, such as apolipoprotein J ("clusterin") and apolipoprotein A-I, reduce the phagocytosis of nanocarriers if they are enriched in the protein corona and act as "stealth proteins" by reducing unspecific cell interactions of nanocarriers, resulting in prolonged circulation times.[10-12]

To complicate the reliable prediction of the nanocarriers' biological fate in the body, the individual blood protein composition can vary significantly depending on many different, subjective factors, such as personal constitution, nutrition and environmental conditions. Igs are a major protein class in human blood, that is particularly affected by the individual state of the immune system and the concentrations of different Ig classes can vary significantly in the course of different diseases.[13]

Therefore, the overall aim of this work is to investigate the specific and unspecific interactions nanocarriers undergo with different Ig classes and how varying physiologically relevant immunoglobulin concentrations in blood plasma affect the protein corona of different nanocarriers. By further understanding nanocarrier-protein interactions, control over the formation process of the protein corona has to be enhanced.

As the name already implies, immunoglobulins (Igs) generally play an important role in the immune system. Interactions between nanocarriers and Igs could potentially result in conformal changes of these antibodies resulting in unwanted behavior of the nanocarriers inside the body, such as (auto)immune reactions, inflammation and allergic reactions. While the adsorption behavior of individual Ig classes, such as IgG, on different nanocarriers is known to be independent on the size of nanocarriers,[14] the influence of the nanocarrier's surface charge on the adsorption mechanism of the different Ig classes is unclear. In order to draw general conclusions for interaction trends between Igs and differently charged nanocarriers, model nanoparticles (NPs) are needed. For this, polystyrene nanoparticles (PS-NPs) with different functional groups (unfunctionalized, carboxyl-functionalized and amino-functionalized) were used as model systems for the investigation of interactions with IgG, IgA and IgM. The presence of NP-Ig interactions is confirmed and the properties of nanocarriers and Igs are investigated before and after incubation with each other. The change of surface charge of each NP due to interactions with the different Igs is investigated by their zeta potential. The binding parameters of the adsorption process give more insight on the interaction mechanisms of Igs with differently charged NPs. Furthermore, the structural stability upon binding to NPs is investigated.

After the interactions between nanocarriers and Igs were characterized by investigating isolated proteins, the influence of these NP-Ig interactions on the protein corona in whole blood plasma is of high interest. As mentioned above, the concentration of different proteins in the blood

may vary vastly depending on individual factors. Usually, pooled blood plasma and serum from multiple healthy donors are used in order to draw conclusions and see general trends in studies of the protein corona, not taking individual fluctuations of protein concentrations in the blood into account. Incidentally, the protein corona formation process in blood plasma has been reported to be dependent on the plasma source[15,16] and the addition of anticoagulants, which are necessary to store the blood.[17] Consequently, studies on the protein corona in pooled blood plasma must not necessarily correlate with the protein corona in the blood of individuals, particularly in patients with a disease. Therefore, the protein coronas of different nanocarriers were compared after incubation in normal blood plasma and blood plasma of varying physiologically relevant immunoglobulin concentrations. For this, the pooled plasma was modified by adding commercially available IgG, IgA or IgM from human serum or by decreasing the IgG concentration *via* fractionation by high performance liquid chromatography (HPLC). In all four cases, a significant alteration of the protein corona was observed compared to the unmodified, normal pooled plasma. As elevated IgG levels in blood are a common finding in medicine due to infections, autoimmunity, inflammation, or malignancy,[18] the case of IgG-enriched plasma was further analyzed in terms of the binding mechanisms of proteins in both plasmas *via* isothermal titration calorimetry (ITC) and in terms of specific cellular interactions caused by the alteration of the protein corona.

After investigating unspecific interactions between different nanocarriers and Igs, specific antibody-antigen interactions were investigated. A common method to reduce unspecific protein adsorption onto nanocarriers and to prolong their circulation time is the attachment of poly(ethylene glycol) (PEG) on the nanocarriers' surface in a so-called PEGylation.[19,20] Coincidentally, PEG is also commonly used in cosmetic and medical products. Upon the increasing exposure to products containing PEG in daily life,[21,22] anti-PEG antibodies were found to be present in humans and animals upon exposure to PEGylated drugs, resulting in detection frequencies up to 36% in humans.[23-26] The PEG-binding properties of these anti-PEG antibodies may result in an accumulation of these Igs in the protein corona of PEGylated nanocarriers. Therefore, the existence and concentration of anti-PEG IgG in normal plasma and in the protein corona of different (PEGylated and non-PEGylated) nanocarriers was investigated *via* enzyme-linked immunosorbent assay (ELISA) and confirmed by a competition assay. A key question was whether or not the PEGylation of nanocarriers ultimately leads to specific interactions with anti-PEG IgG.

2.   State of the Art

In the following, particular parts concerning the theoretical background of blood proteins, nanocarriers and their interactions with each other, which are linked to this work, are discussed. More generalized and extensive information on the biochemistry of blood and blood components[27], as well as colloidal chemistry[28] and physical chemistry[29] are readily available in standard literature.

2.1   Blood

The fundamental task of blood in an animal's organism is to transport oxygen, CO_2, nutrients, and metabolites through the entire body. It consists of cellular (solid) parts and a liquid phase, in which many different substances like proteins, sugars, hormones and salts are dissolved. By separating the cells from blood, the blood's liquid phase (called "blood plasma") is acquired. If this liquid part of the blood is not treated any further, clotting processes of coagulation factors and proteins will take place, ultimately changing its properties while impeding storage and analysis of the blood plasma. Clotting can be prevented by the addition of stabilization agents (e.g. sodium citrate or ethylenediaminetetraacetic acid (EDTA)) to the blood prior to centrifugation and discarding the cellular blood fraction. The resulting blood plasma will have all coagulation factors remaining dissolved within it. It is also possible to induce clotting before the centrifugation actively, in order to remove cellular parts and also coagulation factors and proteins like fibrinogen from blood. The resulting liquid lacking cells and coagulation factors is called "blood serum".[30]

2.1.1 Blood proteome

The blood proteome is the sum of all proteins within the blood plasma and consists of more than 3,000 individual protein types.[31] These proteins can be categorized by their function and appear in different concentrations in the blood. The concentration of all plasma proteins usually ranges from around 60 to 80 g L^{-1}, with only a few proteins making up its majority. Human serum

albumin (HSA) alone makes up more than 50% of the total protein concentration of plasma with approximately 35 - 50 g L^{-1}.[32] Immunoglobulin G (IgG, ~ 11 - 12 g L^{-1})[33], transferrin (~ 2.7 g L^{-1}), fibrinogen (~ 2.7 g L^{-1}), immunoglobulin A (IgA, ~ 2.6 g L^{-1}) and immunoglobulin M (IgM, ~ 1.5 g L^{-1}) are highly abundant in blood plasma as well. Around 90% of the blood's protein mass is made up of ten protein type and further 9% consist of the twelve proteins following in abundance, leaving one remaining percent made up from all other proteins. Following that, immunoglobulins (Igs) are one major protein class and significant part of blood proteome (see Figure 2.1.1).
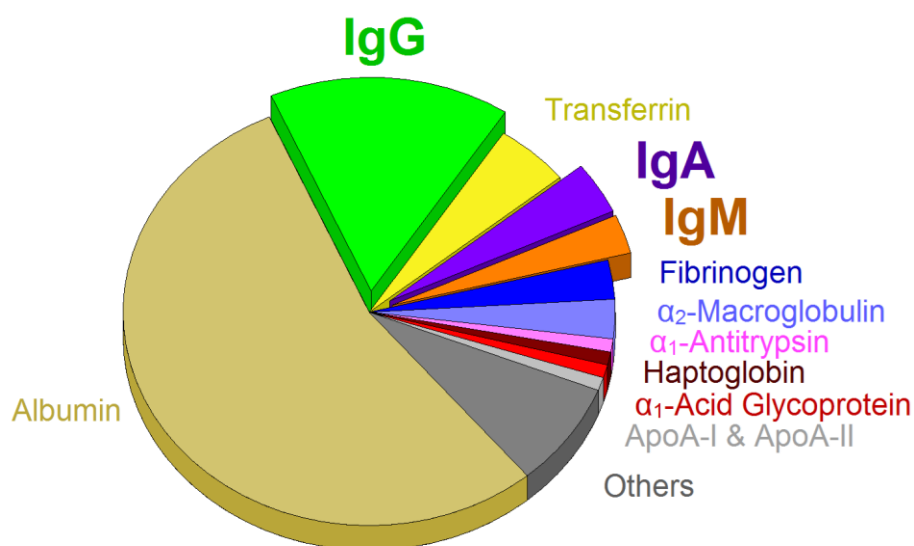
Figure 2.1.1: Most common protein fractions found in blood plasma regarding average relative concentrations found in literature.[31,34] The protein fractions of IgG (green), IgA (purple) and IgM (orange) are highlighted.

2.1.2 Proteins of the immune system

Immunoglobulins, commonly referred to as antibodies, are proteins of the immune system. If Igs interact with compounds foreign to the organism (antigens), these antigens will be recognized and taken up by cells of the immune system (phagocytes). Because of this reaction of the immune system, antigens are cleared from the organism. Furthermore, binding the antigen can deactivate harmful functions of the antigen itself and be followed by activation of the complement system. Igs are categorized in five Ig classes for humans and the most mammals: IgG, IgA, IgM, IgD, and

IgE. All Igs share the same general Y-shaped structure (see Figure 2.1.2 A). Each monomeric Ig molecule consists of two heavy chains (50 kDa for IgG, 55 kDa for IgA and 70 kDa for IgM) and two light chains (25 kDa) which are linked *via* disulfide bonds. The general structure of Igs is divided into the "arms" of the Y-shape (the so-called antigen-binding fragment or F_{ab} fragment) and the "stem" of the Y-shape (the so-called crystallizable region fragment or F_c fragment). The variable part of the F_{ab} fragment contains structures (paratopes) which recognize and bind to specific structures of antigens (epitopes), whereas the F_c fragment is responsible for recognition by cells of the immune system. While IgD (180 kDa), IgE (190 kDa), IgG (150 kDa) and IgA found in serum (160 kDa) appear in a monomeric form, secretory IgA has a dimeric structure (600 kDa) and IgM (970 kDa) has a pentameric structure (see Figure 2.1.2 B).
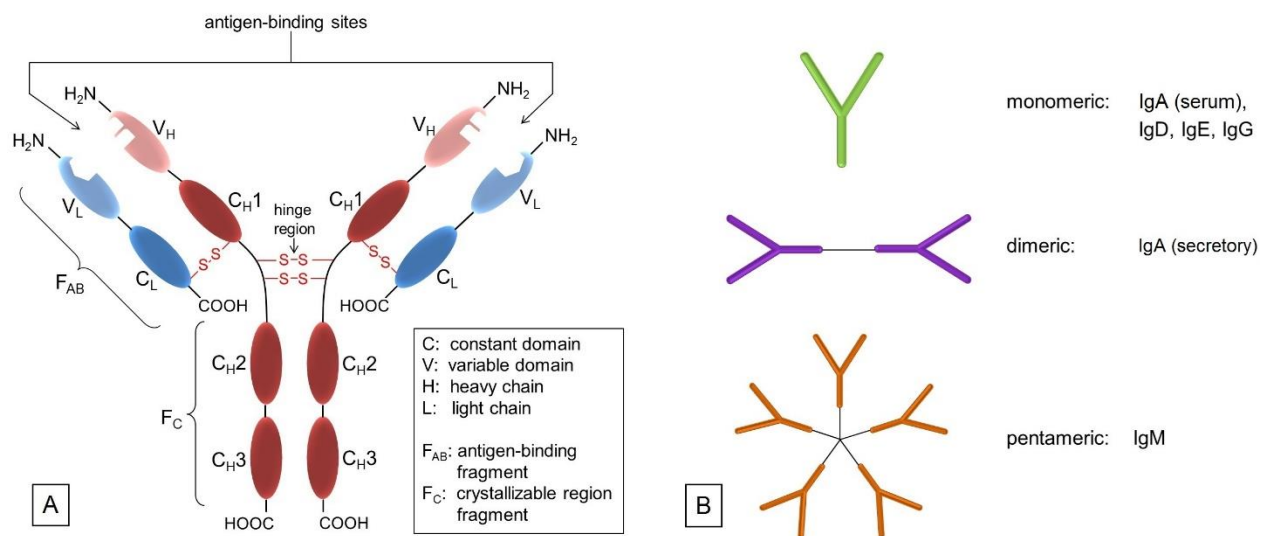
Figure 2.1.2: Structure of Igs. A: general structure of an Ig monomer. Two heavy chains (red domains) and two light chains (blue domains) are linked *via* disulfide bonds (S-S). Black arrows mark antigen-binding sites and hinge region. Brackets indicate the antigen-binding fragment (F_{ab}) and crystallizable region fragment (F_c). B: IgD, IgE, IgG and IgA (serum) appear monomeric (green), while IgA (secretory) has a dimeric (purple) and IgM has a pentameric (orange) structure).

Each Ig class has different tasks in the immune system. Secretory IgA is a dimeric immunoglobulin majorly located in secretory substances, such as tears, and forms a barrier at the mucous membranes in order to prevent pathogens from entering further into the body. Serum IgA

appears in monomeric form in blood and binds pathogens that entered the body and were not stopped by secretory IgA. IgM acts as a first line of defense against pathogens and is primarily produced in the acute phase of a disease. After the acute phase, the IgM concentration in the blood plasma decreases and IgG levels rise for a long-term "memory" effect of the immune system against the pathogen. Levels of the different Ig classes above and below normal range allow indication or diagnosis to specific diseases or the time of the initial infection. For example, in the beginning of an infection only IgM will be elevated and decrease over time, while IgG levels increase. An elevation of solely IgA in blood indicates liver diseases (e.g. liver cirrhosis or intoxication with ethanol).

2.1.3 Apolipoproteins

Apolipoproteins do not occur freely in blood as single proteins, but as stabilizing components of hydrophobic clusters (lipoproteins). As such, they play an important role in the transport of hydrophobic molecules like cholesterol, cholesteryl esters, phospholipids and triglycerides through the blood. In this work, specifically apolipoprotein A-I (apo A-I) and clusterin (apolipoprotein J; apo J) are of particular interest, as they were reported to play an important role in interactions of nanocarriers in previous work.[10] Apo A-I occurs in high-density lipoproteins (HDL) with a molar mass of 28 kDa and a concentration of approximately 1.4 g L^{-1} in blood plasma.[35] Clusterin appears as a heterodimer of approximately 80 kDa (~ 40 kDa per monomer) with a very low abundance in plasma ($0.05\text{-}0.37 \text{ g L}^{-1}$).[36]

2.2   Nanocarriers for biomedical applications

Nanomaterials are being developed in different forms and shapes, from spheres, over fibers and rods, to plates and coatings. Their common property is that the dimensions are in the nanometer-range (1 to 100 nm), which results in vastly different properties compared to the respective bulk material. For that, nanomaterials are established in many different fields with exemplary applications in electronics, catalysis, sensor technology and medicine. While nanomaterials are commonly found in medicine in general (e.g. in the form of coatings for implants), drug delivery by applying mainly spherical nanocarriers is not established widely in medicine yet. The general idea of nanocarrier-based drug delivery systems is to guide a drug to specific locations within the body while avoiding unwanted interactions with the organism and side-effects resulting thereof. By encapsulating the drug within nanocarriers, the circulation time in the blood stream can potentially be prolonged, the cargo is protected against degradation and otherwise insoluble drugs can be transported.[37] Furthermore, unspecific interactions with cellular components can be suppressed. The aim is that by attaching species prone to specific cell interactions to the nanocarriers' surface, targeting properties can be introduced resulting in the increased uptake by these cells (e.g. cancer cells).

For model systems in research, NPs are commonly used, as they can easily be modified and produced with high reproducibility and narrow size distribution. NPs made of polystyrene (PS-NPs) are commonly synthesized *via* miniemulsion polymerization.[38] Functionalization of PS-NPs with amino- ($-NH_2$) or carboxyl groups (-COOH) is feasible by co-polymerization with a respective co-monomer. Furthermore, the surface of NPs may also be modified by adsorption of stabilizing surfactants and covalent attachment of polymeric molecules like poly(ethylene glycol) (PEG) chains. The covalent attachment of PEG chains is a commonly used method to reduce overall protein adsorption and prolong the circulation time in blood.[19,20] This so-called PEGylation is a way to influence NP-protein interactions. However, in order to achieve control over NPs' behavior in blood, the formation process of the protein corona must be understood fully.

In contrast to solid NPs, nanocapsules (NCs) are hollow spheres with an inner cavity, which may be loaded with many different cargos like drugs (in hydrophilic or hydrophobic media), proteins, DNA or RNA. As polystyrene is not applicable for biomedicine due to its lack of biological degradability and compatibility, other materials are needed for the synthesis of NCs. Common materials for biomedically relevant NCs are hydroxyethyl starch (HES) and silica (SiO_2) among others. Like this, the composition of NPs and NCs alike is easily adjustable in terms of their base material, eventual surface modification and functionalization, size and (in case of NCs) shell thickness. However, once the nanocarriers are introduced to biological media like blood or blood plasma, proteins and other biomolecules will adsorb on their surface. This adsorbed protein "cloud" around nanocarriers is commonly referred to as "protein corona". The protein corona influences the properties and behavior of the NPs tremendously, as different proteins will cover the original surface of the nanocarrier in biological media. While this protein adsorption cannot be prevented completely in general, the interaction between the nanocarriers and individual proteins may be reduced or promoted based on the design of the nanocarrier.

2.3   Nanocarrier-protein interactions

Chapter 2.3 is based on a mini review, which we have submitted for publication. Nanocarrier-protein interactions embody a very complex and dynamic process and extensive research investigating the protein corona formation has been conducted in the past decades. Excellent reviews addressing and focusing on the protein adsorption onto nanoparticles,[39-41] and the impact of the protein corona on nanomedicine[42] are available in the literature.

The process of protein corona formation is a competition between different proteins for interactions with the accessible surface of nanocarriers. Result of this competition is a dynamic "cloud" of proteins around the nanocarriers, which continuously changes over time. In the beginning seconds to minutes of this interaction, the more abundant blood proteins such as albumin will be dominant in the corona.[43] Over time, proteins with higher affinity (and lower concentration) will take over the space close to the nanocarrier's surface and proteins with lower

affinity will be attached more loosely in the outer layers around the nanocarrier *via* protein-protein interactions.[43] This kinetically-driven evolution of the corona over time is commonly referred to as "Vroman-effect".[44] Common nomenclature for the more tightly bound proteins is the so called "hard" protein corona, while loosely bound proteins are considered "soft" corona proteins.[9]

Properties of proteins and nanoparticles alike influence their intermolecular interactions with each other. Nanocarriers' properties of interest include size,[45] surface charge and functionalization,[9] stabilizing surfactants,[8] and hydrophilicity.[46] On the other hand, the proteins' properties of interest address their amphiphilic character, which leads to screening of hydrophobic parts of the protein from the surrounding water.[47] Similarly, smaller hydrophobic molecules can be transported by amphiphilic proteins such as lipids attached to apolipoproteins[48]. This amphiphilic nature in turn also leads to preferred interaction with other surfaces such as nanomaterials. The main forces governing the interfacial interactions between nanomaterials and biological systems are listed in Table 2.3.1.[41]

Remaining questions in the field include (but are not limited to) the possibility of protein-multilayers in the corona,[49,50] the exact mechanism of the Vroman-effect with influence of kinetics on the protein corona,[44,51,52] and the thermodynamics of specific nanocarrier-protein interactions.[53] For these open questions, the thermodynamic information obtainable by methods such as ITC can be of significant aid by offering a strong complementary method to the analytical toolbox of protein corona research.

Table 2.3.1: Main forces governing the interfacial interactions between nanomaterials and biological systems (adapted by permission from Springer Nature, Nature Materials, Nel *et al*. Copyright 2009)[41].

Force	Origin and Nature	Range (nm)	Possible impact on the interface
Hydrodynamic interactions	Convective drag, shear, lift and Brownian diffusion are often hindered or enhanced at nanoscale separations between interacting interfaces	10^2-10^6	Increase the frequency of collisions between nanoparticles and other surfaces responsible for transport
Electrodynamic interactions	Van der Waals interactions arising from each of the interacting materials in the intervening media	1-100	Universally attractive in aqueous media; substantially smaller for biological media and cells owing to high salt content
Electrostatic interactions	Charged interfaces attract counter-ions and repel co-ions (Coulombic forces), giving rise to the formation of an electrostatic double layer	1-100	Overlapping double layers are generally repulsive as most materials acquire negative charge in aqueous media, but can be attractive for oppositely charged materials
Solvent interactions	Lyophilic materials interact favourably with solvent molecules Lyophobic materials interact unfavourably with solvent molecules	1-10	Lyophilic materials are stable (thermodynamically) in the solvent and do not aggregate Lyophobic materials are spontaneously expelled from the bulk of the solvent and forced to aggregate or accumulate at an interface
Steric interactions	Polymeric species adsorbed to particles give rise to spring-like repulsive interactions with other interfaces	1-100	Generally increase stability of individual particles but polymers have their own adsorption behavior

2.4   Methods

2.4.1 Isothermal titration calorimetry (ITC)

Chapter 2.4.1 is based on the mini review submitted for publication. Due to the complexity in the multitude of possible interactions nanocarriers and proteins can undergo, one must design, execute and analyze experiments on these interactions with great caution in order to achieve auxiliary and reliable data. Excellent reviews on the fundamentals of isothermal titration calorimetry (ITC) specifically addressing experiment design, execution and analysis in particular are available in literature.[54-58]

In general, ITC is an analytical technique relying on the thermodynamics of binding events. The thermal energy measured stems from binding events resulting from one or multiple titration(s) of one interaction partner to another. These interactions can be of different origins, as previously described for the example of nanocarrier-protein interactions in Table 2.3.1, and cover the entire spectrum for interactions from the formation of covalent bonds to non-covalent interactions such as hydrogen bonding or electrostatics. The first use of titration calorimetry for analyzing the Gibbs-free energy ΔG, the binding enthalpy ΔH and the change of entropy ΔS of the proton ionization from HSO_4^- and HPO_4^{2-} in one single titration was published by Christensen *et al.* in 1966 in form of a method called "entropy titration".[59] In the following years, ITC was developed with interactions between different biomolecules in mind, such as enzyme-substrate interactions.[60,61] One of the first examples for utilizing calorimetric methods in order to determine the activity of enzymes was published in 1976 by Spink and Wadso.[62] However, all processes that lead to the release or absorption of heat during the interaction are accessible with ITC. For example, Chiad *et al.* determined the thermodynamic parameters and stoichiometry for interactions between silica nanoparticles and surface-active amphiphilic copolymers bearing different types of anchor groups (nonionic, zwitterionic, and acidic) in complex organic-inorganic hybrid systems utilizing ITC.[63]

During an experiment, a solution of one compound is titrated to the solution of another compound in an isothermal "measurement cell" in equivoluminar injection(s). Because of this isothermal setup implemented by thermal equilibrium of the measurement cell with a "reference cell", the heat increase or decrease resulting from the two compounds' interaction must be adjusted

by controlling the heating rate of the measurement cell. The general setup of an ITC instrument is depicted in Figure 2.4.1.
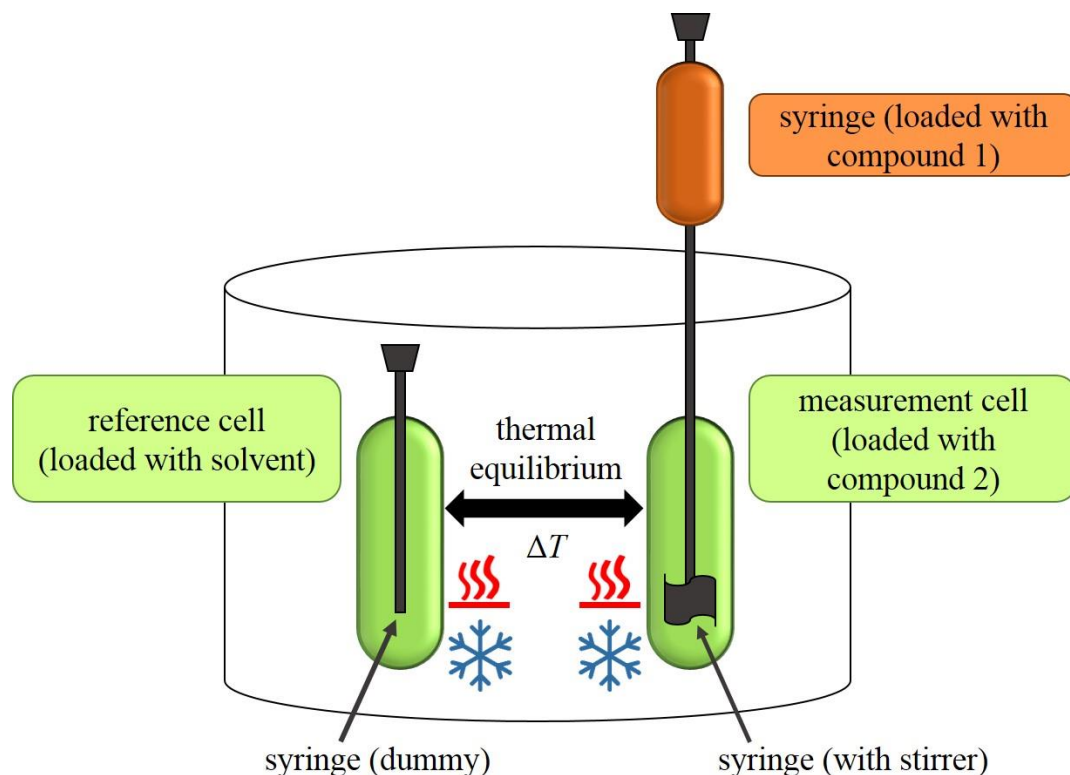
Figure 2.4.1: General setup of an ITC instrument.

The heating rate applied in order to maintain a constant temperature within the measurement cell is monitored for the duration of the titration(s) (see Figure 2.4.2, top). Integration of the heat rate over time, leads to the heat of the interaction process taking place during the respective titration step. It is important to consider, that not only interactions between the two compounds lead to heat changes in the measurement cell, but for example titrations of proteins into water result in heat of dilution already. Subtracting the heat of a titration step with the corresponding heat of dilution yields in the "corrected heat" resulting from interactions between the two compounds. Fitting the corrected heat of consecutive titration steps can be achieved with several mathematical models and the resulting fit (called "adsorption isotherm") yields the thermodynamic parameters of the interactions (see Figure 2.4.2, bottom).
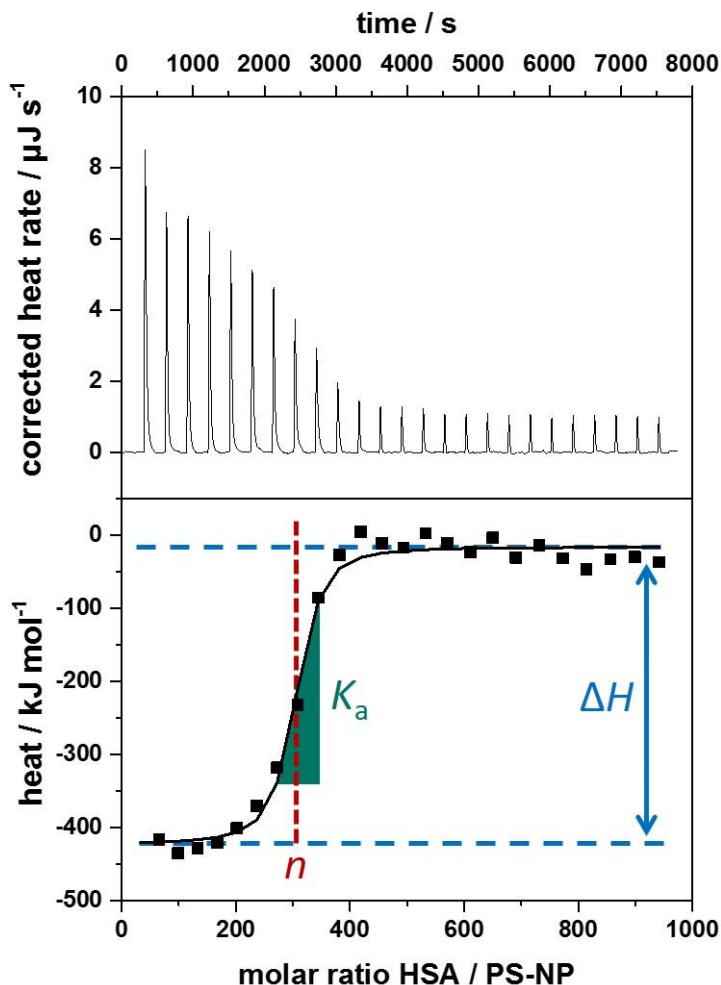
Figure 2.4.2: Typical data obtained from isothermal titration calorimetry measurements of polystyrene nanoparticles (PS-NPs) titrated with human serum albumin (HSA). Top: Corrected heat rate of the titration. Bottom: Integrated normalized heats from each titration step corrected by the heats of dilution (filled squares) together with a fit corresponding to an independent binding model (straight line). Visual representation of the parameters obtained by ITC experiments within the adsorption isotherm. K_a is derived from the curve's slope in its inflection point (green slope ▲), ΔH is represented by the difference between the curve's upper and lower plateaus (blue lines - -) and n is the molar ratio of the two components at the curve's inflection point (red lines --).

Based on the fit resulting from the corrected heat from multiple injections, the association constant K_a, interaction enthalpy ΔH and molar stoichiometry n are obtained. K_a is derived from the curve's slope in its inflection point, ΔH is the difference between the curve's plateaus and n is the molar ratio of the two components at the curve's inflection point (see Figure 2.4.2, bottom).

The *Gibbs* free energy ΔG of the interaction is then calculated using the reaction isotherm equation (see equation 2.4.1).[29] ΔS can then be determined subsequently from the *Gibbs-Helmholtz* equation (see equation 2.4.2).

$$\Delta G = -RT \cdot \ln K_a \tag{2.4.1}$$

$$\Delta G = \Delta H - T\Delta S \tag{2.4.2}$$

In recent years, protein adsorption processes were more and more in the focus of ITC analyses.[58] As a result, several protein corona studies employed ITC for characterizing the physicochemical properties of nanocarrier-protein interactions specifically.[5,8,9,48,64-78] An excellent review elucidating the thermodynamics of NP-biomolecule interactions in general by Huang and Lau is available in the literature.[53]

One big advantage of ITC studies on the protein corona is the unnecessity to separate the formed nanocarrier-protein complexes from the medium for further characterization. This allows analysis of the entire protein corona *in situ*, including low-affinity soft corona proteins, which might have big influence on the nanocarriers, yet are disregarded in most other analytical approaches. Usually, analysis of the protein corona relies on fractionation steps, such as centrifugation, removing low-affinity proteins from the (soft) protein corona.[79] Thus, ITC allows investigation of all nanocarrier-protein interactions, limiting the possibility to oversee important adsorption processes. Furthermore, ITC measurements do not require labels on nanocarriers or proteins, allowing investigation of their interaction without modification of any interaction partner. Also, instead of solely yielding information on the binding affinity, ITC studies give information about the complete thermodynamic parameters of the interaction.

Because of the large amount of possible interactions going on, interpretation of the results that ITC experiments yield about the protein corona in particular is not a simple task. While the significance and meaning of stoichiometry and association constant obtained from ITC studies for single proteins are obvious, interpretation of the thermodynamic parameters concerning the protein

adsorption process appears more complex. For their interpretation, the role of hydration water in particular should not be underestimated. Generally, the formation of non-covalent bonds (see Table 2.3.1; e.g. van der Waals forces, electrostatic interactions or hydrogen bonds) is an exothermic process ($\Delta H < 0$) dominating for hydrophilic surfaces, while desolvation - the release of hydration water from the surface of nanocarriers and proteins - is an endothermic process ($\Delta H > 0$) and is seen more regularly for hydrophobic surfaces as a result of hydrophobic interactions. In a similarly opposing fashion, the conformational restriction and loss of rotational freedom during protein adsorption yields unfavorable entropy loss ($\Delta S < 0$), while desolvation results in an increase of the system's entropy ($\Delta S > 0$) assuming the protein contains its shape. Therefore, the driving force of the adsorption process strongly depends on the interaction mechanism of the individual nanocarrier-protein system and may differ from case to case, requiring cautious analysis. As the heat observed in ITC solely reflects the total energy released or absorbed during the interaction, differentiating the individual contribution of different bonds (see Table 2.3.1) to the total heat is impossible. For example, relative contributions originating from protein denaturation and aggregation, electrostatic and hydrophobic interactions or desolvation cannot be distinguished and thus cannot be quantified individually.

Table 2.3.2: Summary of ITC studies on nanocarrier-protein interactions. [a]: charge of nanocarriers categorized as positively charged ($\oplus$ $\oplus$), mildly positively charged ($\oplus$), neutral (Ø), mildly negatively charged ($\ominus$) or negatively charged ($\ominus$ $\ominus$). [b]: Hydrophilicity of nanocarriers base material categorized ranging from very hydrophilic (*****) to very hydrophobic (*). [c]: charge of protein at physiological pH categorized as overall positively charged ($\oplus$), neutral (Ø), or overall negatively charged ($\ominus$). N/A stands for "not available".

nanocarrier material	protein	parameters of nanocarrier-protein interaction			nanocarrier properties			protein charge[c]	Reference
		K_a / 10^5 M^{-1}	ΔH / kJ mol^{-1}	ΔS / J mol^{-1} K^{-1}	charge[a]	hydrophilicity[b]	surfactant		
polystyrene (PS)	apo A-I	24	−1438	−4700	Ø	*	Lutensol	$\ominus$	[80]
PS	clusterin	371	−1237	−4004	Ø	*	Lutensol	$\ominus$	[80]
PS	HSA	0.6 ± 0.2	−199 ± 54	−487 ± 74	Ø	*	Lutensol	$\ominus$	[81]
PS	HSA	2.4 ± 0.8	−192 ± 45	−540 ± 151	Ø	*	SDS	$\ominus$	[81]
hydroxyethyl starch (HES)	HSA	8 ± 3	−277 ± 43	−818 ± 147	$\ominus$ $\ominus$	*****	SDS	$\ominus$	[9]
HES	apo A-I	3330 ± 1240	−6010 ± 185	−20 000 ± 613	$\ominus$ $\ominus$	*****	SDS	$\ominus$	[9]
HES (carboxyl functionalized)	HSA	4 ± 2	−308 ± 30	−928 ± 103	$\ominus$ $\ominus$	*****	SDS	$\ominus$	[9]
HES (carboxyl functionalized)	apo A-I	1880 ± 790	−5150 ± 787	−17 100 ± 2640	$\ominus$ $\ominus$	*****	SDS	$\ominus$	[9]
HES (amino functionalized)	HSA	5 ± 1	−277 ± 45	−820 ± 152	$\ominus$ $\ominus$	*****	SDS	$\ominus$	[9]
HES (amino functionalized)	apo A-I	54 ± 1	883 000 ± 24000	2.4 ± 0.9 · 10^6	$\ominus$ $\ominus$	*****	SDS	$\ominus$	[9]
copolymer NIPAM/BAM (50:50)	HSA	12.0 ± 0.2	−595 ± 54	−1950 ± 230	Ø	**	none	$\ominus$	[69]
copolymer NIPAM/BAM (85:15)	HSA	62.7 ± 0.2	−104 ± 53	−350 ± 40	$\ominus$	***	none	$\ominus$	[69]
PS (spherical polyelectrolyte brushes)	β-lactoglobulin	10 ± 1	113 ± 3	0.494 ± 0.008	$\ominus$	*	poly(styrene sulfonate)	$\ominus$	[64]

Au	HSA	14 ± 5	-1960 ± 1290	-6200	⊖	***	none	⊖	[82]
Au (amino acid-functionalized)	α-chymotrypsin	≈ 6	≈ - 45	≈ - 50	⊖	*	1-pentanethiol	⊕	[70]
Au (amino acid-functionalized)	histone	≈ 800	≈ 95	≈ 460	⊖	*	1-pentanethiol	⊕	[70]
Au (amino acid-functionalized)	cytochrome c	≈ 100	≈ 50	≈ 330	⊖	*	1-pentanethiol	⊕	[70]
Au (manose functionalized)	concanavalin A	82	$-10.8 * 10^4$	N/A	⊖	*	none	⊖	[83]
Au (17% galactose functionalized)	lecitin PA-IL	1.7 ± 0.3	−37 ± 7	N/A	⊖	*	none	⊖	[84]
Au (100% galactose functionalized)	lecitin PA-IL	200 ± 20	−18 ± 5	N/A	⊖	*	none	⊖	[84]
Carbon NPs	BSA	192	-6477	N/A	Ø	*	none	⊖	[77]
Carbon NPs	HSA	207	-28024	N/A	Ø	*	none	⊖	[77]
Chitosan (cholesterol modified)	BSA	N/A	-46.1 ± 3.3	-50	Ø	*	none	⊖	[85]
Fe_3O_4	BSA	29.8	-58.4	N/A	⊖	****	PEG and oleylamine	⊖	[86]
Fe_3O_4	IgG	26.1	-50.2	N/A	⊖	****	PEG and oleylamine	Ø	[86]
CuO	β -galactosidase	3.7 ± 0.5	-67 ± 5.0	N/A	⊖	****	none	⊖	[87]
ZnO	ToxR protein	9 ± 3	−41.0 ± 3.3	−21.6	⊕	*	none	⊖	[88]
ZnO	BSA	0.26 ±0.06	−18.0 ± 2.9	25	⊕	*	none	⊖	[89]
ZnO (polyethyleneimine-functionalized)	BSA	0.79 ± 0.3	−26.8 ± 6.7	3.14	⊕ ⊕	*	none	⊖	[89]

In order to shed more light onto the trends in correlation between binding mechanism and the properties of nanocarriers and protein, recent ITC studies on nanocarrier-protein interactions are summarized in Table 2.3.2.

It can be seen that most nanocarrier-protein interactions result from enthalpy-driven adsorption processes with a loss of entropy ($\Delta H < 0$ & $\Delta S < 0$) corresponding to a general predominance of van der Waals interactions, electrostatics and hydrogen bond formation.[53] This is present for example in interactions between human serum albumin (HSA) and N-*iso*-propylacrylamide/N-*tert*-butylacrylamide copolymer nanoparticles as reported by Lindman *et al*. in 2007.[69] Similarly, interactions of polymeric polystyrene nanoparticles or hydroxyethyl starch nanocapsules with HSA or different apolipoproteins were dominantly enthalpy-driven under the loss of entropy as reported by Winzen *et al*.[9,81] and Müller *et al*.[80] Notably, many examples can be found where nanocarriers and proteins are of similar charge which also lead to an exothermic interaction that is dominated by van der Waals interactions, electrostatics and hydrogen bond formation, yet appears in weaker forms as nicely seen in the study of Lindman *et al*. mentioned before.[69]

In the case of oppositely charged nanocarrier and protein, the interactions generally result in an increased entropy gain with relatively high association constants and an endothermic process ($\Delta H > 0$ & $\Delta S > 0$) due to stronger binding and promoted desolvation. As an example, interactions between negatively charged, amino acid-functionalized gold nanoparticles and the positively charged histone and cytochrome c show an entropy-driven adsorption process as reported by De *et al*.[70]. However, entropy-driven adsorption processes may also occur in the case of similarly charged nanocarriers and proteins, as reported by Henzler *et al*. for adsorption of β-lactoglobulin onto spherical polyelectrolyte brushes.[64] More highly (positively or negatively) charged nanocarriers generally interact stronger with proteins with higher values for K_a, more negative ΔH and more positive ΔS. This is most likely a result of stronger electrostatic interactions between the charged nanocarrier surfaces and oppositely charged protein patches and the resulting desolvation as discussed above. Furthermore, the more hydrophobic the nanocarrier system is, the higher is the entropy gain for the same protein, presumably due to higher involvement of hydrophobic interactions in the adsorption process. In many cases, this entropy gain is accompanied additionally

by an enthalpy gain, which can also be a result of van der Waals interactions occurring between hydrophobic protein residues and hydrophobic nanocarrier surfaces.

During adsorption events, denaturation of proteins may occur, leading to an entropy gain that is accompanied by an enthalpy loss ($\Delta H < 0$ & $\Delta S > 0$). As an example, such constellations were reported by Chakraborti et al.[89] for the adsorption of negatively charged bovine serum albumin (BSA) at physiological pH onto (positively) charged zinc oxide nanoparticles. In another example, the adsorption of the protein apolipoprotein A-I (apo A-I) onto hydroxyethyl starch (HES) nanocapsules depends on the surface functionality of the nanomaterial - especially comparing unfunctionalized or carboxyl-functionalized with amino-functionalized nanocapsules.[9] An often-disregarded factor in the interpretation and analysis trends in nanocarrier-protein interactions is the influence of surfactants on the properties of the nanocarriers and therefore the whole adsorption process. This becomes apparent regarding the change in net change and hydrophilicity of nanocarriers with the resulting difference in adsorption observed in multiple studies. HSA showed a significantly higher affinity to PS-NPs stabilized by the more hydrophilic surfactant SDS compared to the more hydrophobic PEG-based Lutensol in a study by Winzen et al.[81] In the study by Chakraborti et al.[89] discussed above, zinc oxide NPs which were strongly positively charged due to non-covalent polyethyleneimine-functionalization interacted with a higher K_a and more enthalpy-driven (more negative ΔH and lower, yet still positive ΔS) than similar nanocarriers lacking the surface functionalization.

In conclusion, in order to see trends in surface properties of nanocarriers with the interaction mechanisms they undergo with proteins, one must consider the complete surface composition including all of its components instead of solely focusing on the nanocarrier-material. Based on the summary of ITC studies on the protein corona discussed above, relations between the properties of nanocarriers and the interactions they undergo with proteins can be concluded. More hydrophobic surfaces of nanocarriers generally result in a higher proportion of hydrophobic interactions with proteins observed by stronger binding and a promotion of desolvation at the nanocarrier-protein interface. On the other hand, more hydrophilic surfaces promote van der Waals forces and hydrogen bond formation resulting in enthalpy-driven (exothermic) adsorption processes with a loss of entropy. More highly charged (positively or negatively) surfaces lead to stronger

interactions compared to surfaces of neutral charge, which is observed by a more positive ΔS due to the release of hydration water from the nanocarrier-protein interface. As unspecific nanocarrier-protein interactions are desired to be minimal for engineering the protein corona, we deduce that nanocarriers formed of a hydrophilic material with neutral charge and steric (instead of electrostatic) stabilization experience the weakest interactions with proteins. This brief excerpt of the thermodynamic complexity of nanocarrier-protein interactions depicts the necessity to take information from other methods into account during analysis of ITC studies on the protein corona (for example on the hydrophilicity or surface charge of nanocarriers) in order to make full use of the technique's potential for the field.

While the information obtained from ITC studies on the protein corona nicely complement other methods, ITC also relies on other methods to overcome its own limitations which are discussed in the following. A comprehensive review containing information on the different methods and obtained parameters concerning the protein corona can be found in the literature.[90]

Analyzing data obtained from ITC experiments concerning the protein corona of nanocarriers is particularly complex,[54-56] as multiple pitfalls arise concerning the essentially required molar concentrations of both, nanocarrier dispersion and protein solution. ITC studies of single protein solutions are easily feasible, as calculating the molar concentration of single protein solutions is unproblematic (presupposing knowledge on the molar mass of the respective protein). More complex protein systems (especially in the case of full blood or blood plasma) are more difficult to characterize by their molar protein concentrations. Determining the molar concentration of nanocarrierss by their dispersion's solid content is not trivial, as monodispersity and perfectly spherical particles are an often-unavoidable assumption. This gets even more complicated for hollow particles (nanocapsules or self-assembled systems such as polymersomes/liposomes). Furthermore, many ITC instruments rely on relatively high analyte concentrations in order to detect significant heat changes during titration, which is hard to realize for more exotic (and expensive) proteins.

Fits of the adsorption isotherm in all cases require information on the molar concentration of both interacting components. Usually, ITC studies concerning nanocarrier-protein interactions apply the so called "independent binding model".[55,57] This mathematical model assumes

independent protein binding to the nanoparticle according to a standard Langmuir binding. This means that interacting or bound proteins do not influence the binding of other proteins, excluding possible cooperative effects. In reality, the situation might be different and protein-protein interactions also have to be taken into account. Furthermore, entirely reversible adsorption processes are assumed, which is not trivial considering possible structural changes of proteins if denaturation processes occur during adsorption, leading to changing binding affinities over the course of the experiment.[91] Addressing the problems arising from the independent binding model, Ballauff *et al*. developed a binding model including possible affinity changes of proteins during the interactions of proteins with hydrogel NPs.[67] Ideally, a new model for each ITC study on the protein corona should be developed, which would hardly be possible and would hinder comparability of different studies. Therefore, new standardized models would enhance the method's ability to address nanocarrier-protein interactions dramatically.

Another pitfall for ITC studies concerning the protein corona is neglecting the possibility of interactions between proteins and molecules that stabilize the nanocarriers (e.g. surfactants). It is known that similar nanocarriers that are stabilized by different surfactants engage in strikingly different interactions with proteins.[81] Similarly, the concentration of the surfactant molecules on the surface were shown to be important. Furthermore, the concentration of salts in the different media (protein solution and nanocarrier dispersion) should ideally be identical. Significant differences in salt concentrations may result in large heats during injections due to the dilution heat of the salt and resulting noise, which might make it impossible to analyze the recorded data.

2.4.2 Enzyme-linked immunosorbent assay (ELISA)

The enzyme-linked immunosorbent assay (ELISA) is an assay commonly used to determine the concentration of a certain compound (usually a protein) in a solution utilizing the specific interaction between an antibody and the compound to be quantified (antigen). ELISAs are commonly executed in microtiter plates by immobilizing the antigen in the well directly (*via* unspecific adsorption; direct ELISA) or *via* specific interaction (*via* capturing the antigen with another compound; Sandwich ELISA). After washing steps, an antibody binds the immobilized antigen. Usually this antibody is covalently linked to an enzyme, which is used for quantification in a colorimetric reaction. In this dissertation, an ELISA for the quantification of PEG-binding IgG (anti-PEG IgG) is used. Therefore, anti-PEG IgG is considered as the "antigen" in the ELISA used herein. Only anti-PEG IgG should be quantified by this assay and not any other antibodies. Therefore, instead of using unspecific adsorption to the well, the specific interaction between anti-PEG IgG and PEG chains is used. Like this, PEG-chains are covalently linked to the wells' surface prior to incubation with samples (see Sandwich ELISA described above). Anti-PEG IgG is then allowed to bind the immobilized PEG chains and any unbound proteins are washed away. Subsequently, an antibody specifically binding the F_c-domain of human IgG is used for the detection of all bound anti-PEG IgG proteins. Horseradish peroxidase is covalently linked to the anti-human IgG antibody and facilitates the oxidation of 2,2'-azino-bis(3-ethylbenzothiazoline-6-sulphonic acid) (ABTS) in the presence of hydrogen peroxide to form a stable radical cation with an absorption maximum at 405 nm (see Figure 2.4.3). This reaction product is photometrically quantified after 30 minutes of reaction time.
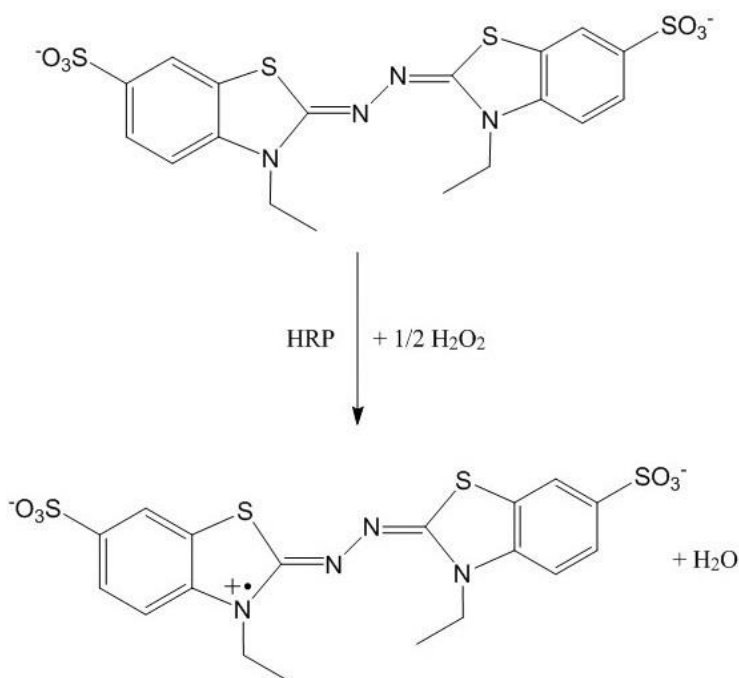
Figure 2.4.3: Oxidation of ABTS for photometric quantification in an ELISA.

In order to analyze the specificity of the proteins' immobilization, a competition assay may be performed in addition to the direct or Sandwich ELISAs. In the case of the Sandwich ELISA for quantification of anti-PEG IgG, free PEG chains may be added to the solution before incubation with biological samples. Subsequently, present anti-PEG IgG molecules will interact with immobilized or free PEG chains respectively and after several washing steps, the measured analyte concentration of the competition assay will be significantly decreased compared to the ELISA solely utilizing immobilized PEG. An overview of the sandwich ELISA and competition assay used in this thesis is depicted in Figure 2.4.4.
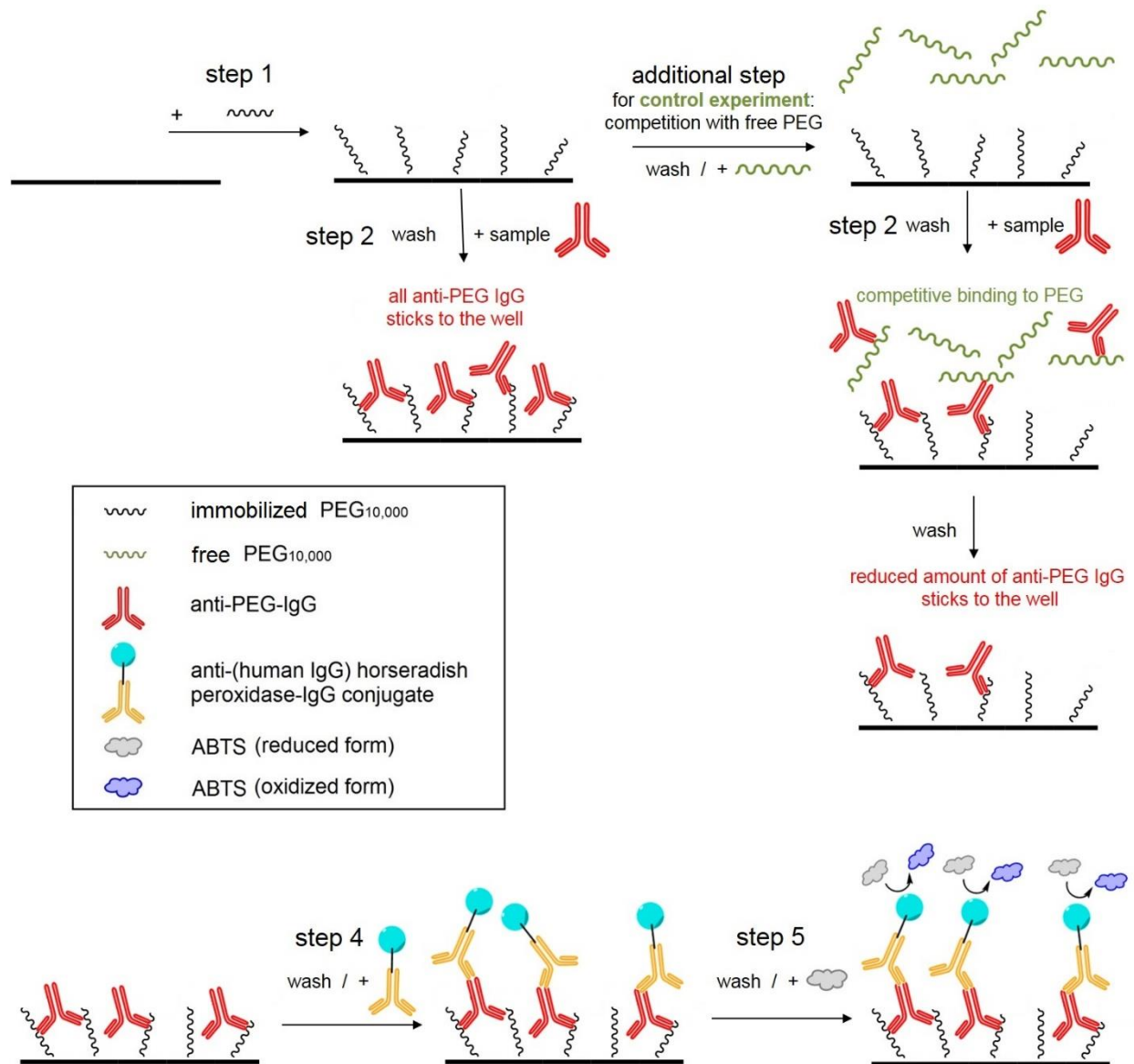
Figure 2.4.4: Schematic overview of the sandwich ELISA method used herein. Step 1: Immobilization of PEG chains to well; additional step (in competition assay): addition of free PEG to the medium; step 2: addition of sample containing anti-PEG IgG; step 3: addition of anti-(human IgG) antibody - horseradish peroxidase conjugate; step 4: addition of ABTS and oxidation of ABTS in the presence of hydrogen peroxide.

2.4.3 Liquid chromatography - mass spectrometry (LC-MS)

Mass spectrometry (MS) is an analytical method used for the selective quantification of molecules and molecule fractions. MS is often coupled to other techniques like gas chromatography (GC) or liquid chromatography (LC) in order to fractionate different substances prior to analysis in the mass spectrometer. The ionization of molecules in GC-MS can be performed in vacuum *via* electron ionization (EI) or chemical ionization (CI) which is not possible for LC-MS as the ionization must be performed at atmospheric pressure. In the case of LC-MS, electrospray ionization (ESI) or atmospheric-pressure chemical ionization (APCI) are available ionization techniques. Both are applicable for the analysis of different substances and work in a different fashion. Therefore, the decision which ionization technique should be used depends on the physicochemical properties of the analyte. ESI is a suitable choice for polar substances with amphiphilic character, while APCI is the appropriate choice for substances of non- or low-polarity. Therefore, analysis of proteins *via* LC-MS is most approachable with ionization using ESI.

The measurable mass/charge (m/z) signal of mass spectrometers on the market can reach m/z of up to 4,000 Da. As the mass of most proteins is too large for analysis with MS, a fractionation (or digestion) step before analysis in MS is required. This digestion of proteins is usually performed utilizing proteases, such as trypsin. Trypsin is a serine protease produced in the pancreas, that specifically cleaves the peptide bonds of proteins and polypeptides after positively charged arginine and lysine residues.[92] Therefore, proteins digested by trypsin yield polypeptide fragments (see Figure 2.4.5) with specific masses based on the sequence of amino acid residues of the original protein, which are in a size range measureable in MS.
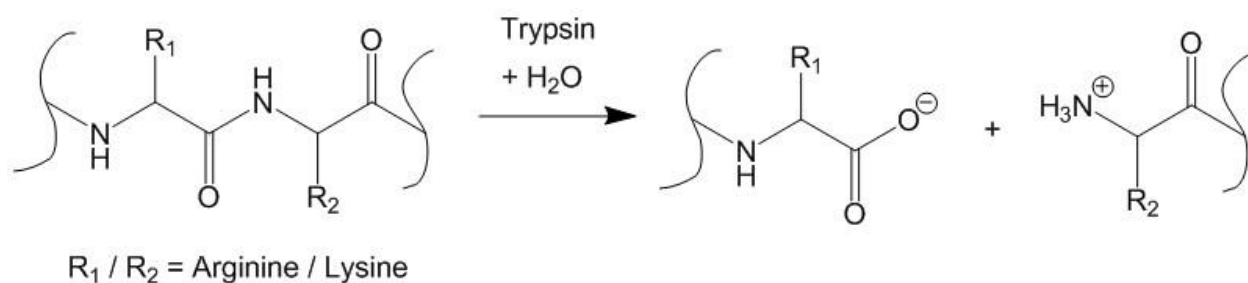

R₁ / R₂ = Arginine / Lysine

Figure 2.4.5: Digestion of proteins by trypsin resulting in the formation of polypeptide fragments.

The peptides resulting from digestion with trypsin are strongly charged, enabling efficient ionization *via* ESI. After analysis *via* MS, the measured *m/z* signals of peptides are matched to peptide masses from proteins from databases in a so-called "peptide mass fingerprinting" process. As the same peptide may appear in multiple proteins, careful analysis of MS experiments regarding proteins is required. For this reason, only proteins with at least 2 unique peptides found in the used database are considered identified successfully.

2.4.4 Dynamic light scattering (DLS)

The theory of light scattering is readily available in standard literature.[93-95] In the following, only certain aspects of dynamic light scattering (DLS) utilized in this dissertation will be discussed.

As light is a periodically oscillating, electromagnetic wave, its interaction with a molecule induces an oscillating dipole. To reach its original state of energy, this dipole emits an electromagnetic wave with the same wave length of the primary light. This emitted wave is irradiated isotropically in all directions perpendicular to the oscillating dipole. As a light source, lasers may be used, as their light has monochromatic and coherent properties and is polarized linearly. If the size of the scattering particle is below $\lambda/20$, only one scattering center per molecule is assumed. However, for larger particles, multiple scattering centers occur per molecule resulting in differently scattered waves. These different waves interfere with each other, resulting in phase shifts. In this case, the scattered wave's intensity loses its isotropy and depends on the scattering angle θ instead. This angle-dependent behavior is described by the scattering vector q. The scattering vector q is expressed by $q = \frac{4\pi n}{\lambda_0} \sin\left(\frac{\theta}{2}\right)$ with n as refractive index of the continuous phase, λ_0 as the wavelength of the scattered light and θ as the scattering angle.

As the scattering particles enter and exit the scattering volume due to Brownian motion, the measured intensity of the scattered light will fluctuate during the experiment. In DLS experiments, the fluctuation of the measured intensity over time is recorded. The scattering intensity at one time point is compared to the intensity at another time point shifted by the time τ_i. The change of intensity is converted to an autocorrelation function for different times τ_i (usually τ ranges from

100 ns to multiple seconds). This fluctuation directly correlates with the diffusion coefficient D of the scattering species. As the diffusion coefficient D depends on the scattering angle θ for polydisperse particles or diffusing species larger than $\lambda/20$, D is determined for different scattering angles. D is subsequently extrapolated for $q^2 \to 0$.

From the diffusion coefficient, the hydrodynamic radius is calculated using the Stokes-Einstein equation (see equation 2.4.3):

$$R_h = \frac{k_B T}{6\pi\eta D} \tag{2.4.3}$$

k_B is the Boltzmann constant, T describes the temperature, η describes the viscosity of the continuous phase and D is the diffusion coefficient of the scattering species.

A method by Rausch et al.[96] has been developed for analysis of multicomponent systems occurring in complex mixtures such as blood plasma. This analysis can be applied for the detection of aggregation of nanocarriers in undiluted plasma or serum and thus serves as a quality control regarding their successful translation to in vitro or in vivo systems. In brief, the autocorrelation function of proteins (single proteins or plasma) $g_{1,P}$ is described by the sum of three exponential terms (see equation 2.4.4), while the autocorrelation function of nanocarriers $g_{1,N}$ is described by the sum of two exponential terms (see equation 2.4.5).

$$g_{1P}(t) = a_{1,P}\, exp\left(-\frac{t}{\tau_{1,P}}\right) + a_{2,P}\, exp\left(-\frac{t}{\tau_{2,P}}\right) + a_{3,P}\, exp\left(-\frac{t}{\tau_{3,P}}\right) \tag{2.4.4}$$

$$g_{1,N}(t) = a_{1,N}\, exp\left(-\frac{t}{\tau_{1,N}}\right) + a_{2,N}\, exp\left(-\frac{t}{\tau_{2,N}}\right) \tag{2.4.5}$$

where a_i describes the amplitudes for the exponential terms, decay times are described by $\tau_i = (q^2 D_i)^{-1}$. D_i is the translational diffusion coefficient.

After determining the individual autocorrelation functions of each component, the mixtures of nanocarriers and proteins can be investigated. If the sum of the autocorrelation functions of both individual components (see equation 2.4.4 and 2.4.5) is sufficient to fit the data of the mixture in a so called "forced fit" (see equation 2.4.6), both components coexist and no aggregation processes occur. However, this forced-fit is not capable of describing the data of the mixture in the case of aggregation events and an additional term describing the diffusion behavior of the aggregate species is needed (see equation 2.4.7).

$$g_{1,m}(t) = f_N g_{1,N}(t) + f_P g_{1,P}(t) \tag{2.4.6}$$

$$g_{1,m}(t) = f_N g_{1,N}(t) + f_P g_{1,P}(t) + f_{Agg} g_{1,Agg}(t) \tag{2.4.7}$$

where f_i describes the intensity contribution factor of the respective species.

3. Results: Nanocarrier-immunoglobulin interactions

3.1 Interactions of isolated immunoglobulins with differently charged polymer nanoparticles

In this chapter, the interactions between different immunoglobulins (Igs) isolated from human serum and differently charged polymer nanoparticles are investigated. Dr. Seah Ling Kuan (MPI-P) created surface charge mapping of IgG and the Fc fragments of IgA and IgM for this project.

3.1.1 Overview

One major protein class and significant part of blood proteome are Igs. The total Ig concentration averages around 16 g L^{-1} with a total protein concentration in human blood of around 60-70 g L^{-1} for adults.[27] The major Ig classes of the proteome consist of IgG at a concentration of approximately 11-12 g L^{-1}, IgA at a concentration of 2.6 g L^{-1} and IgM at a concentration of 1.5 g L^{-1} on average.[33]

As the name already implies, Igs generally play an important role in the immune system. Interactions of Igs with any compound foreign to the organism, including biomedical nanocarriers, trigger the recognition of Igs by cells of the immune system (e.g. macrophages) resulting in immune cascades ultimately leading to the clearance of these foreign compounds from the organism. Therefore, interactions between nanocarriers and immunoglobulins could potentially result in unwanted behavior of the nanocarriers inside the body, such as (auto)immune reactions, inflammation and allergic reactions. Furthermore, Igs behave as opsonins in the protein corona of nanocarriers which means they lead to unspecific cell uptake resulting in a significantly decreased circulation time *in vivo*.[97] Following this, the role of the different Igs in the protein corona of nanocarriers is of importance. Their interaction mechanism has to be fully understood in order to minimize nanocarrier-Ig interactions as much as possible, resulting in a better chance that the nanocarriers will not be cleared by the immune system or even induce adverse effects.

While the adsorption behavior of individual Ig classes, such as IgG, on different nanocarriers is known to be independent on the size of nanocarriers[14], the influence of nanocarriers' surface charge on the adsorption mechanism of the different Ig classes is unclear. In order to draw general conclusions for interaction trends between Igs and differently charged nanocarriers, model nanocarriers are needed. For this, polystyrene nanoparticles with different functional groups (unfunctionalized, carboxyl-functionalized and amino-functionalized) were used as model systems for the investigation of interactions with IgG, IgA and IgM from human plasma. The adsorption of the different immunoglobulin classes on the surface of nanocarriers was confirmed *via* sodium dodecyl sulfate polyacrylamide gel electrophoresis (SDS-PAGE). By investigating the respective zeta potential (ζ), the influence of Igs on the apparent charge of differently charged nanoparticles was analyzed. Furthermore, the thermodynamic adsorption parameters of the respective interactions were analyzed *via* isothermal titration calorimetry (ITC). Analysis of the Ig's influence on the stability and aggregation tendency of nanocarriers was performed *via* dynamic light scattering (DLS). Additionally, the structural stability of immunoglobulins after adsorption was analyzed *via* nano differential scanning fluorimetry (nanoDSF).

3.1.2 Results and Discussion

In this study, the interactions between Igs and different nanocarriers were investigated. For this, dispersions of the respective nanocarrier were incubated with solutions of the respective Ig in PBS. In order to be able to draw conclusions between the resulting Ig-NP interaction and the surface charge of nanocarriers, different model NPs were used in this study (see Table 3.1.1). All NPs used are polystyrene nanoparticles stabilized by minimal amounts of a poly(ethylene glycol) (PEG) based surfactant (Lutensol AT50) and share similar hydrodynamic radii between 50 and 60 nm in order to exclude influences of these parameters. However, different surface functionalities were created by using different comonomers throughout the miniemulsion polymerization in order to achieve differently charged nanocarriers. The resulting polystyrene nanoparticles used were unfunctionalized (PS-NPs), carboxyl-functionalized (PS-NPs-COOH by using acrylic acid as comonomer) or amino-functionalized (PS-NPs-NH$_2$ by using 2-aminoethyl methacrylate hydrochloride (AEMH) as comonomer) respectively.

Table 3.1.1: Characterization of NP systems regarding physico-chemical properties.

	PS-NPs	PS-NPs-COOH	PS-NPs-NH$_2$
material	polystyrene (PS)	polystyrene (PS)	polystyrene (PS)
surfactant	Lutensol AT50	Lutensol AT50	Lutensol AT50
functional group	none	carboxyl (-COOH)	amino (-NH$_2$)
R_h / nm	52 ± 5	57 ± 6	51 ± 5
zeta potential ζ / mV	$- 10 \pm 1$	$- 29 \pm 2$	2 ± 1

First, the presence of Ig chains on the surface of the different PS-NPs was investigated *via* a reducing SDS-PAGE. For that purpose, the different NPs were incubated with each individual Ig type and subsequently separated from free proteins by repeated washing steps. The remaining proteins were detached from the NPs by incubation with SDS and were analyzed afterwards. The identified protein patterns are shown in Figure 3.1.1. The different light and heavy chains of immunoglobulins can be found on the surface of the different PS-NPs and show distinct bands because the connecting disulfide bridges were cleaved during the reducing conditions. Visible differentiation between the different Igs is possible by analyzing the molar weight corresponding to the bands of the heavy chains (between 50 and 70 kDa), while light chains share the same molecular weight around 25 kDa.
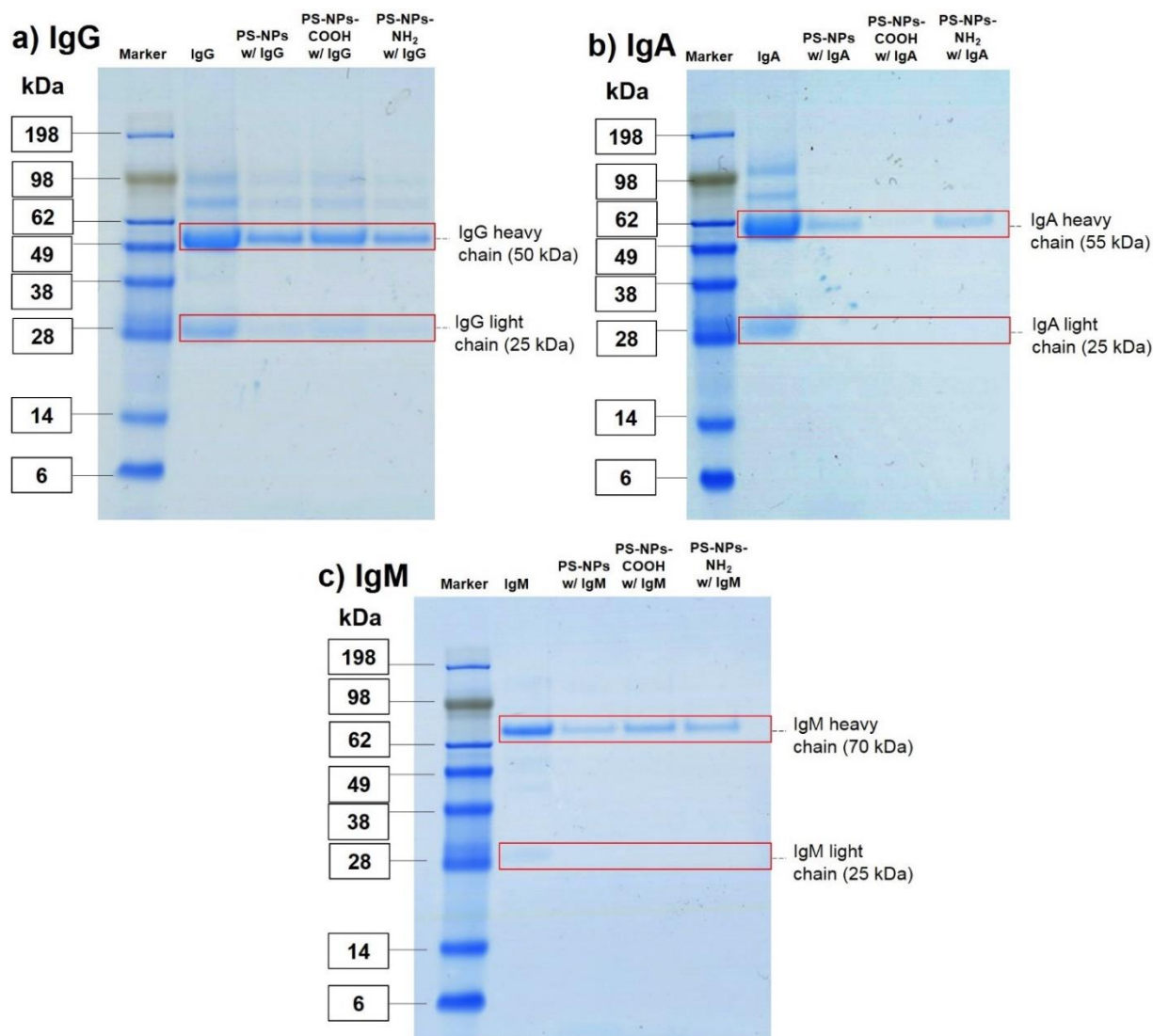
Figure 3.1.1: Reducing SDS-PAGE gel of the protein corona of PS-NPs incubated with a) IgG, b) IgA and c) IgM. Pure Igs are shown as a reference. For staining, a ready-to-use Coomassie staining solution was used according to the manufacturer's instruction.

Additionally, analysis of the antibodies without reduction step prior to electrophoresis are depicted in Figure 3.1.2. Comparing reduced and non-reduced bands gives further information on the original structure of the respective immunoglobulin. IgG and IgA have similar molar weights of around 150 kDa in the non-reduced SDS-PAGE implying monomeric immunoglobulins. However, they can be distinguished by the difference in the molar weight of the heavy chains (50 kDa for IgG and 55 kDa for IgA). IgM appears with a significantly higher molar weight ($\approx$ 1000 kDa) in the non-reduced SDS-PAGE which is explained by the pentameric nature of IgM.
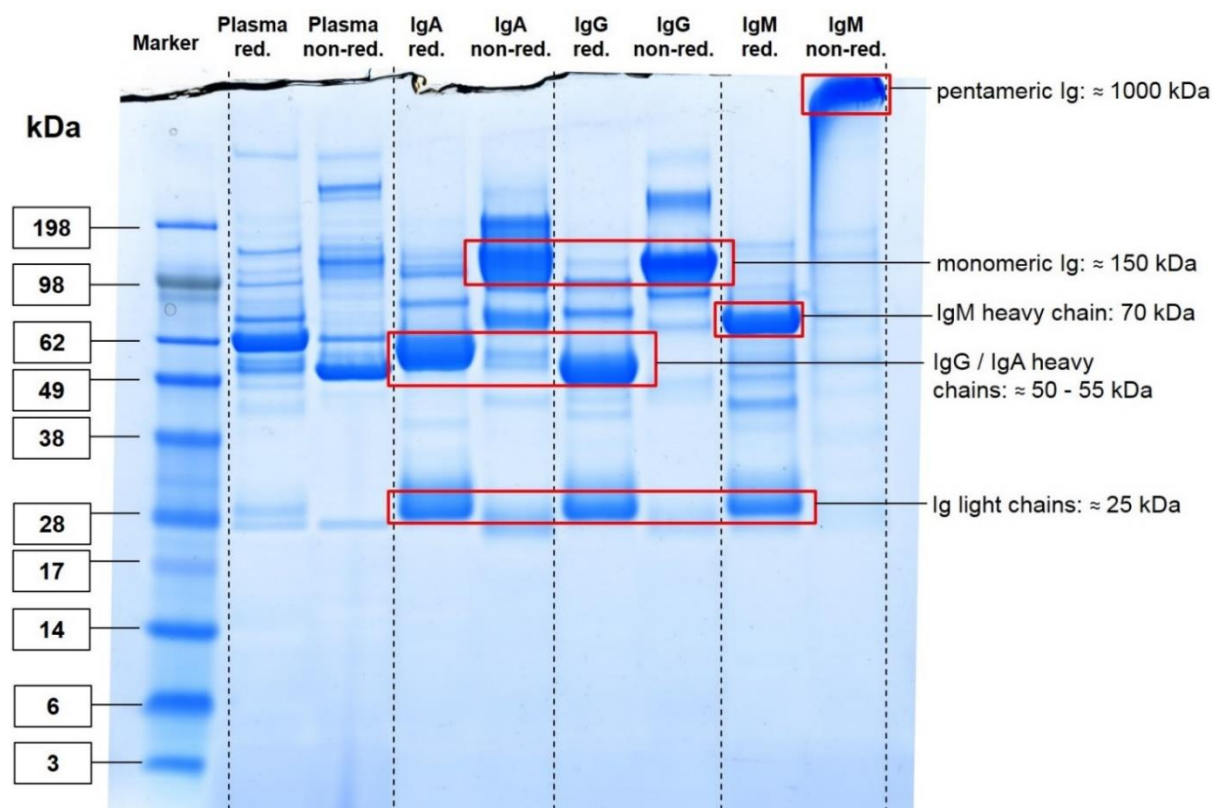
Figure 3.1.2: SDS-PAGE gel of plasma and Igs with ("red.") and without ("non-red.") addition of reducing agent. In reduced SDS-PAGE disulfide bonds are cleaved resulting in bands for heavy and light chains of Igs. In non-reduced SDS-PAGE disulfide bonds remain intact and a single band for the Igs is detected respectively. For IgM, the presence of pentamers is supported by the gel pattern as the detected band is outside the upper limit of the marker range. Different bands belong to different proteins that were not fully removed from the purchased Ig fraction. However, the protein concentration in all columns is rather high and the Ig bands represent the major component by far in each case. For staining, a ready to use Coomassie staining solution was used according to the manufacturer's instruction.

In summary, all Igs are found on the surface of each NP sample, while the interaction between IgA and the three different NPs appears to be rather weak, especially in the case of PS-NPs-COOH. However, a determination of the interaction mechanism cannot be achieved from these results obtained *via* SDS-PAGE. In order to achieve more information on the interaction mechanism, the influence of the NP surface charge was investigated concerning the net charge of the Igs and the subsequent interaction of both using zeta potential measurements (see Figure 3.1.3).
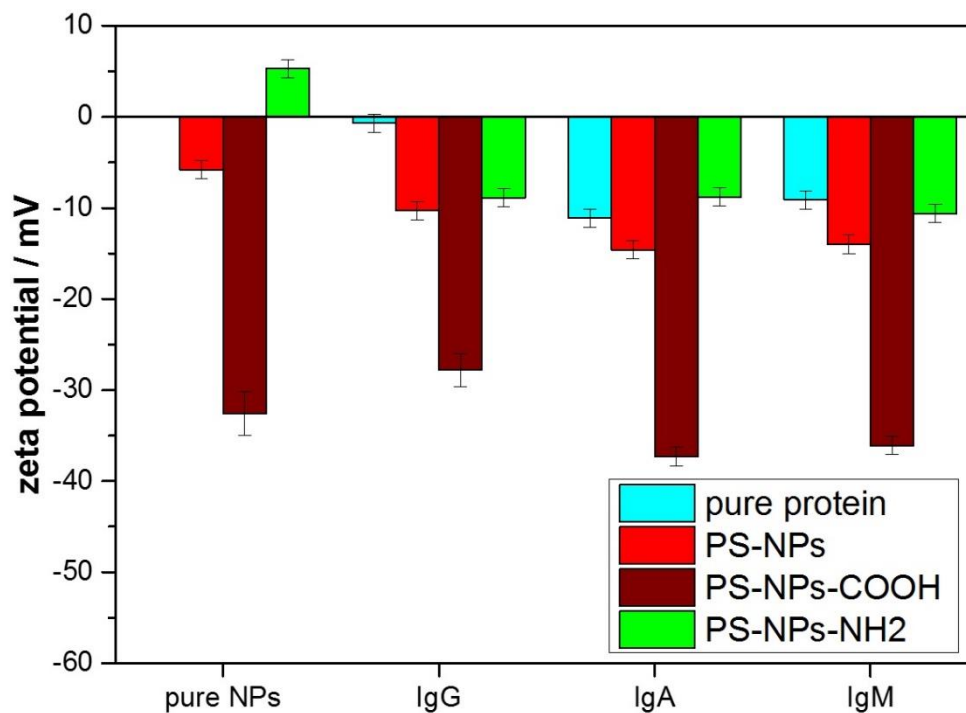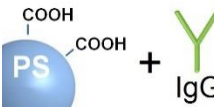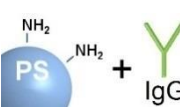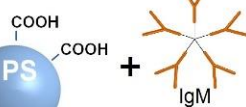
Figure 3.1.3: Bar diagrams for the zeta potentials of the different pure PS-NPs and Igs as well as zeta potentials of the different PS-NPs after incubation with the different Igs and washing at pH = 7 in 1 mM KCl.

According to Figure 3.1.3, Igs themselves exhibit different zeta potentials in accordance with their isoelectric points reported in literature (pI(IgG) = pH 7 - 9.95 ; pI(IgA) = pH 4.7 - 5.9 ; pI(IgM) = pH 5.5 - 6.7)[98]. While the overall surface charge for IgG is almost neutral at pH 7, IgA and IgM overall are slightly negatively charged. The pure PS-NPs themselves (left columns) differ in zeta potential in accordance with their surface charge as well, while PS-NPs-COOH exhibit a more negative zeta potential than the positive zeta potential of PS-NPs-NH$_2$. IgG in the corona leads to a more negative zeta potential of PS-NPs-NH$_2$. While IgA and IgM show a negative zeta potential in their native state, all NPs (especially amino-functionalized ones) exhibit a more negative zeta potential post-incubation with IgA and IgM. Carboxyl-functionalized NPs, which are already highly negatively charged, interestingly keep their surface charge meaning they are not completely and fully covered. These measurements already indicate that the different Ig types interact differently with charged or non-charged surfaces.

Upon further investigation of the adsorption process of Igs onto NPs, the thermodynamic parameters of the respective interaction were investigated *via* isothermal titration calorimetry (ITC). For that, all NP types were titrated with solutions of the different Igs and the corresponding heat of interaction was analyzed. The obtained adsorption parameters are summarized in Table 3.1.2. The obtained heat rates are shown in Figures A1-A9 (see appendix) and their corresponding adsorption isotherms are displayed in Figure 3.1.4. All adsorption isotherms were fitted according to an independent binding model where possible. It has to be noted that all titrations were performed at 15 °C. At higher temperatures, no changes in heat were visible, although interaction was already confirmed by SDS-PAGE. This means that interactions were heat-neutral at higher temperature.

Table 3.1.2: Adsorption parameters obtained from independent binding fits of isotherms from ITC experiments.

	PS + IgG	PS (COOH, COOH) + IgG	PS (NH$_2$, NH$_2$) + IgG	PS (COOH, COOH) + IgM
K_a / 10^6 M^{-1}	4.0 ± 1.0	0.41 ± 0.05	1.8 ± 0.5	2.12 ± 0.57
ΔH / kJ mol^{-1}	-36 ± 5	-274 ± 34	-98 ± 19	-353 · 10^3 ± 49 · 10^3
ΔS / J mol^{-1} K^{-1}	-25 ± 2	-843 ± 118	-211 ± 79	-122 · 10^4 ± 17 · 10^4
ΔG / kJ mol^{-1}	-36.4 ± 0.6	-30.9 ± 0.3	-34.4 ± 0.7	-45.9 ± 0.6
n	121 ± 1	208 ± 18	101 ± 8	1.4 ± 0.1
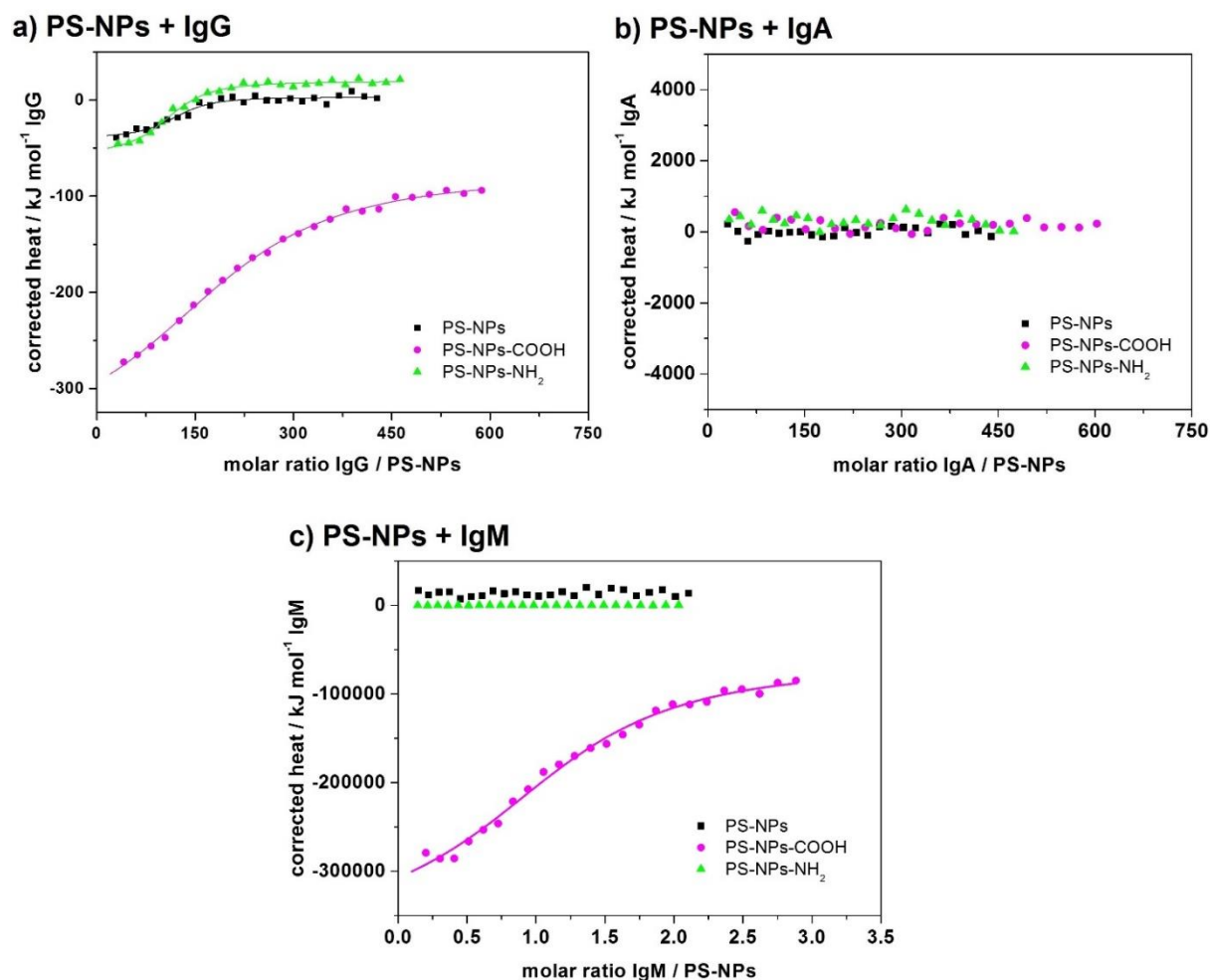
Figure 3.1.4: Adsorption isotherms of a) IgG, b) IgA and c) IgM titrated to the different PS-NPs obtained from ITC experiments. The integrated heat of individual injections is depicted for PS-NPs (■), PS-NPs-COOH (●) and PS-NPs-NH$_2$ (▲). Isotherms were fitted according to an independent binding model (solid lines) where possible.

The adsorption behavior of the different Igs on the different NPs is very different (see Figure 3.1.4 and Table 3.1.2). While the adsorption processes of IgG produces enough heat for obtaining thermodynamic data by independent binding fits, for IgA and IgM almost no heat change is observed during titration. This could be due to relatively weak interactions between the NPs and IgA or IgM respectively (as discussed above *via* SDS-PAGE) or it could be due to the limitation of the protein concentration in the protein source. Only in the case of interaction between PS-NPs-COOH and IgM, large amounts of heat were registered. In the case of IgG, the interaction with all PS-NPs is differently enthalpy driven. PS-NPs without functional groups on the surface

exhibit the highest affinity towards IgG and in relation the smallest enthalpy gain as well as entropy loss. PS-NPs-COOH on the other hand show the least affinity towards IgG and the most enthalpy-driven process with the largest loss of entropy. This suggests that IgG probably undergoes more hydrophobic interactions or less structural rearrangements with plain PS-NPs, while for the functionalized NPs, hydrophilic interactions such as electrostatic interactions become more dominant. This effect is more dominant for PS-NPs-COOH than for PS-NPs-NH$_2$ which is in accordance with the higher net surface charge of PS-NPs-COOH (see Table 3.1.1 and Figure 3.1.3). The large heat generated between interactions of PS-NPs-COOH with IgM does not seem plausible for NP-protein interactions at first sight. In principle, it is likely that denaturation of proteins upon interaction with NPs occurs. However, such denaturation processes are endothermic and entropy-driven, which is not the case for the overall NP-Ig interactions (see Table 3.1.2). Supposedly, the strong enthalpy gain is actually related to a large number of protein residues interacting with the nanoparticle surface. This is supported by the obtained stoichiometry of around 1.4 IgM molecules per NP and the fact that IgM is an immunoglobulin pentamer and thus a much larger molecule than IgG. An enthalpy gain as high as determined here would, as such accordingly, only be possible with a "flat-on" adsorption process of the IgM, yielding the highest available contact area. This raises the question whether the respective surface charge distribution of Igs play a role in the interactions with NPs instead of solely the overall net charge.

In order to investigate if the interactions between NPs and Igs correlate with the surface charge distribution of Igs, surface charge mapping of IgG and the F$_c$ fragments of IgA and IgM were created. The resulting surface charge distribution maps are depicted in Figure 3.1.5.
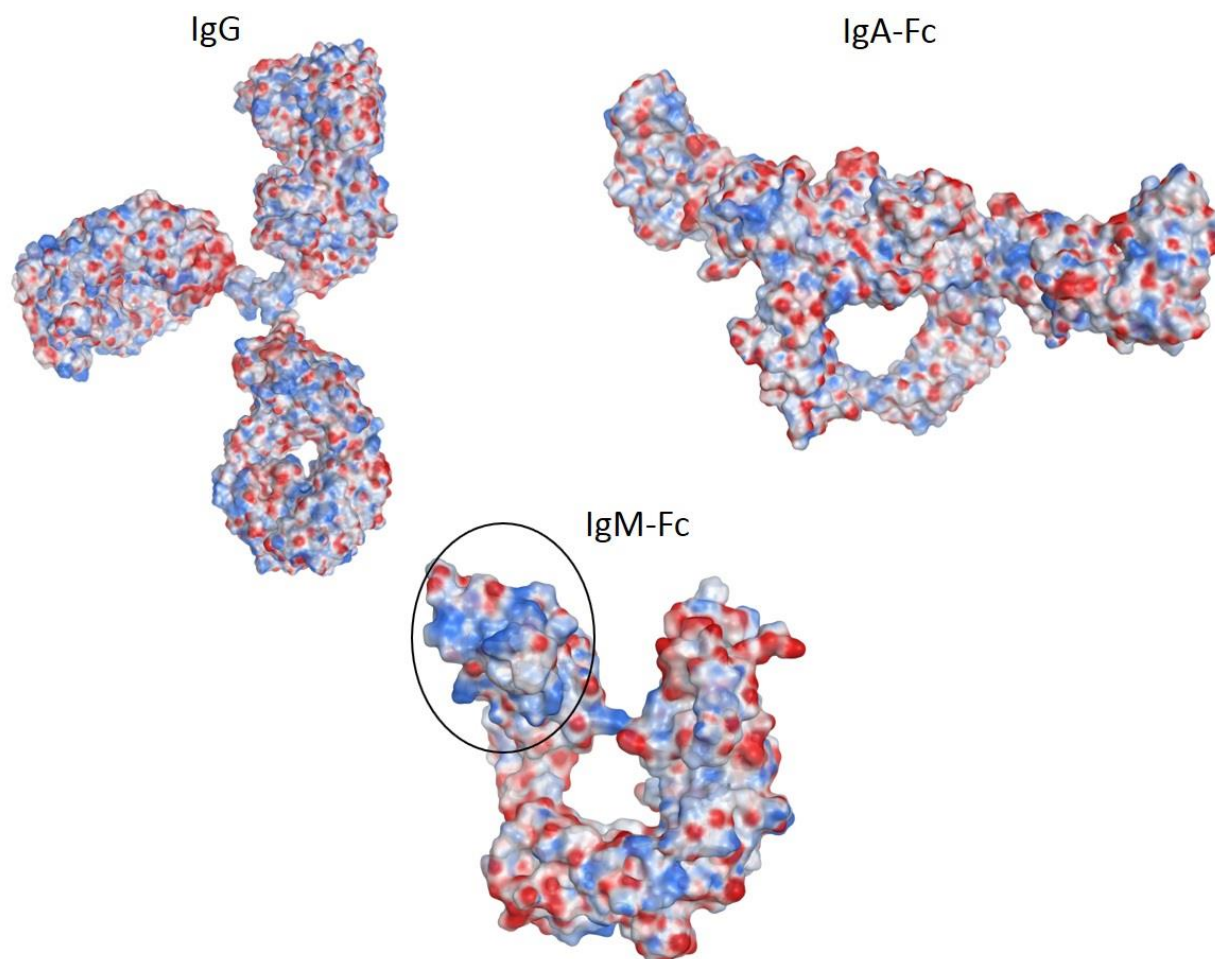
Figure 3.1.5: Surface charge distribution maps of IgG, IgA-F_c and IgM-F_c. Red areas (●) in the graphics represent negatively charged patches, while blue areas (●) represent positively charged patches and white areas (o) are of neutral charge. One pronounced charged patch is indicated by a black circle.

Compared to the other Igs, IgA-F_c appears to have a relatively homogeneous distribution of charges on the surface (smaller patches). This correlates well with the relatively weak interactions of IgA with the NPs observed *via* SDS-PAGE and ITC. The F_c part of IgM appears to have a more heterogeneous distribution of charges (larger patches) compared to IgA. This could be an explanation for the strong (electrostatic) interactions with the strongly (negatively) charged PS-NPs-COOH, as the negative carboxyl groups on the NPs' surface may interact with multiple positively charged patches of IgM (see black circle in Figure 3.1.5).

As another possibility, bridging processes induced by the Igs could occur, which would result in aggregation of the NPs. Accordingly, the stability of the NP-Ig complexes was analyzed *via* DLS (see Figure 3.1.6) using a method by Rausch *et al.*[96] (see chapter 2.4.5) with assistance regarding data analysis from Christine Rosenauer (MPI-P). In brief, the autocorrelation function of all three antibodies and all three NPs are determined individually and in all NP-Ig-combinations. If the sum of the autocorrelation functions of both components, with respect to the individual contribution, is sufficient to fit the data of the mixture in a so-called "forced fit", both components coexist and no aggregation processes occur. However, this forced-fit is not capable of describing the data of the mixture in the case of aggregation events. Then an additional term describing the diffusion behavior of the aggregate species is introduced.
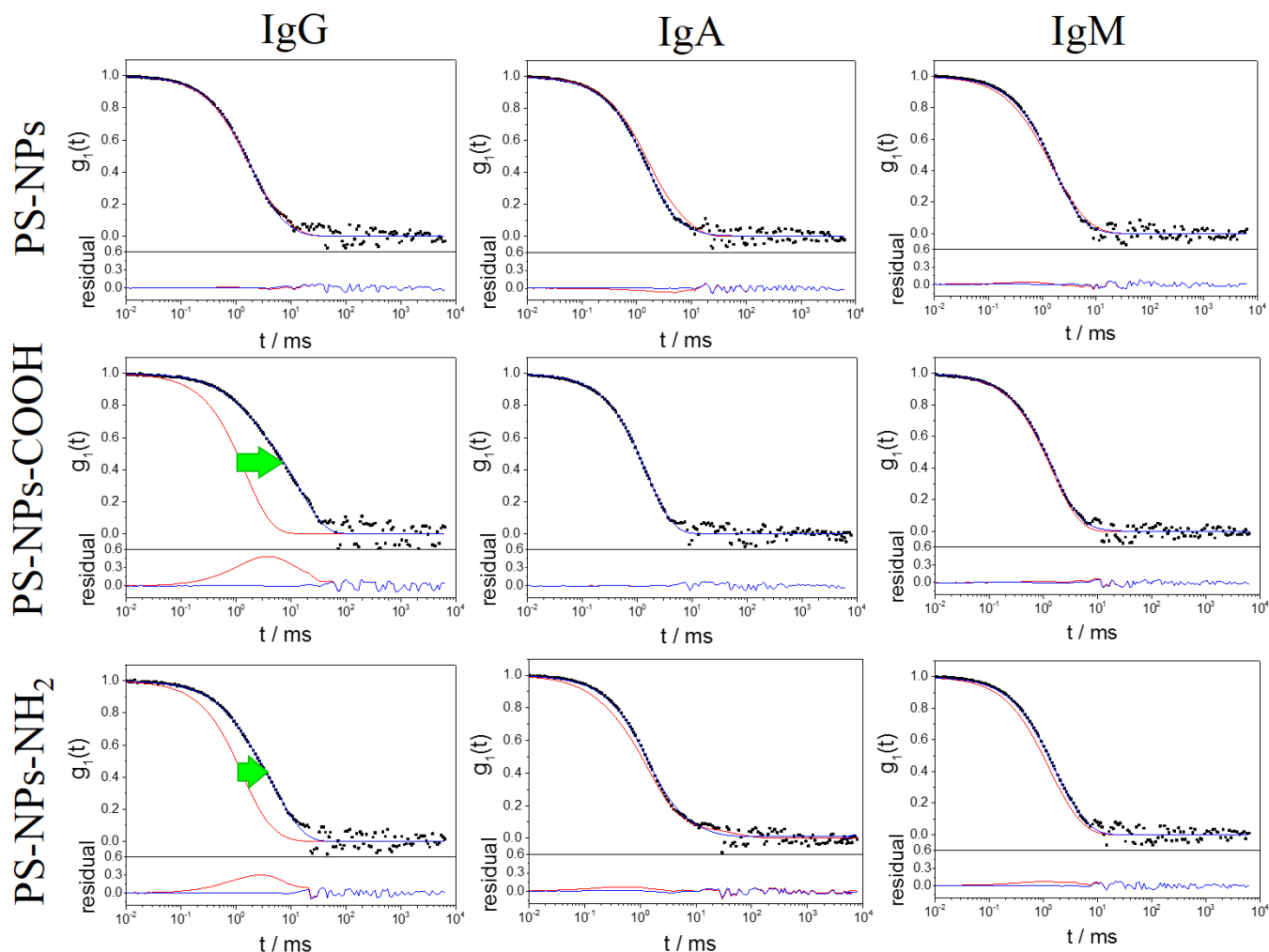
Figure 3.1.6: DLS measurements of the different PS-NPs with IgG, IgA and IgM. In each case the upper graphs: Autocorrelation functions $g_1(t)$ (black circles ●) of PS-NPs, PS-NPs-COOH and PS-NPs-NH$_2$ mixed with IgG, IgA or IgM respectively at $\theta = 60°$. The red line (–) represents the forced fit composed of the sum of the individual components (NPs + Igs) whereas the blue line(–) represents the fit with an additional aggregation term. Green arrows (→) indicate cases of severe aggregation as observed in the difference between fits with or without additional aggregation term. Lower graphs: Corresponding residuals resulting from the difference between the data and the two fits. (scattering angle $\theta = 60°$, temperature $T = 25\ °C$).

Following Figure 3.1.6, larger aggregates in high concentration form in complexes between IgG and PS-NPs-COOH or PS-NPs-NH$_2$ respectively. All other combinations showed little amount of aggregates, which appeared to be not significant in terms of their absolute concentration. This is in accordance with the observation *via* SDS-PAGE and ITC, that IgG interacts the strongest with the NPs, while the more electrostatic interactions with the functionalized NPs result in aggregation processes. Interestingly, no strong aggregation is observed in a mixture of PS-NPs-COOH and IgM for which strong exothermic interactions have been observed prior. It implies that this strong enthalpic interaction is not the result of bridging processes and more likely due to electrostatic interactions between multiple (positively charged) residues of IgM with the negatively charged carboxyl groups of PS-NPs-COOH. This further highlights the influence of NPs' surface charge on the interactions with Igs.

Following the influence Igs have on the colloidal stability of NPs, the subsequent question is if NPs influence the stability of Igs in return. In a next step, the question if Igs appear in the (protein) corona in their native form or denature on the surface of NPs was investigated. Therefore, the stability of Igs in contact with the unfunctionalized PS-NPs was investigated *via* nanoDSF as an initial experiment, as these NPs showed the weakest interaction with Igs in all experiments before and are therefore most likely to show native proteins. Solutions of the native proteins served as positive controls, whereas pure PS-NPs and proteins, which were denatured by thermal treatment in a solution of SDS before the experiment, served as negative controls (see Figure 3.1.7).
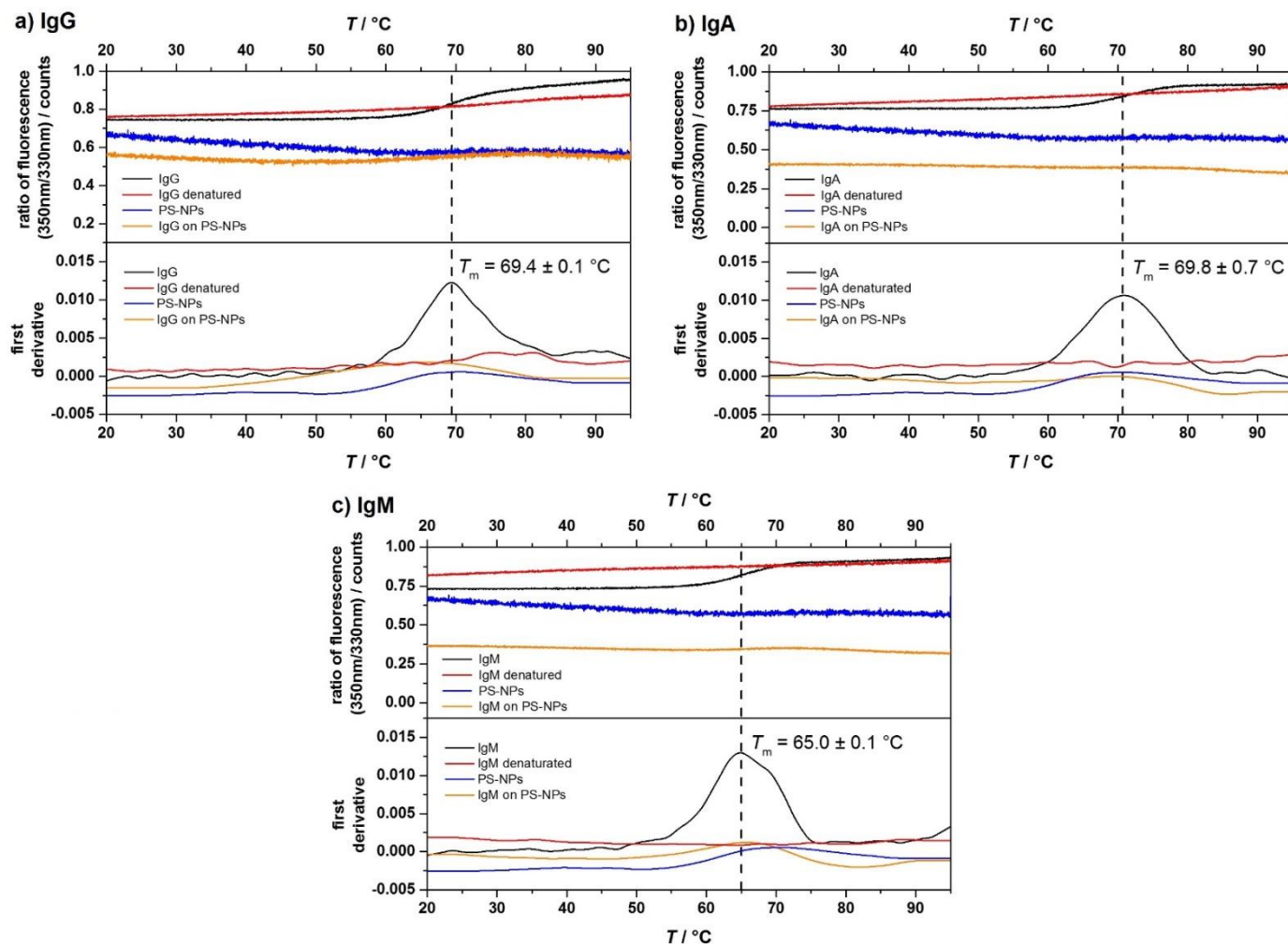
Figure 3.1.7: Differential scanning fluorimetry (nanoDSF) of Igs on PS-NPs. a) IgG, b) IgA and c) IgM showing the protein unfolding (during heating up): 350 nm / 330 nm ratio of fluorescence of Igs (top) together with the first derivative (bottom). Depicted are measurements of a $1\,\mathrm{g\,L^{-1}}$ solution of the respective Ig in its native form (black line —), Ig denatured by thermal treatment in $0.25\,\mathrm{g\,L^{-1}}$ SDS solution (red line —), PS-NPs as negative control (blue line —) and Ig on surface of NPs after three washing steps (orange line —).
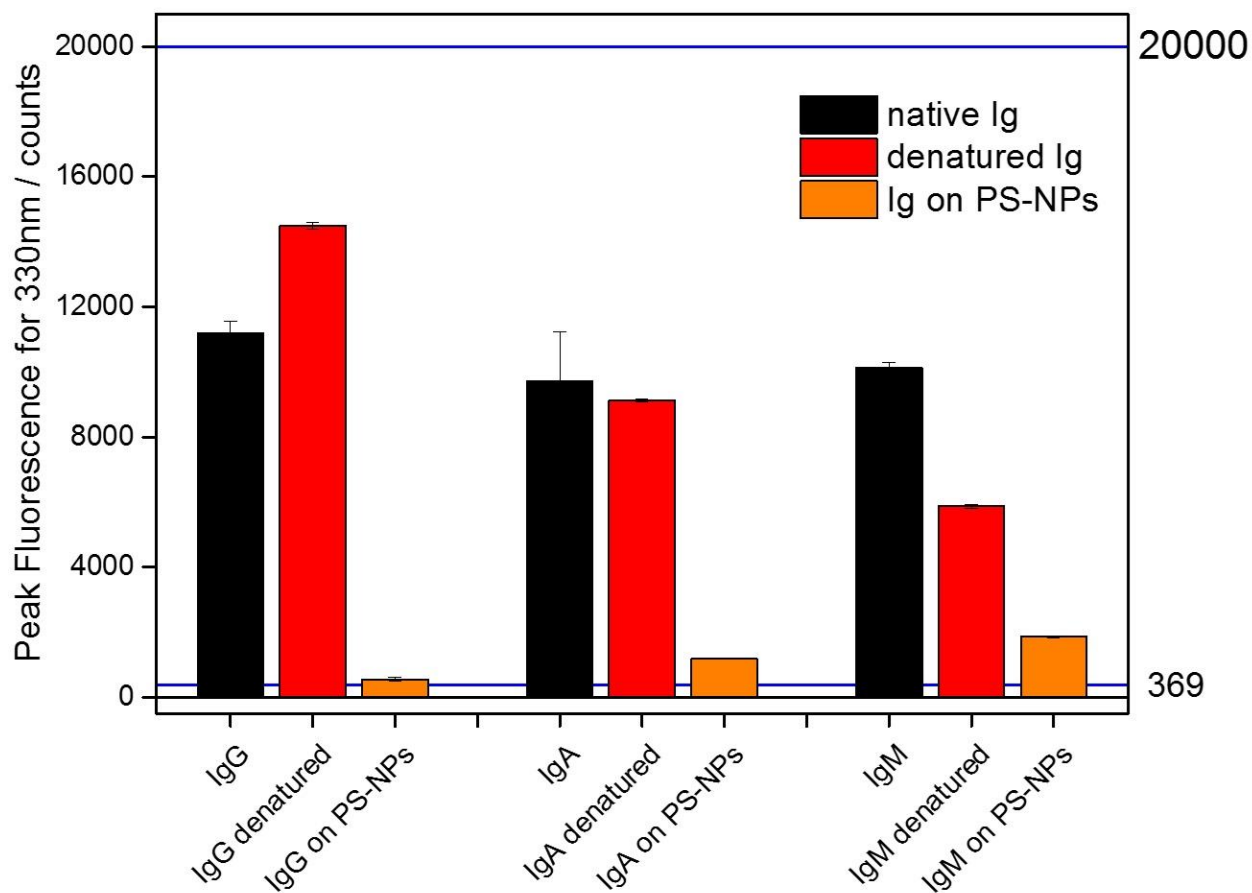
Figure 3.1.8: Peak fluorescence for 330 nm as observed in differential scanning fluorimetry (nanoDSF) of Igs (native and denatured) and Igs on PS-NPs. Depicted are measurements of a 1 g L^{-1} solution of the respective Ig in its native form (black column ■), Ig denatured by thermal treatment in 0.25 g L^{-1} SDS solution (red column ■), and Ig on the surface of PS-NPs after three washing steps (orange column ■). Blue horizontal lines at 369 and 20,000 counts indicate the minimum and maximum peak fluorescence for ensured measurement of protein denaturation. The maximal value for the peak fluorescence of 20,000 counts is a limitation of the instrument, the minimal value for the peak fluorescence is the background fluorescence of the used PS-NPs.

Following Figure 3.1.7, for all native Igs a melting point of around 65 to 70 °C is observed. This transition is completely lost for Igs adsorbed on PS-NPs and is very similar to the reference samples (negative controls) of Igs pre-denatured by treatment in SDS-solution at high temperatures or PS-NPs without proteins present respectively. To verify that enough protein was present in all

samples and that the lack of a melting transition was not due to the protein amount, the peak fluorescence was investigated before each measurement (see Figure 3.1.8). From the peak fluorescence of each sample, it is seen that the fluorescence of each sample containing Igs was between the minimum and maximum fluorescence detection level of the device for a precise measurement of the melting transition. Therefore, it is confirmed, that Igs are present on top of PS-NPs in a denatured form, as no thermal denaturation takes place during the nanoDSF experiments. These conformal changes of Igs on NPs could induce reactions of the immune system as a result. Therefore, interactions between nanocarriers and immunoglobulins should be minimized. This highlights the importance of nanocarriers' design in order to prevent unfavorable denaturation and adsorption processes of immunoglobulins on nanoparticle surfaces.

3.1.3   Conclusion

In conclusion, the influence of different immunoglobulins in the protein corona of differently charged polystyrene nanoparticles was investigated. While all Igs are present on the nanoparticles' surface, Igs influence the properties of nanoparticles upon interaction and *vice versa*. The net charge of nanoparticles was influenced by adsorption of Igs and in the case of interactions between IgG and functionalized nanoparticles, aggregation processes were induced. This was especially the case for interactions between IgG and nanoparticles with charged functional groups. Therefore, nanoparticles with neutral surface charge exhibited less unfavorable interaction with Igs. While IgA and IgM expressed mostly weak interactions with nanoparticles, IgG underwent stronger hydrophobic interactions with unfunctionalized polystyrene nanoparticles and more hydrophilic interactions with carboxylic or amino-functionalized nanoparticles. Only for the adsorption of IgM on carboxylic nanoparticles, strong electrostatic interactions are observed, which do not result in dominant bridging and aggregation processes. Adsorption of IgG on charged nanoparticles resulted in significant aggregation. All Igs appeared to be denatured on the surface of polystyrene nanoparticles with the possible consequence of (unwanted) reactions of the immune system.

3.2   The influence of varied immunoglobulin concentrations in blood plasma on the protein corona

After the interactions between nanocarriers and Igs have been characterized by investigating isolated proteins, the influence of these NP-Ig interactions on the protein corona in whole blood plasma was illuminated. This was studied by investigating the protein corona of different nanocarriers formed in blood plasma of averaged immunoglobulin concentrations and comparing it to the protein corona of the same nanocarriers that formed in blood plasma of varied immunoglobulin concentrations. First, the influence of an increased level of IgG in blood plasma on the protein corona was studied. Next, IgA- and IgM-enriched plasma were investigated. Additionally, the more uncommon case of an immunodeficiency regarding IgG was studied.

3.2.1 Prevention of dominant IgG adsorption on nanocarriers in IgG-enriched blood plasma by clusterin precoating

The work described in chapter 3.2.1 is based on the paper published in the journal *Advanced Science*, volume 6, issue10, 2019, 1802199. The work described in chapter 3.2.1 is licensed under the Creative Commons Attribution 4.0 International License. To view a copy of this license, visit http://creativecommons.org/licenses/by/4.0/ or send a letter to Creative Commons, PO Box 1866, Mountain View, CA 94042, USA.

In this chapter, the adsorption of proteins on different nanocarriers in IgG-enriched plasma and the resulting consequences on the nanocarriers' interactions with different cells were investigated. Precoating of nanocarriers with the protein clusterin, which has been purchased as native proteinisolated from human plasma, was studies as a method to reduce the influence of elevated IgG concentrations in blood plasma on the protein corona and biological behavior of nanocarriers. LC-MS experiments were performed by Dr. Johanna Simon (MPI-P), the cellular uptake of nanocarriers by different cell lines was investigated by Jorge Pereira (MPI-P).

3.2.1.1 Overview

In investigations of the protein corona, pooled blood plasma or blood serum from multiple healthy donors are usually used as biological medium to characterize the interactions of nanocarriers and blood proteins. To complicate the situation, it has been shown that different plasma sources[15,16] or anticoagulants[17] significantly change the corona formation process influencing the biological behavior. Consequently, pooled blood from healthy donors does not necessarily reflect individual concentration fluctuations of blood constituents, especially in patients with a disease.

The blood proteome composition of an individual can vary depending on environmental conditions, nutrition, and constitution. Specifically, immunoglobulins such as immunoglobulin G (IgG) are highly influenced by the personal state of health and an alteration of IgG levels occurs in the process of many diseases. The average immunoglobulin concentration in adults is approximately $16 \, g \, L^{-1}$, which is equivalent to about 20% of the total blood proteome with IgG representing the major immunoglobulin class at a concentration of approximately $12 \, g \, L^{-1}$.[27] High IgG concentrations in the human blood are an uncommon finding and can be caused by infections, autoimmunity, inflammation, or malignancy.[18] IgG blood levels can be increased during immune system activation; by a factor of 2 for autoimmune hepatitis[99], by a factor of 3 for influenza A virus infections[100] and even more drastically by a factor of 4 or higher for multiple myeloma.[101]

As a major protein of the human blood proteome, IgG can also be found in the protein corona of nanocarriers.[7] In literature, IgG is described as an opsonin, meaning that when present in the corona it promotes internalization of nanocarriers into phagocyting cells.[97] Thus, IgG reduces the blood circulation time of nanocarriers, so that other proteins are needed in the corona to counteract this effect.

In this regard, the importance of an enrichment of clusterin (also called apolipoprotein J) in the protein corona of PEGylated nanocarriers was recently discovered. The presence of clusterin resulted in a significant reduction of unspecific cell uptake *in vitro*, which is termed as the "stealth effect".[10-12] Governing of the stealth effect by active engineering of the protein corona can be achieved *via* two possibilities: Firstly, any nanocarrier can be modified by tailored surfactants

forcing the adsorption of clusterin [8] or, secondly, the nanocarriers can directly be pre-coated with clusterin by adsorption.[10] In both cases, unspecific cellular interactions were reduced significantly after exposure to plasma. However, the influence of varying immunoglobulin levels on the effectiveness of the stealth effect has not been investigated yet. As it has been reported that IgG in the protein corona can in extreme cases even lead to pronounced aggregation of the nanocarriers,[102] the presence of IgG should be avoided independent of the blood IgG concentration. Therefore, the influence of elevated IgG levels on the protein adsorption on nanocarriers that feature an enrichment of stealth proteins in "normal" plasma was investigated.

In this study, the protein corona of different nanocarriers (non-covalently PEGylated polystyrene nanoparticles (PS-NPs) and hydroxyethyl starch nanocapsules (HES-NCs)) in pooled "normal" plasma and in plasma exhibiting a 2-fold concentration of IgG were compared. Since the IgG concentration significantly changed the composition of the protein corona, also the cellular uptake was investigated in cell lines with varying presence of IgG binding receptors: murine macrophages (RAW 264,7) and human macrophages (THP-1) which express F_c-receptors, and HeLa cells which lack these receptors. The contribution of IgG receptor binding to cellular internalization was verified using F_c blocking experiments. Subsequently, the effect of pre-coating the nanocarriers with clusterin was determined concerning corona formation as well as cellular uptake, revealing that a stealth effect could indeed be restored in the presence of high IgG concentrations in plasma.

3.2.1.2   Results and Discussion

In this study, interactions of different nanocarriers with human plasma of varying IgG concentration were investigated. For this, pooled human blood plasma with averaged protein levels was obtained from healthy donors (subsequently called "normal plasma"). Furthermore, this normal plasma was modified by addition of commercially available IgG, yielding an artificially "IgG-enriched plasma" of doubled IgG concentration, which represents a physiologically relevant concentration. For ensuring conditions close to *in vivo* situations, IgG extracted from human blood was used for IgG enrichment. Corona formation around nanocarriers in the respective biological media and cellular internalization were then analyzed subsequently. Additionally, nanocarriers

were pre-coated with the stealth protein clusterin before incubation with IgG-enriched plasma to evaluate the potential of negating any IgG effect. Figure 3.2.1 shows a schematic overview of the performed experiments.
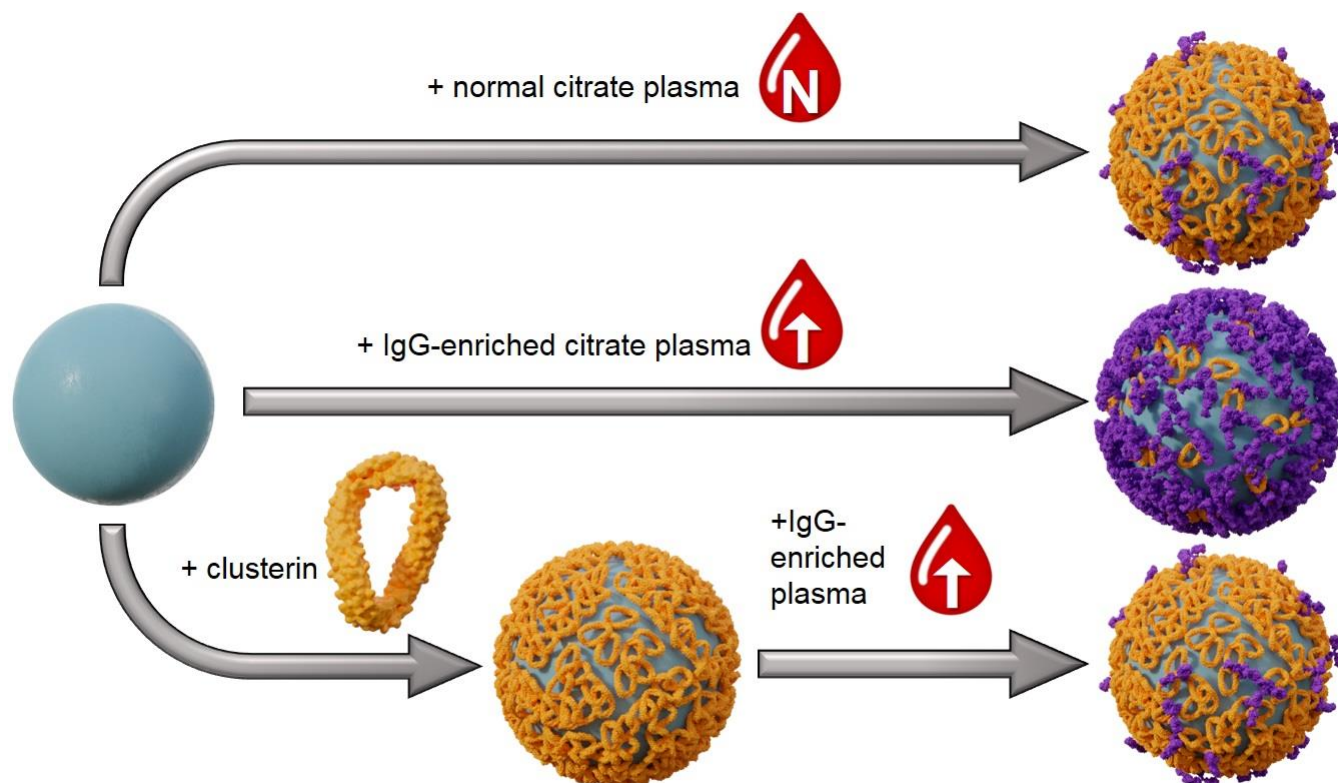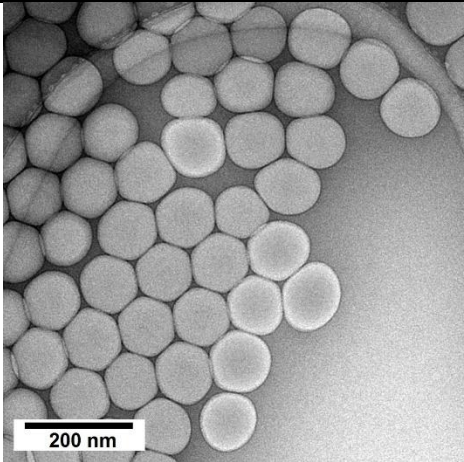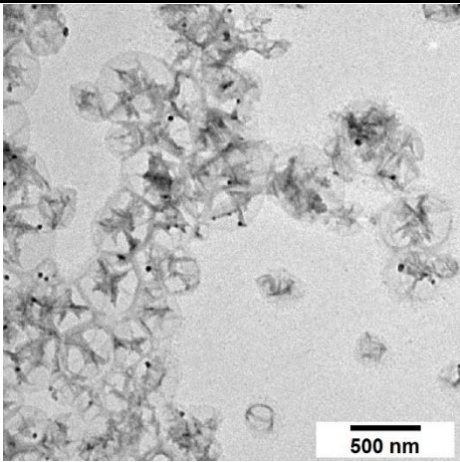
Figure 3.2.1: Overview of the experiment design. Nanocarriers were incubated with normal citrate plasma (top), artificially IgG-enriched citrate plasma (middle) and artificially IgG-enriched citrate plasma after pre–coating with clusterin (bottom). Published by Wiley-VCH.[52]

Non-covalently PEGylated polystyrene nanoparticles (PS-NPs) and hydroxyethyl starch nanocapsules (HES-NCs) were synthesized and thoroughly purified to yield minimum surfactant concentrations in the systems. Both systems are already well characterized regarding their protein corona and feature completely different surface properties, e.g. regarding their material hydrophilicity. [20,103] Table 3.2.1 shows TEM micrographs and physico-chemical characterization data for both nanocarrier systems. TEM micrographs were taken by Christoph Sieber (MPI-P). Besides the nanocarriers' material, the nanocarriers differ in morphology, size, stabilizing surfactant and dye in order to analyze the universality of the corona formation.

Table 3.2.1: Characterization of nanocarrier systems regarding morphology and physico-chemical properties. Published by Wiley-VCH.[52]

	PS-NPs	HES-NCs
TEM micrograph		
material	polystyrene (PS)	hydroxyethyl starch (HES)
surfactant	Lutensol AT50 (PEG-analogue)	sodium dodecyl sulfate (SDS)
R_h / nm	51 ± 5	112 ± 11
zeta potential ζ / mV	$- 8 \pm 1$	$- 8 \pm 1$
dye ($\lambda_{Ex.}$/ $\lambda_{Em.}$)	BODIPY (523 nm/ 536 nm)	Sulforhodamin 101 (586 nm/ 605 nm)

Before investigating the interaction of the nanocarriers with the respective biological media, the used plasma samples were analyzed regarding their protein composition. Therefore, the proteome of normal plasma and IgG-enriched plasma was determined *via* LC-MS. In Figure 3.2.2a, a heatmap indicating the relative amount of the most abundant proteins is depicted. Figure 3.2.2b shows the relative amount of different protein classes (such as immunoglobulins or complement system proteins in general) in the plasma samples.

a)

	normal plasma	IgG-enriched plasma
Alpha-1-acid glycoprotein 1	0.5%	0.3%
Alpha-1-antitrypsin	1.3%	0.7%
Alpha-2-macroglobulin	1.0%	0.6%
Apolipoprotein A-I	0.5%	0.5%
Apolipoprotein B-100	1.2%	0.5%
Clusterin	0.5%	0.3%
Complement C3	0.5%	0.4%
Fibrinogen alpha chain	0.7%	0.5%
Fibrinogen beta chain	1.0%	0.6%
Fibrinogen gamma chain	1.4%	0.8%
Haptoglobin	1.9%	1.1%
Hemopexin	1.4%	0.7%
Ig alpha-1 chain C region	1.8%	1.1%
Ig gamma-1 chain C region	8.7%	19.1%
Ig gamma-2 chain C region	1.6%	4.5%
Ig gamma-3 chain C region	0.7%	1.2%
Ig gamma-4 chain C region	0.4%	0.7%
Ig kappa chain C region	8.8%	20.1%
Ig lambda-2 chain C regions	2.6%	5.4%
Ig mu chain C region	0.7%	0.4%
Immunoglobulin heavy variable 3-7	0.4%	0.6%
Immunoglobulin lambda-like polypeptide 5	1.2%	2.5%
Serotransferrin	2.3%	1.6%
Serum albumin	47.0%	25.6%

b)

Figure 3.2.2: Protein composition of normal and IgG-enriched plasma analyzed *via* LC-MS. a) Heatmap indicating the most abundant proteins in the respective plasma. Only proteins, which constitute at least 0.5% of the total protein composition in one of the plasma samples with at least 2 unique peptides are shown. b) Bar diagram indicating the relative amount of different protein classes. Published by Wiley-VCH.[52]

As anticipated, it can be seen that the relative protein composition of normal and IgG-enriched plasma was different regarding individual proteins and protein classes. The relative concentration of IgG fractions was roughly doubled in the IgG-enriched plasma (e.g. 19.1% IgG-1 chain vs. 8.7% in normal plasma). Consequently, the total fraction of immunoglobulins was increased to approximately 60% in IgG-enriched plasma (vs. approximately 30% in normal plasma). To verify, whether the IgG was still in its native form and no denaturation had occurred,

the melting point was measured with differential scanning fluorimetry (nanoDSF), which yielded a melting point of $T_m = 69.4 \pm 0.1\,°C$ (see Figure 3.2.3). This is in good agreement with values reported in literature for whole IgG isotopes,[104] while two transitions were reported for the IgG domains isolated by cleaving the connecting hinge region ($T_m = 61\,°C$ for the F_{ab} fragment and $T_m = 71\,°C$. for the F_c fragment).[105] Therefore, it can be concluded, that the herein used IgG protein was in its native form.
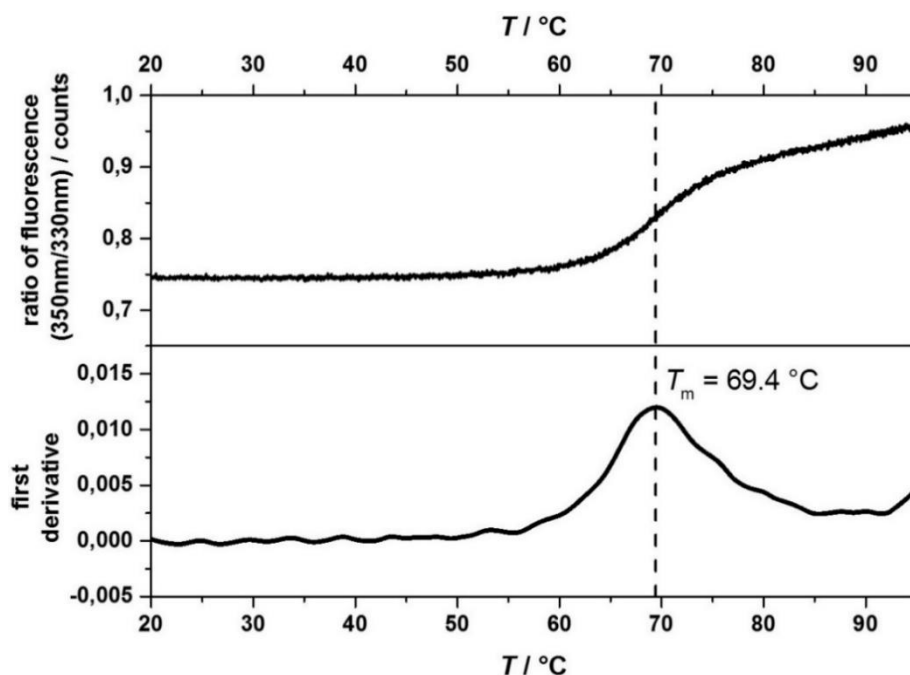
Figure 3.2.3: Differential scanning fluorimetry (DSF) of immunoglobulin G (IgG) showing the protein unfolding (heating): 350 nm / 330 nm ratio of fluorescence of IgG together with the first derivative. The melting point of native IgG (black line —) was observed at $T_m = 69.4\,°C$. Published by Wiley-VCH.[52]

Next, the protein corona formation in both plasma sources was evaluated. For this, PS-NPs and HES-NCs were incubated in both plasma sources (20%-diluted plasma to ensure solubility of additional IgG, see Materials and Methods section) and subsequently centrifuged and washed to remove excess free proteins. The protein composition of the protein coronas analyzed *via* LC-MS is shown in Figure 3.2.4a) for PS-NPs and Figure 3.2.4b) for HES-NCs. Additionally, the protein adsorption was verified by zeta potential measurements of each nanocarrier with and without protein corona obtained from the different plasmas (see Table 3.2.2).

a) PS-NPs

	normal plasma	IgG-enriched plasma	
Antithrombin-III	0.0%	0.0%	0%
Apolipoprotein A-I	19.4%	6.0%	
Apolipoprotein A-II	0.4%	0.8%	
Apolipoprotein A-IV	1.1%	1.4%	
Apolipoprotein B-100	0.1%	1.4%	
Apolipoprotein C-II	0.2%	0.6%	
Apolipoprotein C-III	3.5%	2.0%	10%
Apolipoprotein E	2.6%	0.8%	
Clusterin	38.8%	5.1%	
Coagulation factor V	0.2%	0.7%	
Complement C1q subcomponent subunit B	0.3%	1.6%	
Complement factor H-related protein 5	0.1%	0.8%	20%
E3 ubiquitin-protein ligase RNF135	0.2%	2.6%	
Fibrinogen alpha chain	0.1%	0.6%	
Gem-associated protein 8	4.5%	0.4%	
Haptoglobin	0.1%	1.8%	
Ig gamma-1 chain C region	0.5%	19.6%	
Ig gamma-2 chain C region	0.2%	5.8%	30%
Ig gamma-3 chain C region	0.1%	0.6%	
Ig kappa chain C region	0.6%	18.5%	
Ig lambda-2 chain C regions	0.1%	1.6%	
Ig mu chain C region	0.1%	0.3%	
Immunoglobulin lambda-like polypeptide 5	0.2%	3.6%	
Keratin, type II cytoskeletal 1	0.2%	0.1%	40%
Mitochondrial in. membrane protease SU 2	1.3%	0.2%	
Phospholipid transfer protein	2.1%	0.6%	
Serum albumin	0.6%	2.2%	
Transthyretin	0.1%	0.7%	
Vitronectin	0.4%	0.6%	
Zinc finger protein basonuclin-2	3.0%	0.2%	50%

b) HES-NCs

	normal plasma	IgG-enriched plasma	
Alpha-1-antichymotrypsin	0.9%	0.3%	0%
Apolipoprotein A-I	2.8%	3.0%	
Apolipoprotein A-IV	1.5%	1.4%	
Apolipoprotein E	8.4%	1.4%	
Clusterin	43.2%	3.6%	
Complement C3	0.9%	2.6%	10%
Fibrinogen alpha chain	0.7%	0.6%	
Fibrinogen beta chain	1.6%	0.7%	
Fibrinogen gamma chain	1.3%	1.1%	
Haptoglobin	0.4%	1.5%	
Ig alpha-1 chain C region	0.9%	0.5%	20%
Ig gamma-1 chain C region	1.5%	22.2%	
Ig gamma-2 chain C region	1.6%	6.0%	
Ig gamma-3 chain C region	0.3%	0.9%	
Ig gamma-4 chain C region	0.3%	2.0%	
Ig kappa chain C region	3.4%	20.7%	30%
Ig lambda-2 chain C regions	0.4%	1.7%	
Ig mu chain C region	0.9%	0.5%	
Ig mu heavy chain disease protein	0.6%	0.3%	
Immunoglobulin kappa variable 2D-29	1.6%	2.1%	
Immunoglobulin kappa variable 3-20	0.2%	0.7%	40%
Immunoglobulin lambda-like polypeptide 5	0.9%	4.0%	
Keratin, type I cuticular Ha5	0.2%	1.0%	
Keratin, type I cytoskeletal 18	0.5%	0.7%	
RING finger protein 39	2.0%	0.1%	
Serum albumin	6.7%	1.5%	
Vitronectin	1.8%	1.0%	50%

Figure 3.2.4: Composition of protein corona after incubation with normal and IgG-enriched plasma analyzed *via* LC-MS for a) PS-NPs and b) HES-NCs. Only those proteins, which constitute at least 0.5% of the protein corona on one of the nanocarriers with at least 2 unique peptides are shown. Published by Wiley-VCH.[52]

Table 3.2.2: Zeta potential of nanocarriers before and after incubation with different citrate plasmas measured in a 1 mM KCl solution. Published by Wiley-VCH.[52]

	zeta potential of PS-NPs / mV	zeta potential of HES-NCs / mV
nanocarriers alone	- 8 ± 1	- 8 ± 1
nanocarriers + plasma (normal)	- 25 ± 1	- 19 ± 1
nanocarriers + plasma (IgG-enriched)	- 15 ± 1	- 13 ± 1
nanocarriers + clusterin + plasma (IgG-enriched)	- 27 ± 2	- 23 ± 2

Following Figure 3.2.4, the composition of the protein corona of both nanocarriers differs a lot for the different plasmas. For the incubation in normal plasma, clusterin was the main protein corona component, followed by apolipoprotein A-I (PS-NPs) and apolipoprotein E (HES-NCs), while IgG and its fractions were not a major component of both nanocarriers' protein corona. This agrees well with the corona composition for both systems already reported before.[9,102] However, after incubation in IgG-enriched plasma the relative amount of IgG chains in the protein coronas was significantly increased (e.g. 19.6% IgG-1 chain vs. 0.5% for PS-NPs). For both nanocarrier systems, the overall protein corona consists of almost 50% immunoglobulins after incubation in IgG-enriched plasma. Clusterin and other proteins enriched before were still present, although in much lower amounts. Strikingly, the enrichment of IgG components in the protein corona was far greater than the enrichment of IgG in the plasma sample itself (enrichment by a factor of around 40 in the corona vs. factor of around 2 in the plasma sample). This suggests that the interactions between nanocarriers and plasma proteins strongly depend on the individual protein concentration (in this case IgG) in the biological medium and are not purely a result of the individual protein binding affinities. While clusterin levels in blood average around only 0.1 g L^{-1},[14] elevated IgG levels might lead to suppression of clusterin interactions with the nanocarriers by simply blocking its access to the surface due to the high concentration. This is in agreement with the commonly described "Vroman effect", which defines the first step of protein adsorption as a kinetically controlled process.[44,106] According to that effect, proteins with a high abundance and high mobility may adsorb first to a nanocarrier and after longer time be replaced by proteins with a lower abundance/mobility but higher binding affinity. In our case, the initial adsorption of IgG might block the nanocarrier surface from adsorbing clusterin, which has a higher binding affinity, but very low abundance especially in IgG-enriched plasma. Usually, the timescale of such kinetically driven changes in the protein adsorption occurs within one hour of incubation time.[68,107,108] However, for the system described here, this is apparently not the case, as the incubation time of experiments discussed in this study was one hour as well. This might be due to the high initial concentration of IgG so that further rearrangements were outside of the experimental timeframe.

Accordingly, the dominant IgG adsorption might be prevented by previous incubation of the nanocarriers with clusterin in order to allow a pre-coating of the nanocarrier surface with the desired stealth protein possessing a high binding affinity but low plasma concentration. Thus, the protein corona of both nanocarrier systems after pre-coating with clusterin and subsequent incubation in IgG-enriched plasma was analyzed by LC-MS and compared to the protein patterns shown in Figure 3.2.4. Moreover, the identified proteins were normalized by the total protein mass detected in the corona *via* a Pierce 660 nm quantification assay (see Figure 3.2.5) to determine whether immunoglobulins replaced the apolipoproteins or were adsorbed additionally (see Figure 3.2.6).
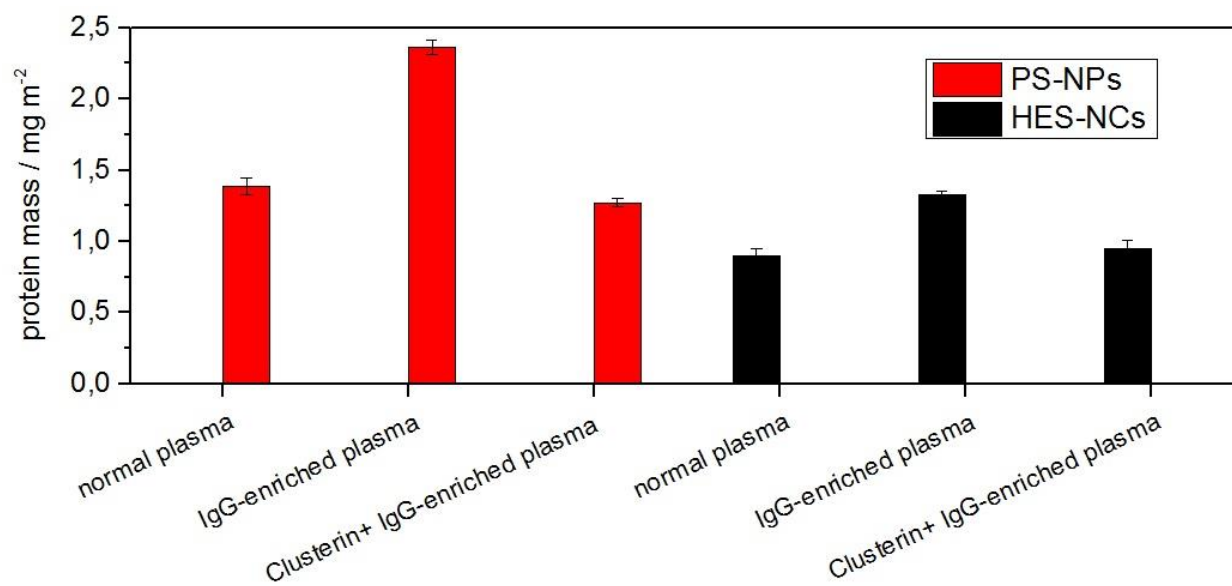
Figure 3.2.5: Protein mass on the surface of a) PS-NPs and b) HES-NCs after incubation with normal plasma, IgG-enriched plasma or IgG-enriched plasma after pre-incubation with clusterin detected by a Pierce 660 nm protein assay. Published by Wiley-VCH.[52]
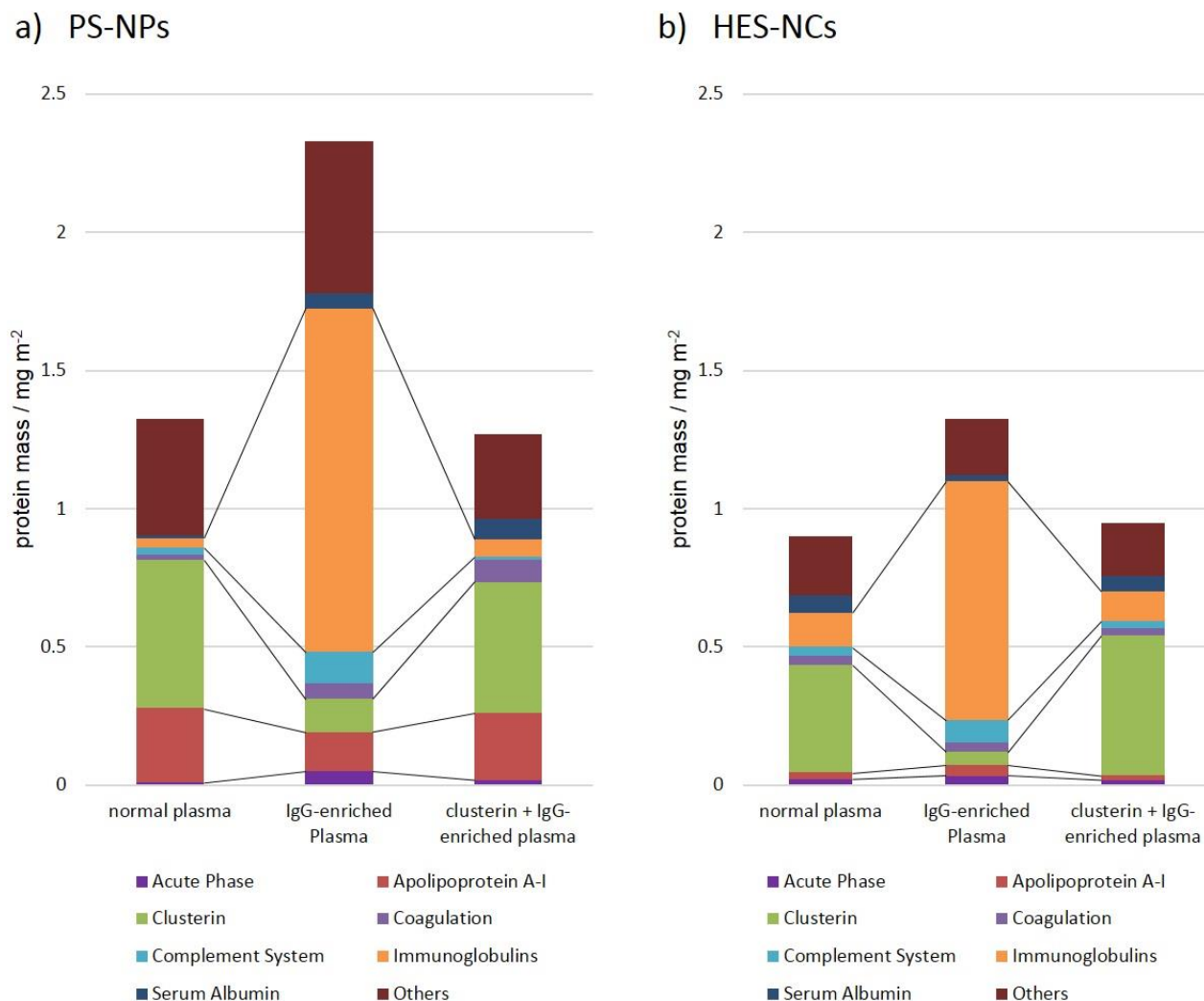
a) PS-NPs

b) HES-NCs

Figure 3.2.6: Composition of protein corona of a) PS-NPs and b) HES-NCs according to protein class after incubation with normal plasma, IgG-enriched plasma or IgG-enriched plasma after pre-incubation with clusterin analyzed *via* LC-MS normalized for protein amounts detected by a Pierce 660 nm protein assay. Published by Wiley-VCH.[52]

For both nanocarriers, pre-coating with clusterin and subsequent incubation with IgG-enriched plasma yielded a protein corona that was similar compared to the respective nanocarriers, which were incubated with normal plasma, both qualitatively and quantitatively for individual protein masses and total protein adsorption. This effect of dominant IgG adsorption and its prevention by clusterin-pre-coating were also observed in the analysis of the protein coronas of both nanocarriers in the different plasmas *via* SDS-PAGE (see Figure 3.2.7 to 3.2.9). Without the

pre-coating of nanocarriers with clusterin, the total mass of proteins adsorbed on the respective nanocarriers increased significantly after incubation with IgG-enriched plasma (see Figure 3.2.5). This resulted not only in the previously discussed relative enrichment of IgG fractions in the corona, but also a higher absolute mass of immunoglobulins and a lower absolute mass of apolipoproteins (clusterin and apo A-I) was found on the nanocarriers. Therefore, it can be concluded that a replacement of these apolipoproteins by IgG took place in IgG-enriched plasma, which could be prevented by pre-coating with clusterin. The LC-MS (Figure 3.2.6) and SDS-PAGE (Figure 3.2.7 to 3.2.9) results show near identical amounts of clusterin in the corona of both NPs incubated with normal plasma and IgG-enriched plasma after clusterin pretreatment. This raises the possibility that the corona is saturable with clusterin, and saturation is reached by a dose less than the externally added amount. Interestingly, the corona composition after clusterin-coating is very similar to the corona in normal plasma, which could be explained by the Vroman-effect as described above. The effect of IgG-enrichment in the protein corona post-incubation with IgG-enriched plasma is not only observed for the two nanocarrier systems discussed, but for a multitude of different nanocarriers (Table 3.2.3 and Figure 3.2.10 to 3.2.14) and further investigated in the following for both nanocarriers discussed so far.
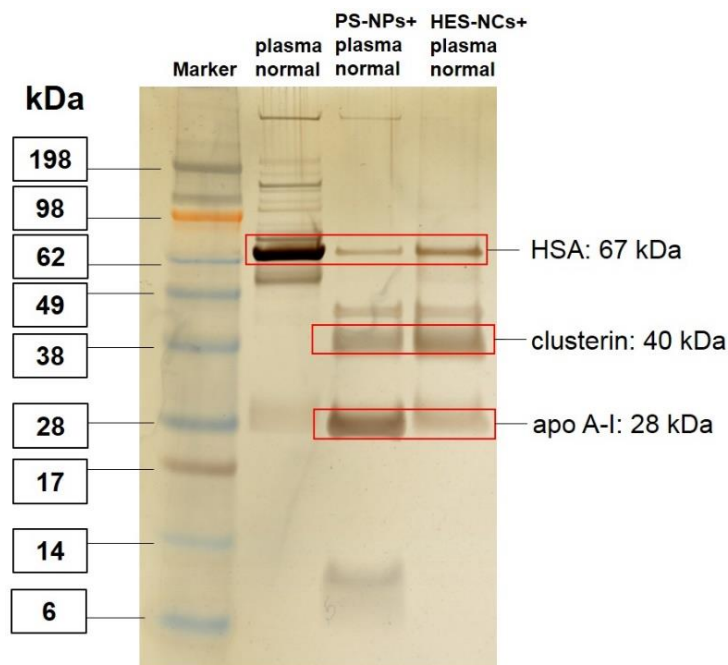
Figure 3.2.7: SDS-PAGE gel of the protein coronas of PS-NPs and HES-NCs incubated with normal plasma. Pure plasma is shown as a reference. For staining, a silver staining kit was used according to manufacturer's instruction. Published by Wiley-VCH.[52]

Figure 3.2.8: SDS-PAGE gel of the protein coronas of PS-NPs and HES-NCs incubated with IgG-enriched plasma. Pure IgG-enriched plasma is shown as a reference. For staining, a silver staining kit was used according to manufacturer's instruction. Published by Wiley-VCH.[52]
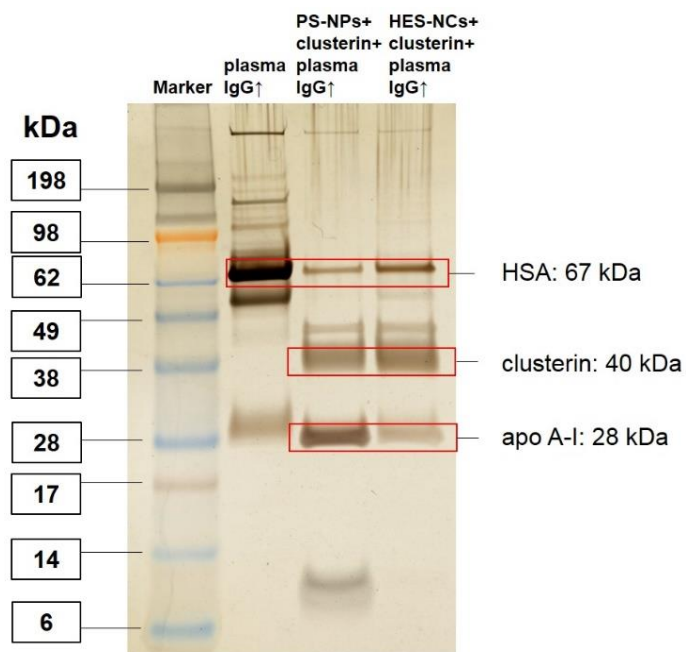
Figure 3.2.9: SDS-PAGE gel of the protein coronas of PS-NPs and HES-NCs incubated with IgG-enriched plasma after pre-incubation with clusterin. Pure IgG-enriched plasma is shown as a reference. For staining, a silver staining kit was used according to manufacturer's instruction. Published by Wiley-VCH.[52]

Table 3.2.3: Nanocarriers that were incubated with normal and IgG-enriched plasma respectively. Published by Wiley-VCH.[52]

abbreviation	material	surfactant	hydrodynamic radii *via* multi-angle-DLS / nm	zeta potential / mV
PS-NPs	polystyrene	Lutensol	52 ± 5	-10 ± 1
PS-NPs-COOH	polystyrene-COOH	Lutensol	57 ± 6	-29 ± 2
PS-NPs-NH$_2$	polystyrene-NH2	Lutensol	51 ± 5	2 ± 1
PS-NPs-SDS	polystyrene	SDS	53 ± 5	-50 ± 3
HES-NCs	hydroxyethyl starch	SDS	112 ± 11	-11 ± 1
SiO$_2$-NCs-CTAC	silica	CTMA-Cl	171 ± 17	-10 ± 1
SiO$_2$-NCs-LUT	silica	Lutensol	87 ± 9	-10 ± 1
OVA-NCs	ovalbumin	SDS	272 ± 27	-24 ± 1
OVA-NCs-PEG	ovalbumin - PEGylated	SDS	261 ± 26	-31 ± 1
PS-NPs-PMEP	polystyrene	poly(methyl ethylene phosphate)	52 ± 5	-48 ± 1
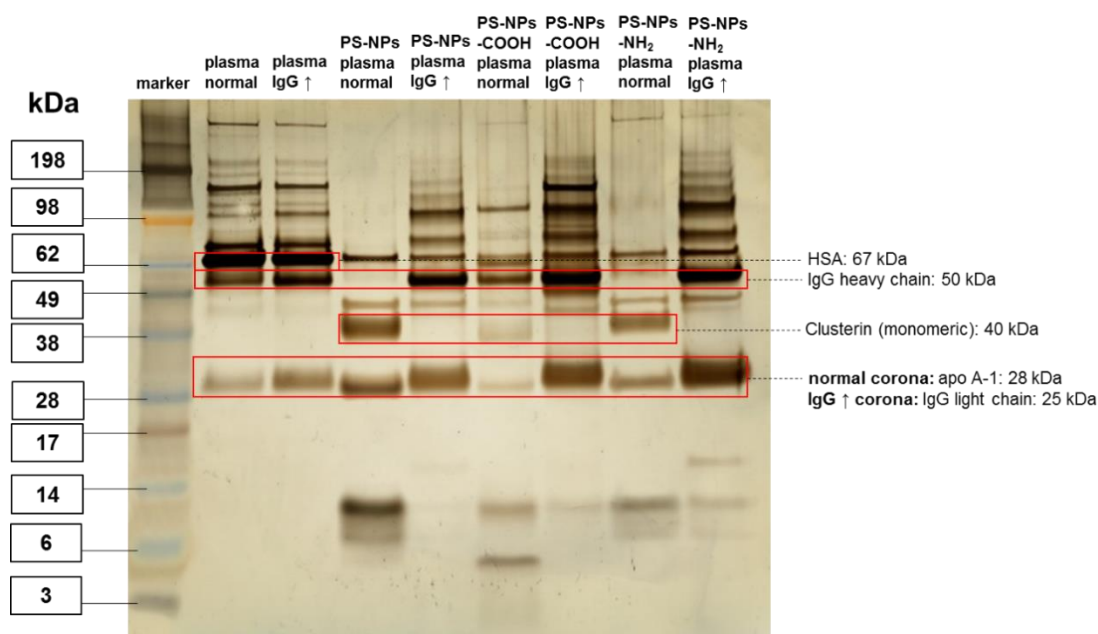
Figure 3.2.10: SDS-PAGE gel of the protein coronas of different NPs incubated with normal and IgG-enriched plasma. Pure normal and IgG-enriched plasma is shown as a reference. For staining, a silver staining kit was used according to manufacturer's instruction. Published by Wiley-VCH.[52]
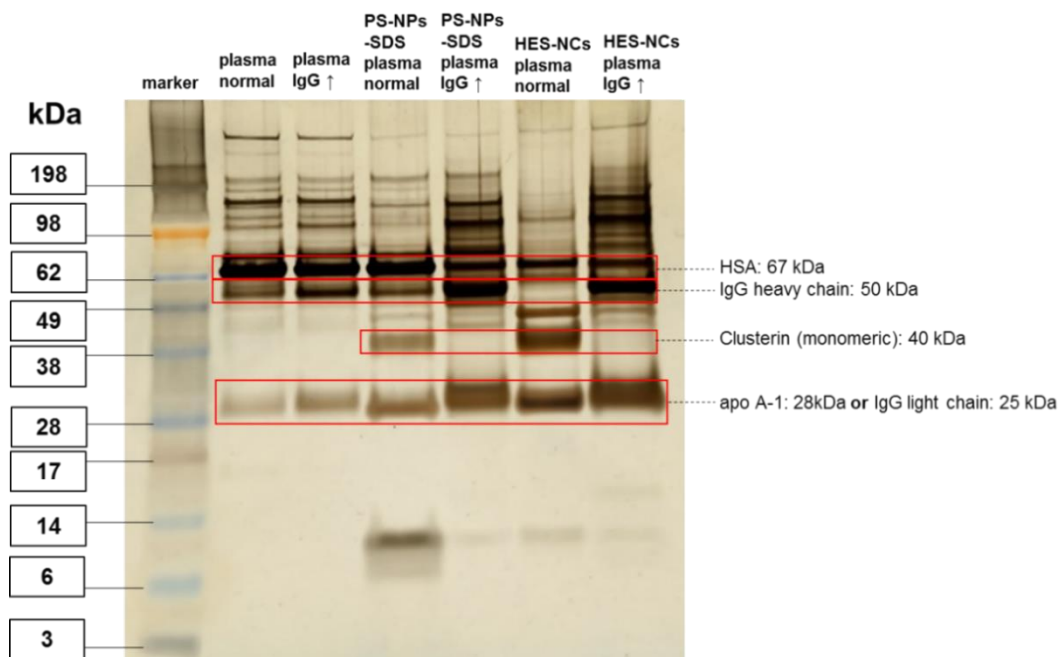
Figure 3.2.11: SDS-PAGE gel of the protein coronas of different nanocarriers incubated with normal and IgG-enriched plasma. Pure normal and IgG-enriched plasma is shown as a reference. For staining, a silver staining kit was used according to manufacturer's instruction. Published by Wiley-VCH.[52]
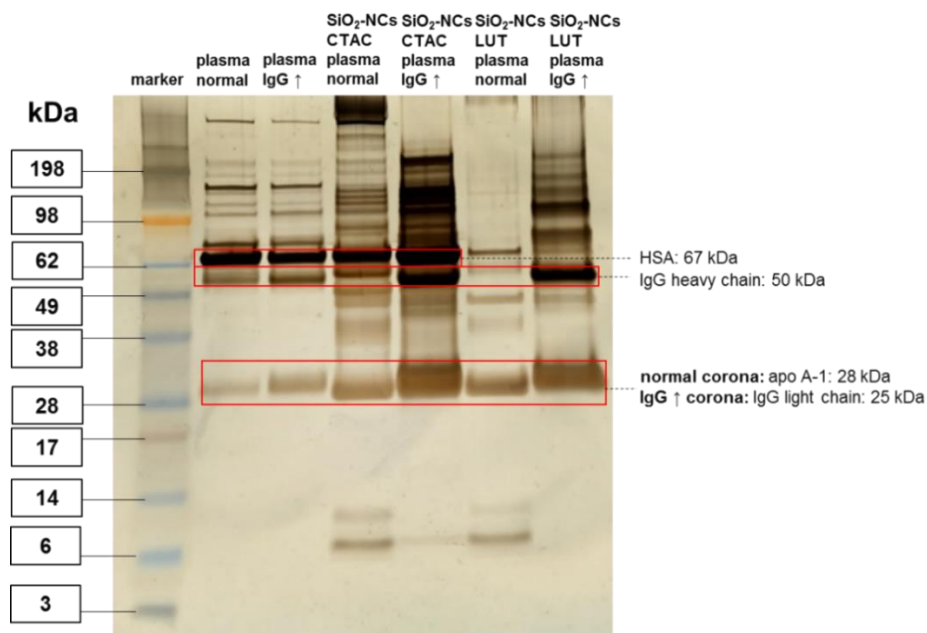
Figure 3.2.12: SDS-PAGE gel of the protein coronas of different NCs incubated with normal and IgG-enriched plasma. Pure normal and IgG-enriched plasma is shown as a reference. For staining, a silver staining kit was used according to manufacturer's instruction. Published by Wiley-VCH.[52]
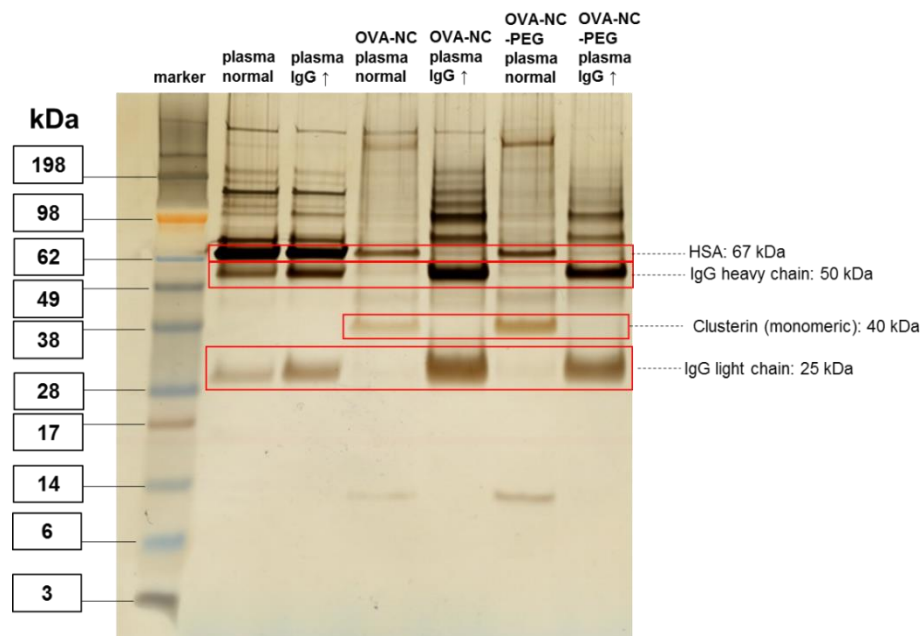
Figure 3.2.13: SDS-PAGE gel of the protein coronas of different NCs incubated with normal and IgG-enriched plasma. Pure normal and IgG-enriched plasma is shown as a reference. For staining, a silver staining kit was used according to manufacturer's instruction. Published by Wiley-VCH.[52]
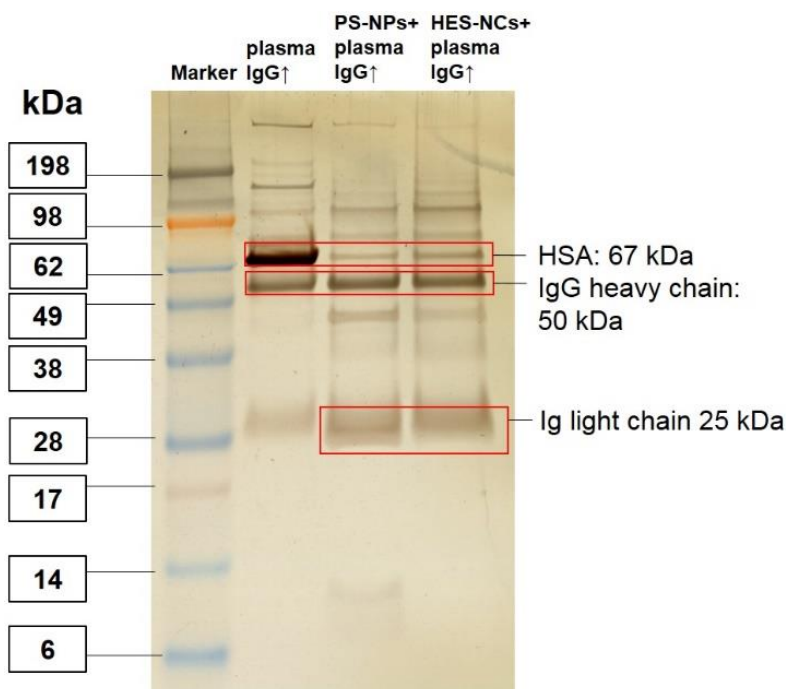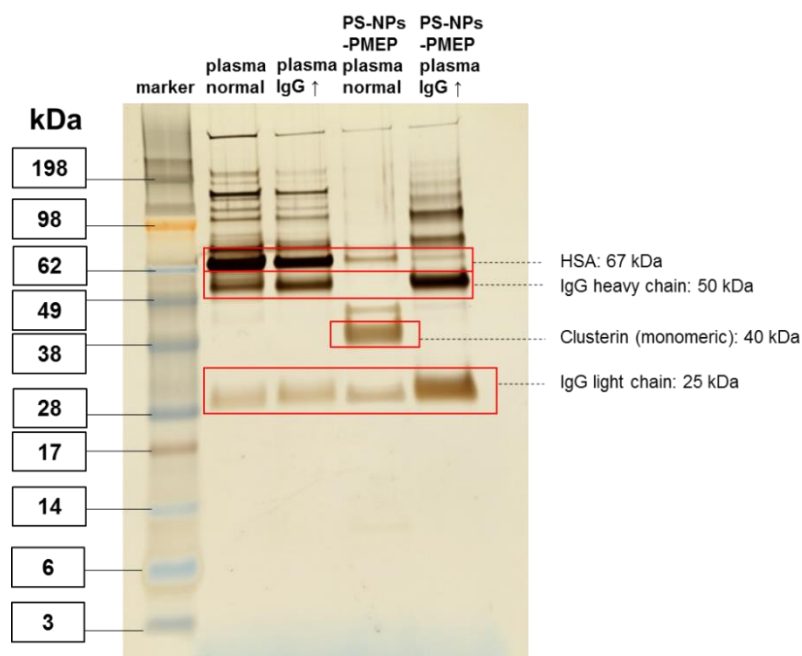

Figure 3.2.14: SDS-PAGE gel of the protein coronas of different NPs incubated with normal and IgG-enriched plasma. Pure normal and IgG-enriched plasma is shown as a reference. For staining, a silver staining kit was used according to manufacturer's instruction. Published by Wiley-VCH.[52]

Since the IgG level of the plasma had a large impact on the formation of the hard protein corona as observed *via* LC-MS, further information about the total interaction (including the soft corona) between nanocarriers and the different plasmas were of high interest. Therefore, calorimetric measurements of both nanocarriers were performed *via* isothermal titration calorimetry (ITC) to obtain information about the overall influence of the IgG on interaction thermodynamics. In each experiment, normal or IgG-enriched plasma was titrated into a suspension of the respective nanocarriers (with or without pre-coating with clusterin). Additionally, the heat of dilution of plasma (titration of plasma into buffer) was determined and subtracted from the initial measurement. The obtained corrected injection heats were fitted with an independent binding model. For this, the total molar concentration of plasma proteins was calculated based on the composition determined by LC-MS. Figure 3.2.15 shows the resulting adsorption isotherms and parameters of these ITC experiments.

a) PS-NPs

PS-NPs	plasma (normal)	plasma (IgG↑)	clusterin coated + plasma (IgG↑)
K_a / 10^6 M^{-1}	0.28 ± 0.04	1.74 ± 0.34	0.36 ± 0.06
ΔH / kJ mol^{-1}	-117 ± 3	-109 ± 10	-130 ± 10
ΔS / J mol^{-1} K^{-1}	-302 ± 13	-258 ± 35	-344 ± 36
ΔG / kJ mol^{-1}	-30.0 ± 0.3	-34.4 ± 0.5	-30.6 ± 0.4
n	309 ± 15	296 ± 14	366 ± 14

b) HES-NCs

HES-NCs	plasma (normal)	plasma (IgG↑)	clusterin coated + plasma (IgG↑)
K_a / 10^6 M^{-1}	0.39 ± 0.07	2.86 ± 0.72	0.58 ± 0.06
ΔH / kJ mol^{-1}	-99 ± 5	-44 ± 5	-54 ± 2
ΔS / J mol^{-1} K^{-1}	-237 ± 18	-31 ± 20	-76 ± 6
ΔG / kJ mol^{-1}	-30.8 ± 0.4	-29.0 ± 0.3	-31.8 ± 0.2
n	19800 ± 4400	21300 ± 1000	17600 ± 1300

Figure 3.2.15: Adsorption isotherms and parameters of plasma proteins titrated to a) PS-NPs and b) HES-NCs obtained from ITC experiments. The average molar concentration of plasma proteins was calculated by dividing the mass concentration of plasma proteins by the mean molar mass of all plasma proteins according to their relative contribution determined *via* LC-MS (see details in the SI). Isotherms were fitted according to an independent binding model (solid lines). Color code indicates relative deviation (white = no deviation, red = strong deviation) of adsorption parameters from the parameters obtained from titrations with normal plasma (second column of each table). Published by Wiley-VCH.[52]

Certainly, it has to be pointed out that all obtained adsorption parameters present an average over all involved proteins and processes so that the absolute values cannot be interpreted reliably. However, the relative values obtained for the different adsorption scenarios (1) normal plasma, 2) IgG-enriched plasma, 3) Clusterin pre-incubation + IgG-enriched plasma) can be compared to each other. According to Figure 3.2.15, it is clear that the adsorption parameters of plasma proteins in

normal and IgG-enriched plasma significantly deviate from each other for both systems. Significantly higher average association constants K_a were obtained for the titration of uncoated nanocarriers with IgG-enriched plasma (indicated by the color coding in the tables), meaning that overall the affinity to bind plasma proteins is higher. This correlates with the elevated level of IgG in the nanocarriers' corona as demonstrated *via* LC-MS and the fact that the overall amount/mass of adsorbed protein is higher in IgG-enriched plasma (compare Figure 3.2.6). When the nanocarriers were pre-coated with clusterin and subsequently titrated with IgG-enriched plasma, the observed average binding affinities were decreased again and similar to the parameters in normal plasma. From the other parameters such as enthalpy and entropy, in principle information about the driving force of the interactions can be concluded. ΔH and ΔS change similar to the binding affinity when changing the plasma source. This is expected because as the protein corona composition changes also the involved interaction mechanisms might differ (electrostatic interactions, hydrogen bonding etc.). When introducing the clusterin pre-coating, ΔH and ΔS again change in the titration with IgG-enriched plasma, but do not completely go back to the values obtained in normal plasma. This is especially the case for the HES-NCs and probably a result of the fact that HES is a more hydrophilic material compared to PS. Therefore, a larger contribution of more loosely bound corona proteins is expected, which would only be visible in the ITC experiments as no washing takes place.[9] While loosely bound proteins are mainly removed from the nanocarriers in the washing steps during corona preparation (as prepared for MS experiments), adsorption of all proteins are measured in ITC including proteins of lower affinity. Accordingly, from the ITC experiments it is concluded, that increasing the IgG level in plasma indeed also changes the thermodynamic parameters and, thus, the mechanism of interaction of the proteins overall.

As a significant effect of elevated IgG levels in plasma on the protein corona formation was observed, the influence of this altered protein corona on cellular uptake of different cell lines was investigated subsequently by Jorge Pereira (MPI-P). The aim of this was to figure out if nanocarriers with increased IgG concentration in their corona would exhibit an elevated endocytosis mediated by F_c receptors, which specifically bind the F_c region of antibodies. For this, both nanocarriers with the different protein coronas discussed before were incubated with macrophages that express F_c receptors (human macrophage cell line: THP-1 or mouse macrophage

cell line: RAW 264.7) and HeLa cells (human cancer cell line), which lack F_c receptors (see Figure 3.2.16).[109] No additional proteins were added to the cell culture medium. For reference, nanocarriers without protein corona were incubated with each cell line. Cellular uptake was verified *via* confocal laser scanning microscopy (cLSM, see Figure 3.2.16 and Figures A10 - A15 in the appendix). Cell viability was verified with Zombie Aqua viability kits (see Figure A16 in the appendix).
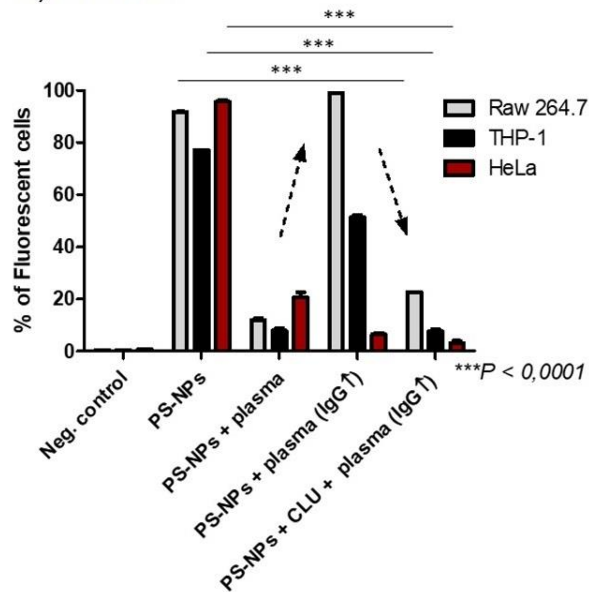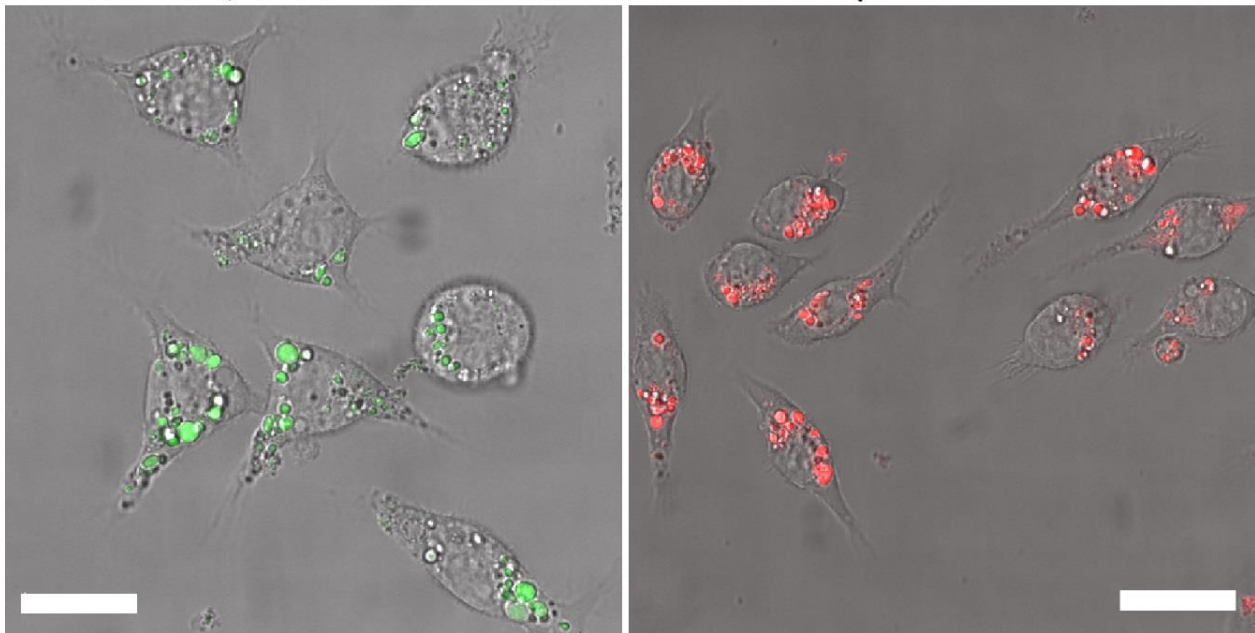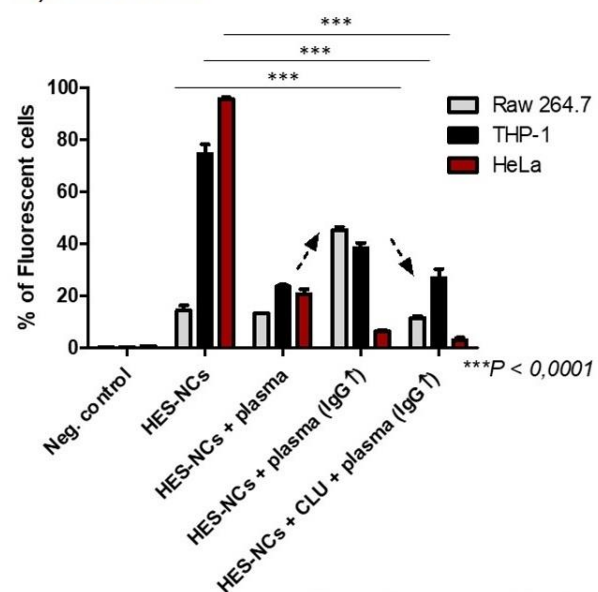
Figure 3.2.16: Top: Cellular uptake of a) PS-NPs and b) HES-NCs before and after incubation with normal plasma, IgG-enriched plasma and clusterin followed by IgG-enriched plasma. RAW 264,7 (murine macrophages), THP-1 (human macrophages) and HeLa cells (human cancer cells)

were used as cell lines. For the negative control, only cells in medium were measured without addition of sample. Values are mean values with standard deviation of three biological replicates. The ANOVA two-way test was used for statistical analysis yielding ***$p < 0.0001$ corresponding to the individual types of nanocarriers. Arrows indicate the increased cell uptake after incubation in IgG-enriched plasma and decreased uptake after preincubation with clusterin. Bottom: Exemplary cLSM pictures of a) PS-NPs (pseudo-colored in green) and b) HES-NCs (pseudo-colored in red) without protein corona in RAW 264.7 cells. Exemplary cLSM pictures of a) PS-NPs and b) HES-NCs without protein corona in RAW 264.7 cells were chosen to distinguish cellular uptake from cell membrane decoration. The scale bar corresponds to a length of 20 μm. Published by Wiley-VCH.[52]

According to the flow cytometry results, pristine nanocarriers (without protein corona) were readily taken up by the different cells, while nanocarriers incubated with normal plasma showed significantly decreased uptake due to their protein corona with the exception of HES-NCs in RAW 264.7 cells. In contrast, after incubation in IgG-enriched plasma both nanocarriers showed a significantly increased uptake in RAW 264.7 and THP-1 cells while uptake in HeLa cells was slightly decreased. Pre-coating with clusterin before incubation in IgG-enriched plasma again reduced the cellular uptake for both systems to a similar level as with the "normal" protein corona. I suggest that the increased uptake of uncoated nanocarriers incubated with IgG-enriched plasma was due to the increased IgG concentration in the corona, as RAW 264.7 and THP-1 cells express F_c-receptors, which HeLa cells lack completely.

In order to further investigate the uptake mechanism of the nanocarriers regarding IgG specificity, F_c blocking experiments were performed in which the different F_c receptors were blocked by adding purified anti- CD64, anti-CD16 and/or anti-CD32 before incubation with nanocarriers. For determining the exact uptake pathway, the receptors CD16/CD32 (binding aggregated IgG with low affinity for the ligand[109]) and CD64 (the only receptor that can bind monomeric IgG and has high affinity for the ligand[110]) were blocked individually and additionally all three at the same time. The results of these blocking experiments are depicted in Figure 3.2.17 showing the median of fluorescence intensity (percentage of fluorescent cells see Figure 3.2.18).
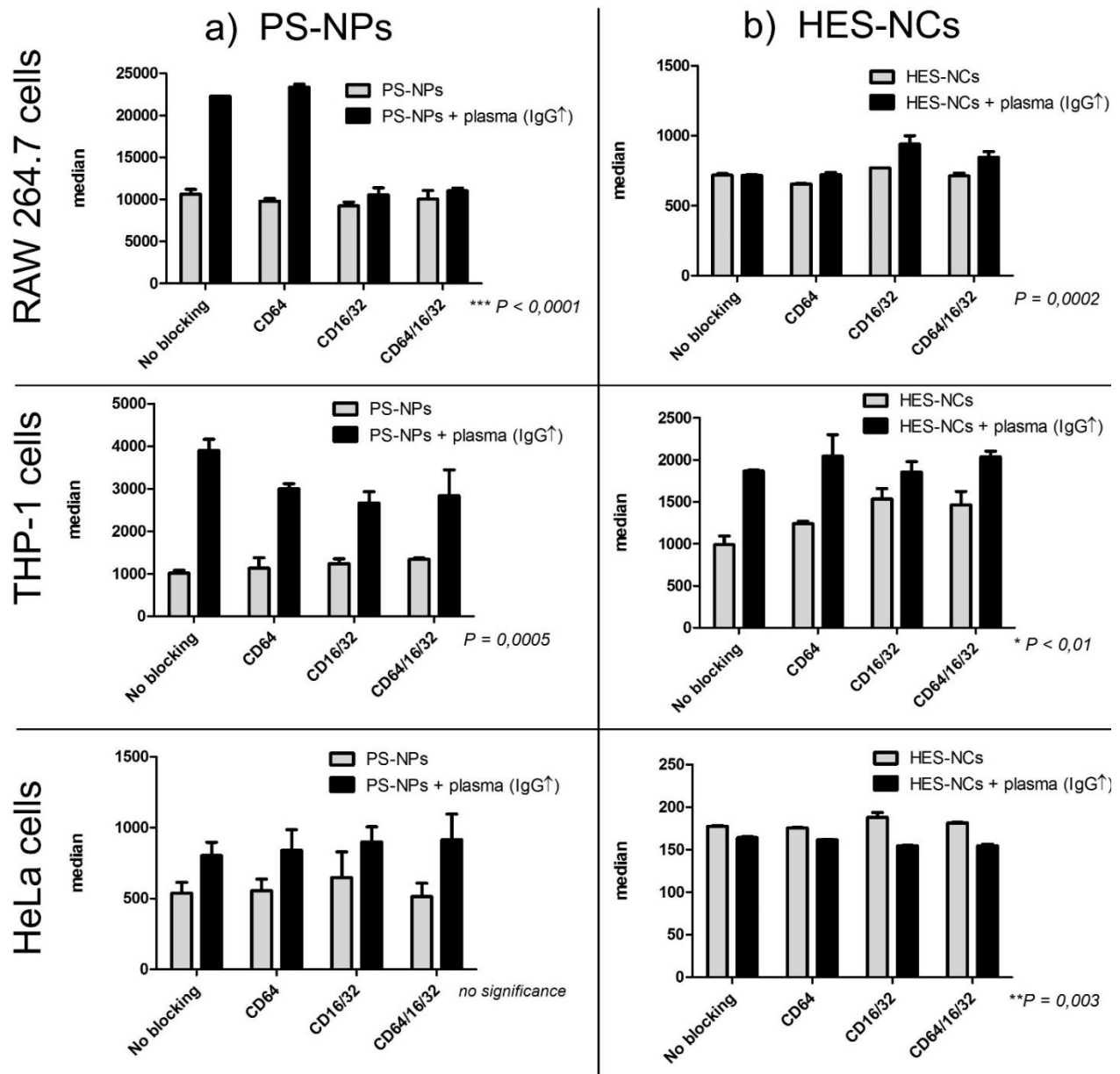
Figure 3.2.17: F_c blocking experiments of a) PS-NPs and b) HES-NCs before and after incubation with IgG-enriched plasma. RAW 264,7 (murine macrophages), THP-1 (human macrophages) and HeLa cells (human cancer cells) were used as cell lines. Values are mean values with standard deviation of three biological replicates. The ANOVA two-way test was used as statistical analysis. P-values describe the interaction between nanocarriers (without protein corona or with corona from IgG-enriched plasma) and blocked/unblocked receptors. CD16/CD32 (binding aggregated IgG with low affinity for the ligand) and CD64 (binding monomeric IgG with high affinity for the ligand) receptors were either blocked individually or all three at the same time. Published by Wiley-VCH.[52]
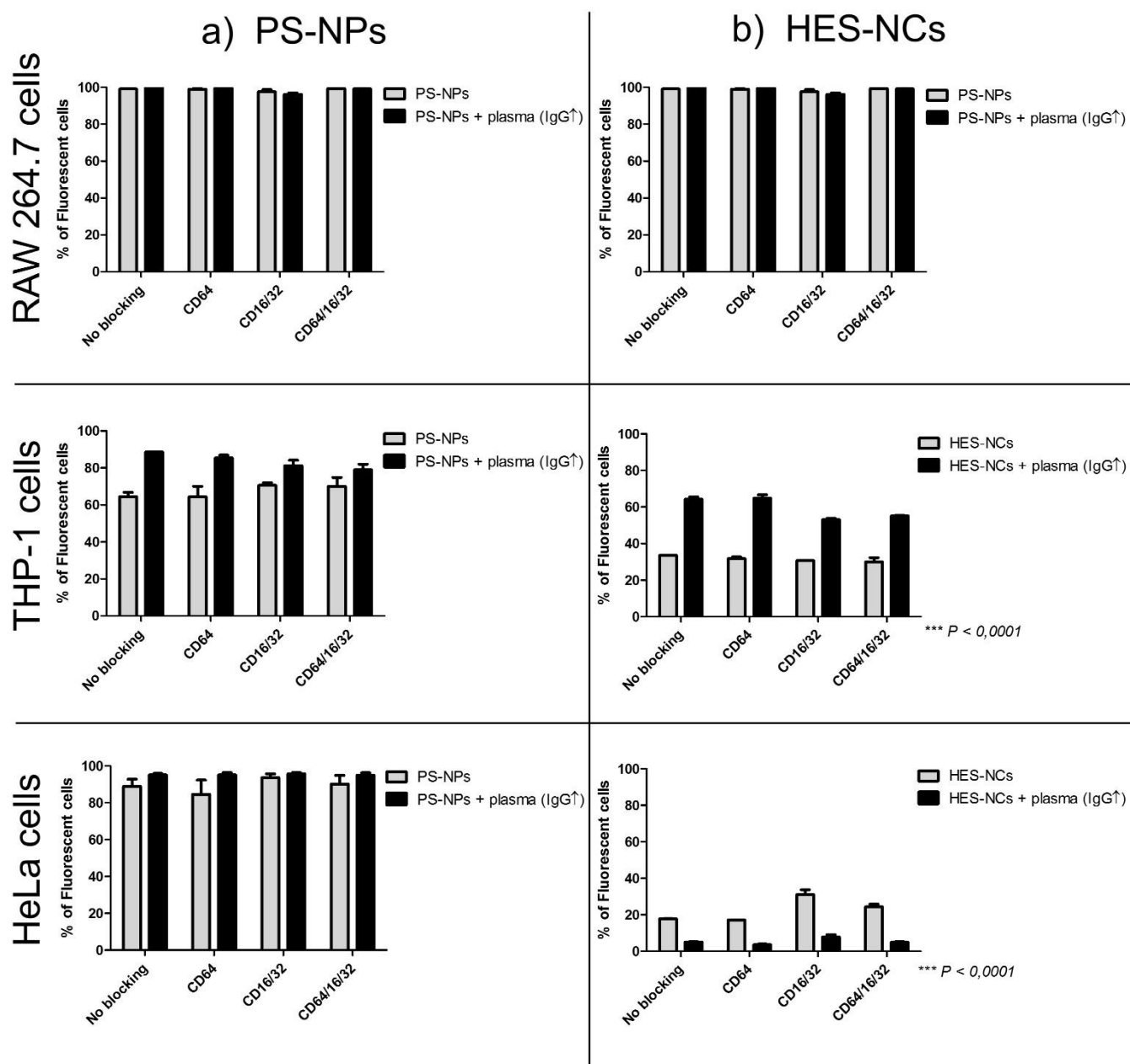
Figure 3.2.18: Percentage of fluorescent cells for Fc blocking experiments of a) PS-NPs and b) HES-NCs before and after incubation with IgG enriched plasma. RAW 264,7 , THP-1 and HeLa cells were used as cell lines. Values are mean values with standard deviation of three biological replicates. The ANOVA two-way test was used as statistical analysis. P-values describe the interaction between nanocarriers (without protein corona or with corona from IgG-enriched plasma) and blocked/unblocked receptors. Where no significance was observed, p-values are not shown. Published by Wiley-VCH.[52]

As it can be seen, the uptake of nanocarriers without protein corona did not change significantly when any F_c-receptors were blocked. However, for PS-NPs incubated with IgG-enriched plasma the uptake was reduced to the same level as for PS-NPs without protein corona in RAW 264.7 cells when CD16/CD32 were blocked, suggesting the binding to these receptors to be majorly responsible for the initially increased uptake.[97] This is in good agreement with differential scanning flourimetry (nanoDSF) experiments showing that IgG exists in denatured configuration on the surface of PS-NPs (see Figure 3.2.19). Only blocking CD64, however, did not affect the uptake. In THP-1 cells, the uptake of PS-NPs in IgG-enriched plasma was decreased significantly when CD16/CD32 and/or CD64 were blocked. The uptake was not decreased to the level of bare nanocarriers though, highlighting that human macrophages are more complex than mouse macrophages. Blocking all three F_c-receptors in THP-1 cells still showed an uptake higher than the negative control so that the uptake mechanisms for these nanocarriers are unclear. Experiments with the macrophage cell lines for HES-NCs showed no significant decrease of uptake which is most likely linked to the generally low absolute uptake of these nanocarriers as observed in the median fluorescence values (approximately 700 for HES-NCs vs. approximately 10,000 for PS-NPs). Uptake in HeLa cells was not affected by blocking for any of the nanocarriers, which is in accordance with the fact that these cells lack respective receptors.
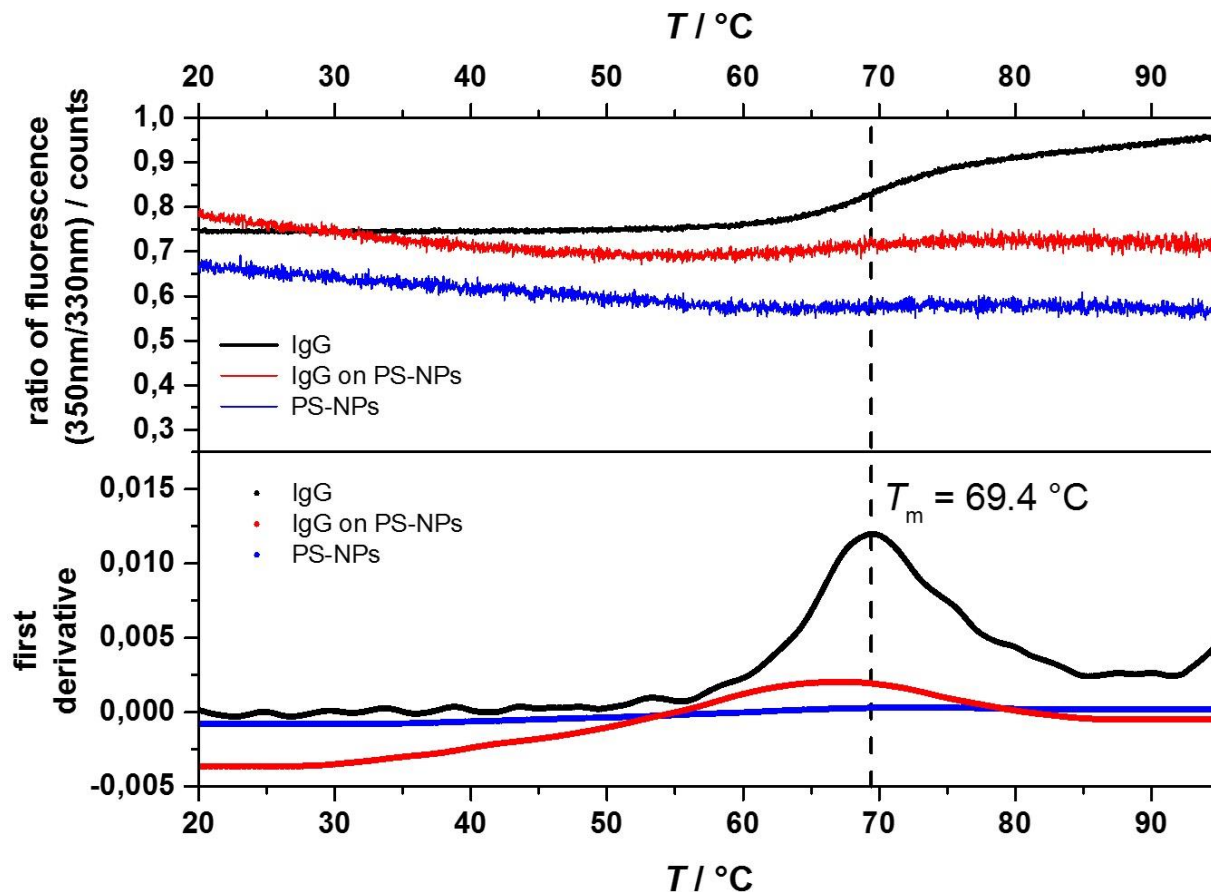
Figure 3.2.19: DSF of native IgG (black line —, positive control), pure PS-NPs (blue line —, negative control) and IgG on PS-NPs (red line —) showing the protein unfolding (heating): 350 / 330 nm ratio of fluorescence together with the first derivative. The melting point of native IgG was observed at $T_m = 69.4$ °C. For pure PS-NPs no change in fluorescence was observed. IgG on PS-NPs after incubation and washing steps did not exhibit any melting transition. This indicates that the protein was already in its denatured form on the surface of the PS-NPs and no native protein remains after the corona preparation. Published by Wiley-VCH.[52]

Summing up the *in vitro* experiments, cellular uptake strongly depended on the composition of the protein corona while the uptake mechanisms differed based on the nanocarriers' material and cell type. While the uptake of PS-NPs was mediated by aggregated IgG *via* the CD16/CD32 receptors, the uptake of HES-NCs seemingly was not connected to this pathway. This could potentially be related to the accessibility of the antibodies' F_c regions on the surface of the different nanocarriers. It could be possible that IgG bound with different orientation on the respective

nanocarriers resulting in the recognition of its F_c region on PS-NPs, which is not an apparent pathway of internalization for HES-NCs. Also, it could be that other proteins adsorbed on the HES-NCs shielded the F_c parts of the IgGs in a different way than for the PS nanocarriers. The IgG enrichment and effect in the protein corona was lower for the HES-NCs than for the PS-NPs and can be prevented by pre-coating with clusterin, negating the hard to predict outcome for cellular uptake.

3.2.1.3   Conclusion

In this study, the influence of varying immunoglobulin blood plasma levels on the formation of the protein corona was illuminated. The protein corona composition and resulting cellular response for polymeric nanocarriers exposed to blood plasma with normal and artificially elevated IgG levels was characterized regarding the protein corona composition and subsequent effect on cellular internalization. Strikingly, upon doubling the IgG concentration in plasma, the fraction of IgG in the respective coronas was elevated by a factor of 40, while the adsorption of stealth proteins such as clusterin was promoted for nanocarriers in normal plasma. This IgG enrichment in the protein corona led to significantly increased uptake in human and murine macrophages *via* F_c-receptor mediated endocytosis, as supported by F_c blocking experiments. Pre-coating of the nanocarriers with clusterin before protein corona formation successfully prevented dominant IgG-adsorption and additionally reduced cellular internalization. Following this, precoating with clusterin or potentially other stealth proteins with high binding affinities can be regarded as a powerful method to reduce the influence of individual blood composition variations (e.g., as an outcome of different health states) on the biological identity of nanocarriers. Ultimately, the data presented suggest that nanocarriers can be precisely engineered using "body-own" materials such as the blood proteins to achieve a universal performance. In my opinion, this methodology could pave the way to gain control over the behavior of nanocarriers in biological media and, thus, allow for more successful translation of nanocarriers into the clinics.

3.2.2 IgA- and IgM-enriched blood plasma

3.2.2.1 Overview

As discussed in chapter 3.1, the different immunoglobulin classes interact very differently with differently charged model nanoparticles (see chapter 3.1.1) and an elevated concentration of IgG in the plasma has a tremendous effect on the composition of each nanocarrier's corona composition (see chapter 3.2.1). Therefore, the question arises whether or not an elevated concentration of IgA or IgM in plasma might have a similar IgA- or IgM-enrichment effect on the protein composition of different nanocarriers respectively, as elevated concentrations of IgA and IgM occur in the course of many diseases as well. As an example, the IgA-concentration in blood increases from normal values $(0.7\text{-}4.0 \text{ g L}^{-1})$ to roughly 9 g L^{-1} in the course of alcoholic cirrhosis[111]. The IgM-concentration in blood increases first as an initial immune response after encountering an antigen. As esamples, the concentrations of serum IgM changes from normal values $(0.4\text{-}2.3 \text{ g L}^{-1})$ to roughly 3 g L^{-1} in the case of brain tumors[112] and to 6 g L^{-1} in the case of primary biliary cirrhosis.[113]

In order to investigate this, the protein corona composition of different nanocarriers were investigated *via* SDS-PAGE and LC-MS after incubation with IgA- and IgM-enriched plasma. For this, normal plasma (see chapter 3.2.1) was modified by addition of commercially available IgA or IgM respectively, yielding an artificially "IgA-enriched plasma" and an artificially "IgM-enriched plasma" of roughly five-fold concentration of the respective Ig, which represent physiologically relevant concentrations. LC-MS experiments were performed by Dr. Johanna Simon (MPI-P).

3.2.2.2   Results and Discussion

Before incubating any nanocarriers with the respective plasma, the protein composition of IgA-enriched and IgM-enriched plasma was compared to normal plasma. Therefore, the proteome of "normal", IgA-enriched and IgM-enriched plasma was determined *via* LC-MS. In Figure 3.2.20, a heatmap indicating the relative amount of the most abundant proteins is depicted.

	normal plasma	IgA-enriched plasma	IgM-enriched plasma
Alpha-1-acid glycoprotein 1	0.5%	0.6%	0.8%
Alpha-1-antitrypsin	1.3%	2.0%	1.0%
Alpha-2-macroglobulin	1.0%	1.0%	1.4%
Apolipoprotein A-I	0.5%	0.9%	0.5%
Apolipoprotein B-100	1.2%	0.9%	0.5%
Beta-2-glycoprotein 1	0.3%	1.1%	0.8%
Complement C3	0.5%	2.8%	2.7%
Complement C4-B	0.1%	0.6%	0.5%
Fibrinogen alpha chain	0.7%	0.6%	0.5%
Fibrinogen beta chain	1.0%	3.5%	1.8%
Fibrinogen gamma chain	1.4%	0.7%	1.4%
Haptoglobin	1.9%	2.0%	1.5%
Hemopexin	1.4%	1.0%	1.1%
Ig alpha-1 chain C region	1.8%	14.1%	2.0%
Ig alpha-2 chain C region	0.2%	1.5%	0.2%
Ig gamma-1 chain C region	8.7%	3.5%	5.1%
Ig gamma-2 chain C region	1.6%	1.0%	1.0%
Ig gamma-3 chain C region	0.7%	0.6%	0.6%
Ig gamma-4 chain C region	0.4%	0.8%	0.6%
Ig kappa chain C region	8.8%	13.7%	11.1%
Ig lambda-1 chain C regions	0.0%	2.8%	2.5%
Ig lambda-2 chain C regions	2.6%	2.9%	3.6%
Ig mu chain C region	0.7%	0.5%	3.1%
Ig mu heavy chain disease protein	0.1%	0.8%	7.8%
Serotransferrin	2.3%	2.4%	2.3%
Serum albumin	47.0%	28.5%	37.3%
Vitamin D-binding protein	0.4%	1.0%	0.8%
Zinc-alpha-2-glycoprotein	0.1%	1.4%	0.7%

Figure 3.2.20: Protein composition of normal, IgA-enriched and IgM-enriched plasma analyzed *via* LC-MS. Heatmap indicating the most abundant proteins in the respective plasma. Only proteins, which constitute at least 0.5% of the total protein composition in one of the plasma samples with at least 2 unique peptides are shown.

As anticipated, the relative amount of individual proteins and protein classes was different comparing the three plasmas with respect to IgA- and IgM-fractions. The relative concentration of

IgA-fractions was roughly seven-fold in the IgA-enriched plasma (e.g. 14.1% Ig alpha-1 chain vs. 1.8% in normal plasma). Similarly, the relative concentration of IgM-fractions was roughly five-fold in the IgM-enriched plasma (e.g. 3.1% Ig mu chain vs. 0.7% in normal plasma).

Consequently, the protein corona composition of different nanocarriers was investigated after incubation with IgA- and IgM-enriched plasma. As nanocarriers, all four nanocarriers investigated in the chapters above (PS-NPs, PS-NPs-COOH, PS-NPs-NH$_2$ and HES-NCs) were used for easy comparability with the previous results. For this, all four nanocarriers were incubated in IgA- and IgM-enriched plasma respectively and subsequently centrifuged and washed to remove excess free proteins. The protein composition of the protein coronas was analyzed *via* SDS-PAGE (see Figure 3.2.21) and LC-MS (see Figure 3.2.22 for IgA- and Figure 3.2.23 for IgM-enriched plasma).

Figure 3.2.21: SDS-PAGE gels of the protein coronas of different nanocarriers incubated with a) IgA-enriched plasma and b) IgM-enriched plasma. Pure IgA- and IgM-enriched plasma are shown as a reference. A ready to use Coomassie staining solution was used according to the manufacturer's instruction.

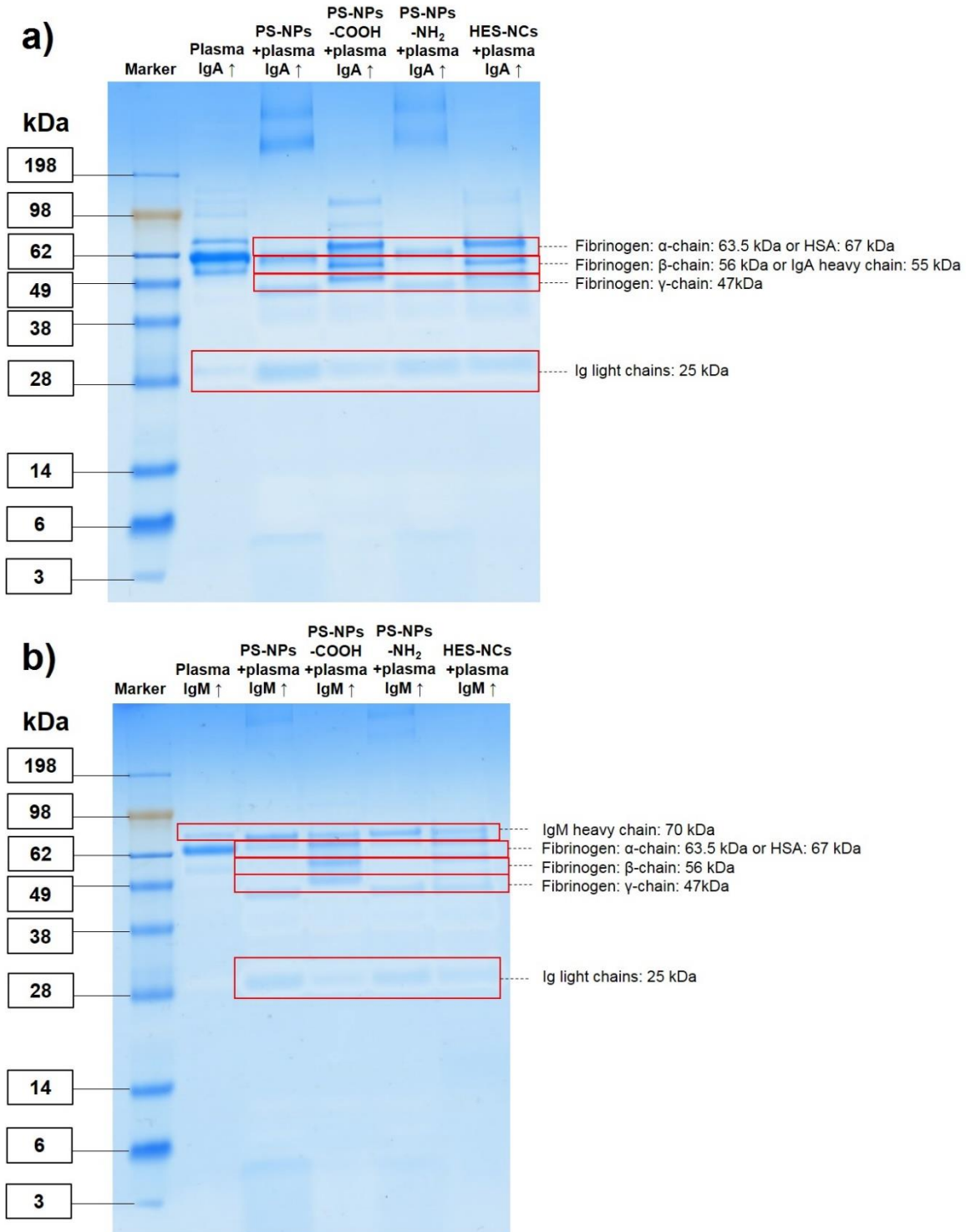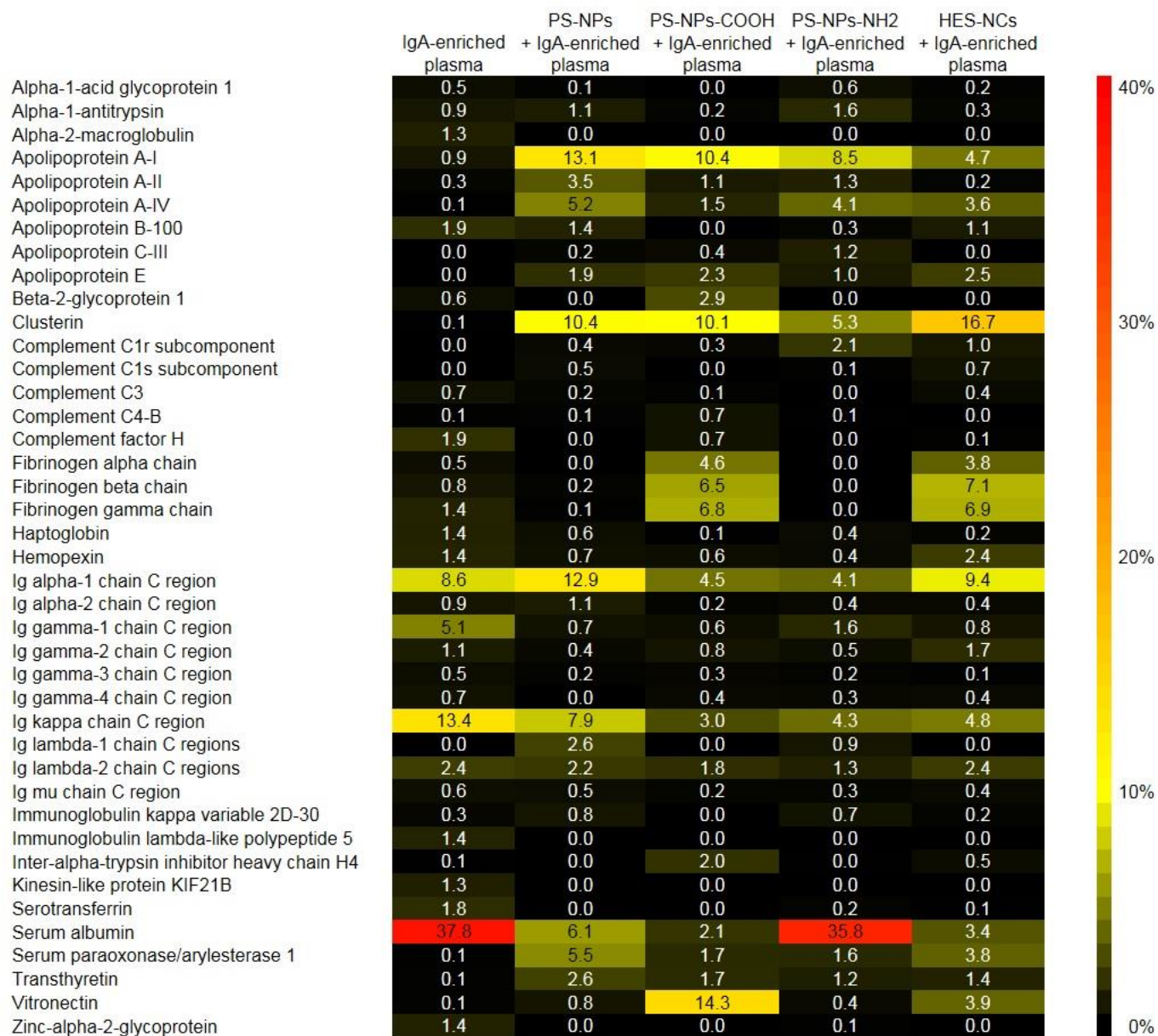|	IgA-enriched plasma	PS-NPs + IgA-enriched plasma	PS-NPs-COOH + IgA-enriched plasma	PS-NPs-NH2 + IgA-enriched plasma	HES-NCs + IgA-enriched plasma
Alpha-1-acid glycoprotein 1	0.5	0.1	0.0	0.6	0.2
Alpha-1-antitrypsin	0.9	1.1	0.2	1.6	0.3
Alpha-2-macroglobulin	1.3	0.0	0.0	0.0	0.0
Apolipoprotein A-I	0.9	13.1	10.4	8.5	4.7
Apolipoprotein A-II	0.3	3.5	1.1	1.3	0.2
Apolipoprotein A-IV	0.1	5.2	1.5	4.1	3.6
Apolipoprotein B-100	1.9	1.4	0.0	0.3	1.1
Apolipoprotein C-III	0.0	0.2	0.4	1.2	0.0
Apolipoprotein E	0.0	1.9	2.3	1.0	2.5
Beta-2-glycoprotein 1	0.6	0.0	2.9	0.0	0.0
Clusterin	0.1	10.4	10.1	5.3	16.7
Complement C1r subcomponent	0.0	0.4	0.3	2.1	1.0
Complement C1s subcomponent	0.0	0.5	0.0	0.1	0.7
Complement C3	0.7	0.2	0.1	0.0	0.4
Complement C4-B	0.1	0.1	0.7	0.1	0.0
Complement factor H	1.9	0.0	0.7	0.0	0.1
Fibrinogen alpha chain	0.5	0.0	4.6	0.0	3.8
Fibrinogen beta chain	0.8	0.2	6.5	0.0	7.1
Fibrinogen gamma chain	1.4	0.1	6.8	0.0	6.9
Haptoglobin	1.4	0.6	0.1	0.4	0.2
Hemopexin	1.4	0.7	0.6	0.4	2.4
Ig alpha-1 chain C region	8.6	12.9	4.5	4.1	9.4
Ig alpha-2 chain C region	0.9	1.1	0.2	0.4	0.4
Ig gamma-1 chain C region	5.1	0.7	0.6	1.6	0.8
Ig gamma-2 chain C region	1.1	0.4	0.8	0.5	1.7
Ig gamma-3 chain C region	0.5	0.2	0.3	0.2	0.1
Ig gamma-4 chain C region	0.7	0.0	0.4	0.3	0.4
Ig kappa chain C region	13.4	7.9	3.0	4.3	4.8
Ig lambda-1 chain C regions	0.0	2.6	0.0	0.9	0.0
Ig lambda-2 chain C regions	2.4	2.2	1.8	1.3	2.4
Ig mu chain C region	0.6	0.5	0.2	0.3	0.4
Immunoglobulin kappa variable 2D-30	0.3	0.8	0.0	0.7	0.2
Immunoglobulin lambda-like polypeptide 5	1.4	0.0	0.0	0.0	0.0
Inter-alpha-trypsin inhibitor heavy chain H4	0.1	0.0	2.0	0.0	0.5
Kinesin-like protein KIF21B	1.3	0.0	0.0	0.0	0.0
Serotransferrin	1.8	0.0	0.0	0.2	0.1
Serum albumin	37.8	6.1	2.1	35.8	3.4
Serum paraoxonase/arylesterase 1	0.1	5.5	1.7	1.6	3.8
Transthyretin	0.1	2.6	1.7	1.2	1.4
Vitronectin	0.1	0.8	14.3	0.4	3.9
Zinc-alpha-2-glycoprotein	1.4	0.0	0.0	0.1	0.0

Figure 3.2.22: Composition of protein corona after incubation with IgA-enriched plasma analyzed *via* LC-MS. Only those proteins, which constitute at least 0.5% of the protein corona on one of the nanocarriers with at least 2 unique peptides are shown.
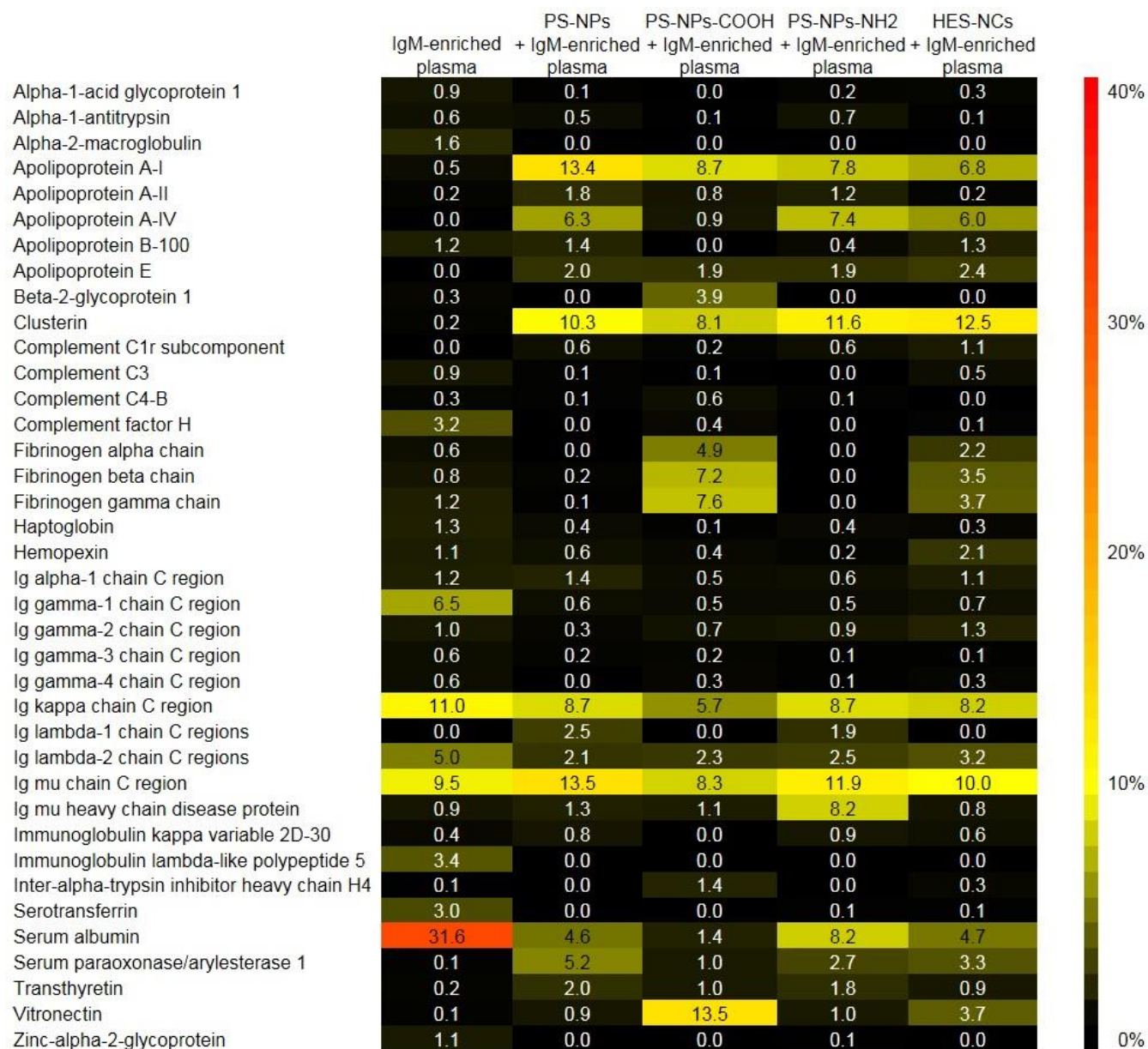
	IgM-enriched plasma	PS-NPs + IgM-enriched plasma	PS-NPs-COOH + IgM-enriched plasma	PS-NPs-NH2 + IgM-enriched plasma	HES-NCs + IgM-enriched plasma
Alpha-1-acid glycoprotein 1	0.9	0.1	0.0	0.2	0.3
Alpha-1-antitrypsin	0.6	0.5	0.1	0.7	0.1
Alpha-2-macroglobulin	1.6	0.0	0.0	0.0	0.0
Apolipoprotein A-I	0.5	13.4	8.7	7.8	6.8
Apolipoprotein A-II	0.2	1.8	0.8	1.2	0.2
Apolipoprotein A-IV	0.0	6.3	0.9	7.4	6.0
Apolipoprotein B-100	1.2	1.4	0.0	0.4	1.3
Apolipoprotein E	0.0	2.0	1.9	1.9	2.4
Beta-2-glycoprotein 1	0.3	0.0	3.9	0.0	0.0
Clusterin	0.2	10.3	8.1	11.6	12.5
Complement C1r subcomponent	0.0	0.6	0.2	0.6	1.1
Complement C3	0.9	0.1	0.1	0.0	0.5
Complement C4-B	0.3	0.1	0.6	0.1	0.0
Complement factor H	3.2	0.0	0.4	0.0	0.1
Fibrinogen alpha chain	0.6	0.0	4.9	0.0	2.2
Fibrinogen beta chain	0.8	0.2	7.2	0.0	3.5
Fibrinogen gamma chain	1.2	0.1	7.6	0.0	3.7
Haptoglobin	1.3	0.4	0.1	0.4	0.3
Hemopexin	1.1	0.6	0.4	0.2	2.1
Ig alpha-1 chain C region	1.2	1.4	0.5	0.6	1.1
Ig gamma-1 chain C region	6.5	0.6	0.5	0.5	0.7
Ig gamma-2 chain C region	1.0	0.3	0.7	0.9	1.3
Ig gamma-3 chain C region	0.6	0.2	0.2	0.1	0.1
Ig gamma-4 chain C region	0.6	0.0	0.3	0.1	0.3
Ig kappa chain C region	11.0	8.7	5.7	8.7	8.2
Ig lambda-1 chain C regions	0.0	2.5	0.0	1.9	0.0
Ig lambda-2 chain C regions	5.0	2.1	2.3	2.5	3.2
Ig mu chain C region	9.5	13.5	8.3	11.9	10.0
Ig mu heavy chain disease protein	0.9	1.3	1.1	8.2	0.8
Immunoglobulin kappa variable 2D-30	0.4	0.8	0.0	0.9	0.6
Immunoglobulin lambda-like polypeptide 5	3.4	0.0	0.0	0.0	0.0
Inter-alpha-trypsin inhibitor heavy chain H4	0.1	0.0	1.4	0.0	0.3
Serotransferrin	3.0	0.0	0.0	0.1	0.1
Serum albumin	31.6	4.6	1.4	8.2	4.7
Serum paraoxonase/arylesterase 1	0.1	5.2	1.0	2.7	3.3
Transthyretin	0.2	2.0	1.0	1.8	0.9
Vitronectin	0.1	0.9	13.5	1.0	3.7
Zinc-alpha-2-glycoprotein	1.1	0.0	0.0	0.1	0.0

(color scale: 40% / 30% / 20% / 10% / 0%)

Figure 3.2.23: Composition of protein corona after incubation with IgM-enriched plasma analyzed *via* LC-MS. Only those proteins, which constitute at least 0.5% of the protein corona on one of the nanocarriers with at least 2 unique peptides are shown.

Based on the SDS-PAGE gels depicted in Figure 3.2.21, it is seen that the overall protein composition of PS-NPs and PS-NPs-NH$_2$ is rather similar after incubation with both plasmas respectively. The same can be said for PS-NPs-COOH and HES-NCs, as further seen in Figure 3.2.22 and Figure 3.2.23. Compared to the corona compositions found after incubation in normal

plasma (up to 1% Ig alpha-1 and Ig mu chains and roughly 40% clusterin for PS-NPs and HES-NCs; see chapter 3.2.1), the corona composition found after incubation with IgA- or IgM-enriched plasma was very different for both plasmas. The elevated concentrations of IgA- or IgM-fractions in the respective plasma resulted in an increase of these fractions in the coronas of all four nanocarriers. In a similar fashion to the results reported in chapter 3.2.1 and the case of IgG-enriched plasma, other protein fractions than immunoglobulins were affected as well. Exemplarily, the concentrations of the "stealth proteins" apo A-I and clusterin were significantly lower after incubation with IgA- or IgM-enriched plasma compared to normal plasma. Furthermore, fibrinogen fractions were found in an increased concentration on the surface of PS-NPs-COOH and HES NCs. This agrees well with the IgG-enrichment of the protein corona of different nanocarriers reported before, as the enrichment of IgA- and IgM-fractions in the corona seem to be a direct consequence of the individual protein concentration (in this case of IgA or IgM) in the plasma and not purely depend on each protein's binding affinity.[52] This is in agreement with the "Vroman-effect" as described in chapter 3.2.1, as the incubation time of one hour might not be enough time for the system to rearrange due to high initial concentrations of the (less affine) immunoglobulins compared to the low concentrated, yet very affine clusterin. Interestingly, the concentration of serum albumin increased a lot on PS-NPs-NH$_2$ after incubation with IgA-enriched plasma specifically. This could be a result of the generally low affinity of IgA to each nanocarriers' surface paired with a generally high concentration of serum albumin in plasma or a result of protein-protein interactions. In other words, the concentration of clusterin might be too low to compete with IgA for the surface of PS-NPs-NH$_2$, while serum albumin could have the most optimal adsorption conditions in this case with a high concentration in plasma and relatively high binding affinity compared to IgA.

3.2.2.3   Conclusion

In this study, the protein corona composition of different nanocarriers was investigated after incubation with IgA- and IgM-enriched plasma. In conclusion, not only does an increased IgG-concentration of blood plasma result in an enrichment of IgG in the corona of different nanocarriers, but a similar enrichment of IgA or IgM is found after incubation with IgA- or IgM-

enriched plasma respectively. In a similar fashion to the case of IgG-enrichment, an enrichment of IgA- or IgM-fractions in the corona also affects the adsorption process of other proteins, such as apo A-I, clusterin, fibrinogen or serum albumin. This means that not only the individual IgG-concentrations in blood may affect the protein corona and behavior of different nanocarriers, yet the same could be said for IgA and IgM as well. This further highlights the influence of the individual immunoglobulin composition on NP-protein interactions as a whole and the binding mechanisms of immunoglobulin adsorption must be understood further.

3.2.3 Absence of IgG in the blood proteome

3.2.3.1 Overview

After discovering that an increased concentration of an Ig class in blood plasma has a tremendous effect on the protein corona composition and cellular interactions of nanocarriers, the question arises whether or not a complete lack of individual Ig classes in the blood plasma could influence the composition of the protein corona as well. This becomes even more considerable since cooperative protein-protein interactions play an important role in NP-protein interactions.[114]

Compared to the more common case of increased or mildly decreased blood levels of individual Ig classes or subclasses, which occur in the course of most diseases, the deficiency and complete lack of individual immunoglobulins (a so-called immunodeficiency) is much rarer with an estimated overall prevalence of 0.1% in live births.[115,116] While it is not fully understood what causes certain immunodeficiencies, genetics are expected to play a crucial role.[115] Following that, a significantly different composition of the protein corona might occur, if complete Ig classes or subclasses were missing in the blood due to such genetic disorders.

In the following, the impact of the absence of IgG on the formation of the protein corona was investigated, as IgG is the highest concentrated Ig of the blood proteome. In order to achieve this, pooled human blood plasma with averaged protein levels obtained from healthy donors (subsequently called "normal plasma") was treated in order to remove all IgG from this normal plasma resulting in an "IgG-depleted plasma". Subsequently, the protein corona of different NPs

was compared after incubation with normal or IgG-depleted plasma in order to investigate the influence that the absence of IgG in the blood proteome has on the formation of the protein corona. LC-MS experiments were performed by Dr. Johanna Simon (MPI-P),

3.2.3.2 Results and Discussion

IgG must be isolated from normal plasma selectively, in order to obtain IgG-depleted plasma. This can be achieved using different proteins, which specifically bind the F_c-domains of the respective Ig, such as protein A. Protein A is a protein produced by the bacterium *Staphylococcus aureus* and is widely used for isolating IgG due to its high affinity.[117] Because of this, an HPLC setup utilizing a column functionalized with protein A was used in order to isolate IgG from normal plasma (see chapter 4.3.5 for more details on the procedure). Before incubating different NPs with normal and IgG-depleted plasma, the protein composition of both plasma sources (normal and IgG-depleted) were investigated *via* LC-MS. In Figure 3.2.24, a heat map visualizing the relative amount of the most abundant proteins in both plasmas is shown.
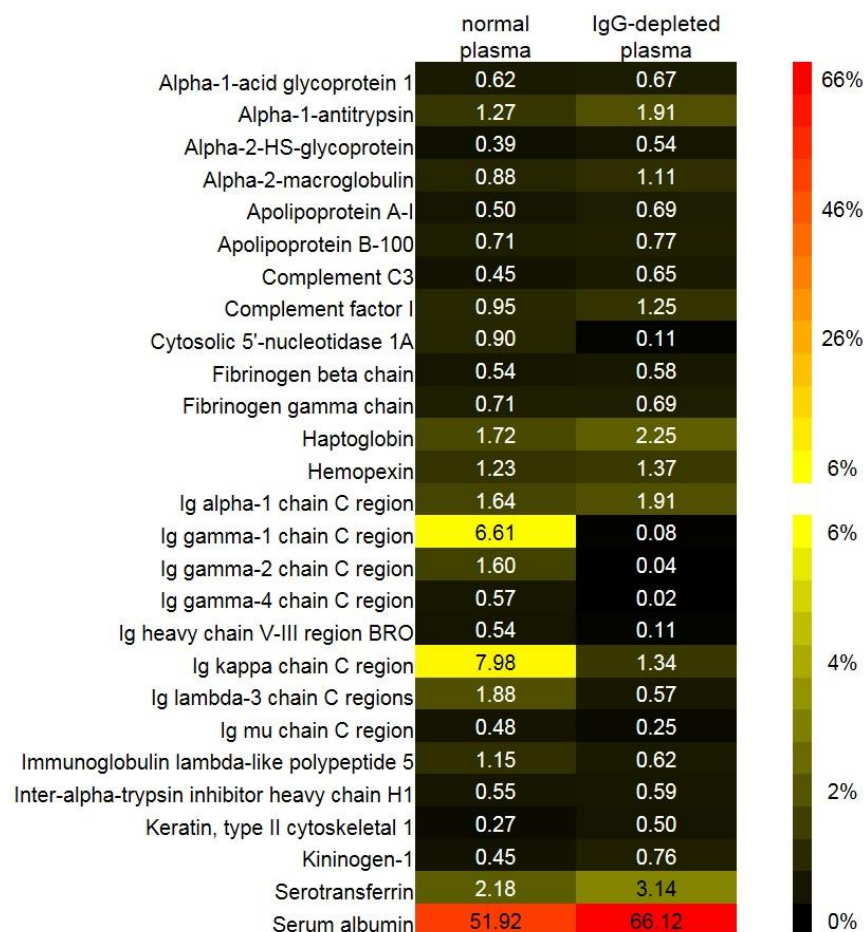
Figure 3.2.24: Protein composition of normal and IgG-depleted plasma analyzed *via* LC-MS. Heat map is indicating the most abundant proteins in the respective plasma. Only proteins, which constitute at least 0.5% of the total protein composition in one of the plasma samples with at least 2 unique peptides are shown.

As anticipated, it can be seen that the overall picture of relative protein concentrations of normal and IgG-depleted plasma is quite similar except for IgG chains. All other proteins have rather similar concentrations in both plasmas, most appear in a slightly higher relative concentration in IgG-depleted plasma, due to the decreased overall protein concentration as a result of the IgG isolation. Therefore, the depletion of IgG from plasma was successful, yet the salt concentration of both plasmas is different after the treatment of normal plasma, as during the isolation process of IgG from normal plasma *via* HPLC, 10mM Tris · HCl is used as a running buffer. To restore a more physiological salt environment for the obtained IgG-depleted plasma, it was desalted using a desalting column and diluted by 90% with 10x PBS (see chapter 4.3.6 for more information on the procedure).

Subsequently, the formation of the protein corona in both plasma sources was investigated. For this, the same Lutensol-based model NPs as discussed in the previous chapter 3.1.1 (see Table 3.1.1) were incubated in both plasma sources, washed and centrifuged to remove excessive free proteins. Firstly, the protein corona composition was analyzed *via* SDS-PAGE (see Figure 3.2.25).
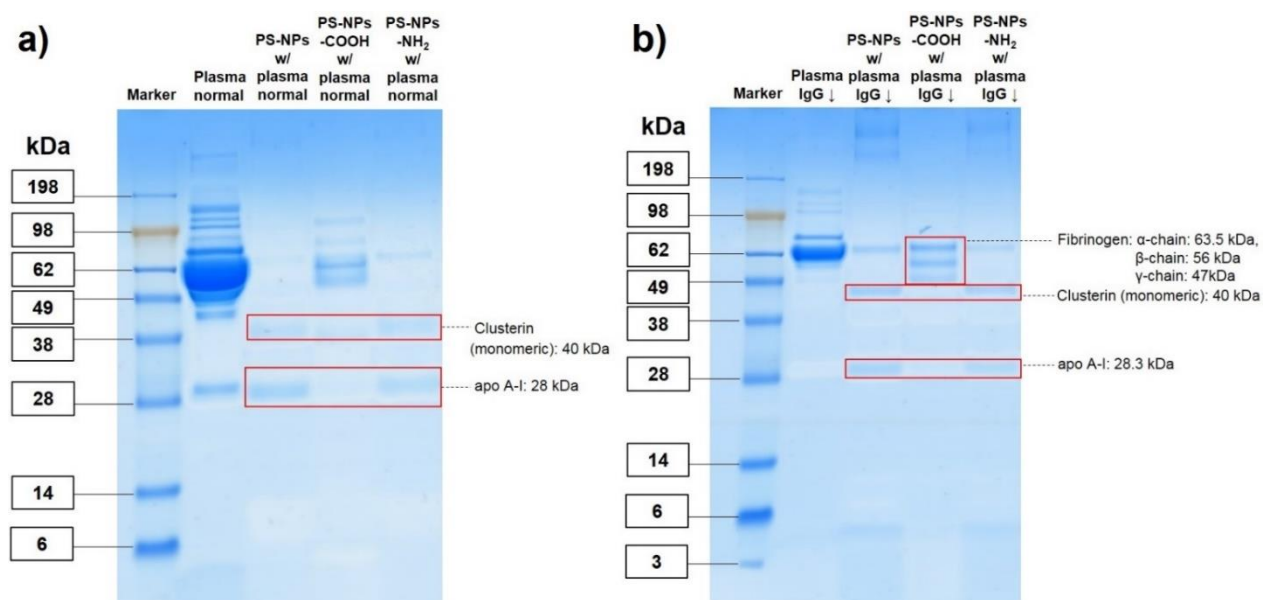

Figure 3.2.25: Reducing SDS-PAGE gel of the protein corona of PS-NPs incubated with a) normal plasma and b) IgG-depleted plasma. Both plasmas are shown as a reference. For staining, a ready-to-use Coomassie staining solution was used according to the manufacturer's instruction.

From the gels in Figure 3.2.25, it can be seen that the bands corresponding to the heavy chain (50 kDa) and light chain (25 kDa) of IgG are missing in the reference of IgG-depleted plasma. The bands of the protein coronas of PS-NPs and PS-NPs-NH$_2$ look rather similar for the same plasma, while PS-NPs-COOH show a completely different protein pattern in both cases. Comparing both plasmas, the protein corona of the same NP appear to have a different protein composition after incubation in the different plasmas.

In order to gain more information concerning the exact composition of the nanocarriers' protein corona composition, the proteins detached from the nanocarriers' surfaces were analyzed *via* LC-MS (see Figure 3.2.26).
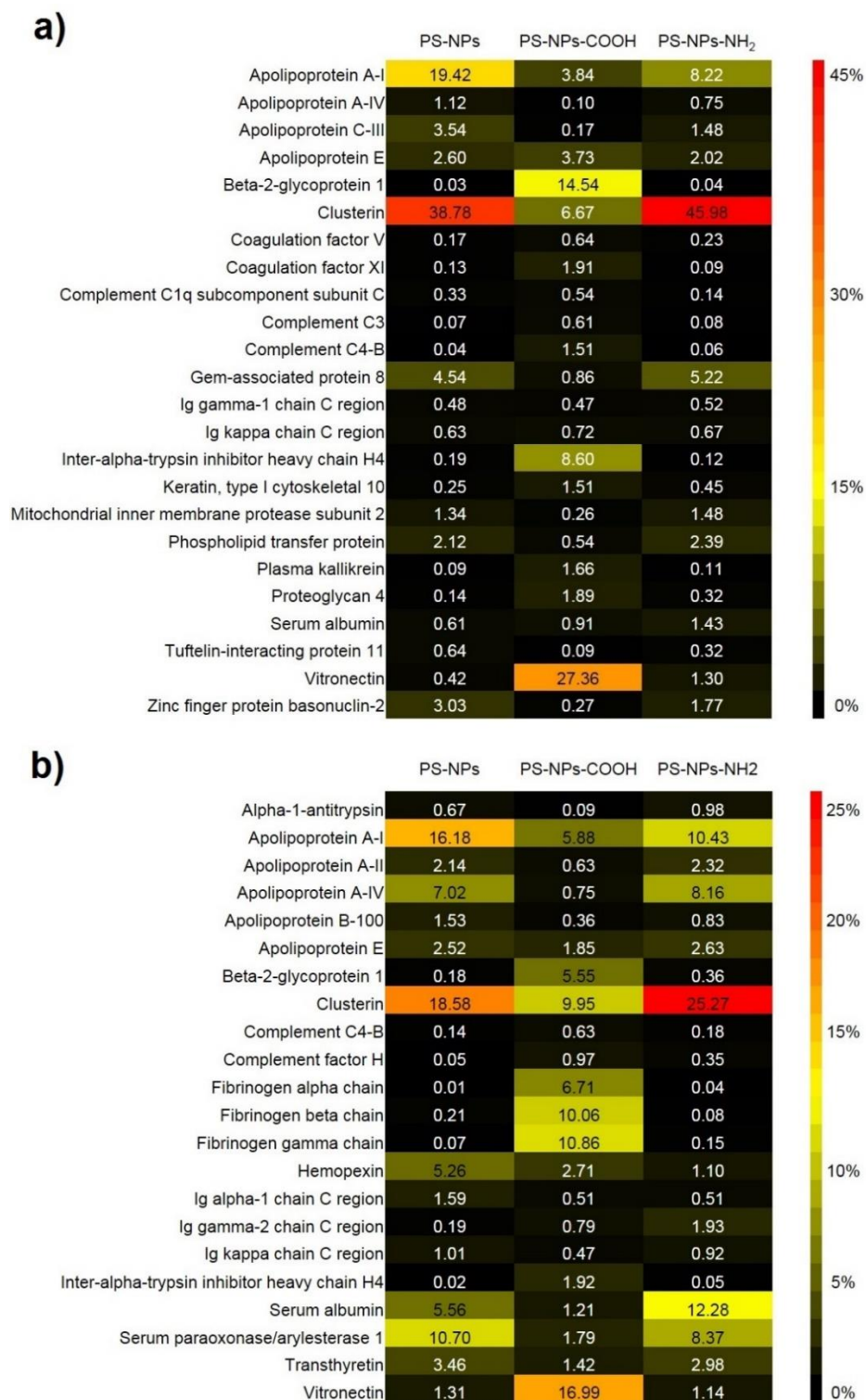
a)

	PS-NPs	PS-NPs-COOH	PS-NPs-NH$_2$
Apolipoprotein A-I	19.42	3.84	8.22
Apolipoprotein A-IV	1.12	0.10	0.75
Apolipoprotein C-III	3.54	0.17	1.48
Apolipoprotein E	2.60	3.73	2.02
Beta-2-glycoprotein 1	0.03	14.54	0.04
Clusterin	38.78	6.67	45.98
Coagulation factor V	0.17	0.64	0.23
Coagulation factor XI	0.13	1.91	0.09
Complement C1q subcomponent subunit C	0.33	0.54	0.14
Complement C3	0.07	0.61	0.08
Complement C4-B	0.04	1.51	0.06
Gem-associated protein 8	4.54	0.86	5.22
Ig gamma-1 chain C region	0.48	0.47	0.52
Ig kappa chain C region	0.63	0.72	0.67
Inter-alpha-trypsin inhibitor heavy chain H4	0.19	8.60	0.12
Keratin, type I cytoskeletal 10	0.25	1.51	0.45
Mitochondrial inner membrane protease subunit 2	1.34	0.26	1.48
Phospholipid transfer protein	2.12	0.54	2.39
Plasma kallikrein	0.09	1.66	0.11
Proteoglycan 4	0.14	1.89	0.32
Serum albumin	0.61	0.91	1.43
Tuftelin-interacting protein 11	0.64	0.09	0.32
Vitronectin	0.42	27.36	1.30
Zinc finger protein basonuclin-2	3.03	0.27	1.77

Scale: 45% / 30% / 15% / 0%

b)

	PS-NPs	PS-NPs-COOH	PS-NPs-NH2
Alpha-1-antitrypsin	0.67	0.09	0.98
Apolipoprotein A-I	16.18	5.88	10.43
Apolipoprotein A-II	2.14	0.63	2.32
Apolipoprotein A-IV	7.02	0.75	8.16
Apolipoprotein B-100	1.53	0.36	0.83
Apolipoprotein E	2.52	1.85	2.63
Beta-2-glycoprotein 1	0.18	5.55	0.36
Clusterin	18.58	9.95	25.27
Complement C4-B	0.14	0.63	0.18
Complement factor H	0.05	0.97	0.35
Fibrinogen alpha chain	0.01	6.71	0.04
Fibrinogen beta chain	0.21	10.06	0.08
Fibrinogen gamma chain	0.07	10.86	0.15
Hemopexin	5.26	2.71	1.10
Ig alpha-1 chain C region	1.59	0.51	0.51
Ig gamma-2 chain C region	0.19	0.79	1.93
Ig kappa chain C region	1.01	0.47	0.92
Inter-alpha-trypsin inhibitor heavy chain H4	0.02	1.92	0.05
Serum albumin	5.56	1.21	12.28
Serum paraoxonase/arylesterase 1	10.70	1.79	8.37
Transthyretin	3.46	1.42	2.98
Vitronectin	1.31	16.99	1.14

Scale: 25% / 20% / 15% / 10% / 5% / 0%

Figure 3.2.26: Composition of the protein corona for PS-NPs- PS-NPs-COOH and PS-NPs-NH$_2$ after incubation with a) normal plasma and b) IgG-depleted plasma analyzed *via* LC-MS. Only those proteins, which constitute at least 0.5% of the protein corona on one of the nanocarriers with at least two unique peptides, are shown.

Interestingly, IgG is not a major component in any protein corona, including the coronas resulting from incubation in normal plasma. Yet, still the corona composition is significantly different for both plasmas (see Figure 3.2.26). After incubation with normal plasma, the protein coronas of PS-NPs and PS-NPs-NH$_2$ showed apo A-1 and clusterin as major components, while the corona of PS-NPs-COOH consisted majorly of vitronectin and beta-2-glycoprotein 1. In contrast, the protein coronas of PS-NPs and PS-NPs-NH$_2$ after incubation with IgG-depleted plasma showed less apo A-1 and clusterin, but significantly more of other proteins like serum albumin, apolipoprotein A-IV, and serum paraoxonase/arylesterase 1. Similarly, the protein corona of PS-NPs-COOH have a significantly different composition after incubation with IgG-depleted plasma as well. Here, the relative concentration of vitronectin and beta-2-glycoprotein 1 was lower, yet other proteins showed a higher concentration in the corona of these carboxylated NPs. This was especially the case for fibrinogen. This means, that even if the concentration of IgG was rather low (roughly 1%) in the corona of NPs in normal plasma in the first place, the complete lack of IgG in the plasma still had a tremendous impact on the overall interaction between nanocarriers and proteins in general. This might potentially be a result of protein-protein interactions between IgG and other proteins, which can occur in normal plasma and cannot occur in IgG-depleted plasma. Yet, it could also be an effect of the affected salt content of IgG-depleted plasma in the course of the depletion process. This affected salt content was tried to be compensated by desalting and dilution with concentrated PBS, but still could have an effect on the proteins within the used IgG-depleted plasma.

Following that, further information on the total interaction between all NPs and the proteins of both plasmas are of high interest. Therefore, calorimetry measurements of all three NPs were performed *via* isothermal titration calorimetry (ITC) for both plasmas. In an ITC experiment, IgG-depleted plasma or normal plasma was titrated into a dispersion of the respective NPs in multiple injections (see chapter 2.4.1 for more information on ITC). The resulting adsorption isotherms and parameters of each NP in both plasmas are depicted in Figure 3.1.12.

a)

	PS-NPs+ plasma (normal)	PS-NPs-COOH+ plasma (normal)	PS-NPs-NH$_2$+ plasma (normal)
K_a/ 10^6 M^{-1}	0.30 ±0.04	0.18 ± 0.02	0.30 ± 0.04
ΔH/ kJ mol^{-1}	-115 ± 3	-296 ± 14	-125 ± 5
ΔS/ J mol^{-1} K^{-1}	-295 ± 10	-927 ± 49	-329 ± 19
ΔG/ kJ mol^{-1}	-30.2 ± 0.3	-29.0 ± 0.3	-30.2 ± 0.4
n	309 ± 15	505 ± 10	366 ± 5

b)

	PS-NPs+ plasma (IgG ↓)	PS-NPs-COOH+ plasma (IgG ↓)	PS-NPs-NH$_2$+ plasma (IgG ↓)
K_a/ 10^6 M^{-1}	6.1 ± 1.3	1.0 ± 0.1	1.7 ± 0.1
ΔH/ kJ mol^{-1}	-126 ± 11	-1500 ± 130	-539 ± 65
ΔS/ J mol^{-1} K^{-1}	-308 ± 41	-5070 ± 470	-1750 ± 225
ΔG/ kJ mol^{-1}	-37.4 ± 0.5	-33.2 ± 0.3	-34.4 ± 0.2
n	325 ± 26	360 ± 6	281 ± 10

Figure 3.2.27: Adsorption isotherms and parameters of a) normal plasma and b) IgG-depleted plasma titrated to PS-NPs, PS-NPs-COOH and PS-NPs-NH$_2$ respectively as obtained from ITC experiments. Isotherms were fitted according to an independent binding model (solid lines).

Comparing the adsorption isotherms of the different NPs, it can be seen that the interactions of PS-NPs-COOH are significantly different from for the other NPs in both plasmas. While PS-NPs and PS-NPs-NH$_2$ undergo very similar interactions with plasma proteins in normal plasma, they interact very differently in IgG-dependent plasma. This is well in accordance with the differences in protein corona composition observed *via* LC-MS (as discussed above). For both plasmas, the association constants K_a are lower for PS-NPs-COOH, while ΔH and ΔS are more negative. The

relatively low affinity of proteins to the carboxylated NPs can be explained by the relatively low concentration of the proteins apo A-1 and clusterin in the corona, as these proteins were shown to have high affinities to the NPs' surfaces. If proteins are not very affine to the negatively charged surface of PS-NPs-COOH ($K_a < 10^6 \, M^{-1}$), the overall lower affinity of plasma proteins to their surface is plausible. The more negative binding enthalpy and entropy observed for IgG-depleted plasma correspond with a higher contribution of electrostatics and hydrogen bond formation during the interaction and less hydrophobic interactions. This further shows that by the lack of IgG in the plasma, the overall mechanism of the interactions between NPs and plasma protein changes. This becomes even more striking if it is considered that IgG is not a major component of these NPs' coronas in normal plasma.

3.2.3.3 Conclusion

In this chapter, the influence of a depletion of IgG from blood plasma on the formation of the protein corona was illuminated. It was shown that the protein corona composition of differently charged nanocarriers is different comparing the protein corona resulting from incubation in normal plasma to the protein corona resulting from incubation in IgG-depleted plasma. While the concentration of IgG was rather low (roughly 1%) in the protein corona of each nanocarrier in normal plasma in the first place, the lack of IgG in the plasma still had a tremendous impact on the overall interaction between nanocarriers and proteins in general. If the results presented in this chapter are not an effect of the preparation of IgG-depleted plasma as discussed above, it has to be noted that a relatively low concentration of a single protein or protein class on a nanocarrier's surface does not necessarily correlate with a low impact on the nanocarrier's overall protein interactions. In the specific case of immunodeficiencies, it means that it has to be considered that the lack of specific immunoglobulin classes or subclasses in the blood may result in altered NP-protein interactions in general. Therefore, the individual protein composition of blood towards high and low concentrations may play a crucial role in all NP-protein interactions.

3.3   Anti-PEG immunoglobulin G in the protein corona

3.3.1   Overview

PEGylation is commonly used to improve the physicochemical properties of nanoparticles, liposomes, proteins and small molecules.[118] PEGylating nanocarriers leads to an overall reduction of unspecific protein adsorption on the nanocarriers' surfaces in biological media and prolongs their circulation times in blood significantly.[19,20] Because of this, multiple PEGylated drugs, such as PEG-liposomal doxorubicin (Doxil®, Caelyx®, LipoDox®),[119] are approved for clinical use.[120-122]

However, anti-PEG antibodies may be generated by the organism upon exposure to PEGylated drugs, changing the blood composition of the patient's blood significantly after one single injection. The "accelerated blood clearance (ABC) phenomenon" describes the loss of the long-circulation properties of PEG-liposomes and other species containing PEG-chains in a second injection a few days after their first injection caused by the promoted production of anti-PEG antibodies in mice, rats and rhesus monkeys.[123] It was shown that in the first days after the first injection with PEG-liposomes, anti-PEG IgM is dominantly produced in the spleen[124] and after several more days anti-PEG IgG is produced as well.[125,126] Furthermore, pre-existing anti-PEG antibodies were detected in humans with detection frequencies of up to 36% in naive individuals,[23-26] supposedly caused by long-time exposure to PEG in cosmetics and medicine.[21,22] Interestingly, in a study by Chen *et al.* regarding pre-existing anti-PEG IgG and IgM in the blood of healthy Han Chinese donors, it was reported that younger and female individuals showed higher prevalence and concentration of pre-existing anti-PEG antibodies compared to older and male subjects.[22]

Anti-PEG antibodies in the protein corona could lead to F_c-receptor mediated phagocytosis, preventing an efficient therapy as discussed in previous chapters. Furthermore, interactions between anti-PEG immunoglobulins and PEGylated nanocarriers and liposomes may induce reactions of the complement system and ultimately lead to allergic reactions.[21,127] The PEG-binding properties of these anti-PEG antibodies may result in an accumulation of these Igs in the protein corona of PEGylated nanocarriers and therefore negatively influence their behavior *in vivo*

as discussed above. This means that further knowledge on the influence of specific anti-PEG antibody-nanocarrier interactions on the protein corona of different (PEGylated and non-PEGylated) nanocarriers are needed in order to control the behavior of nanocarriers more reliably in biological media. Therefore, the existence and concentration of anti-PEG IgG, as one mayor class of anti-PEG antibodies, in the pooled, normal plasma used in this thesis and in the protein corona of different (PEGylated and non-PEGylated) nanocarriers prepared from the same plasma was investigated *via* enzyme-linked immunosorbent assay (ELISA) and confirmed by a competition assay in the following.

3.3.2 Results and Discussion

Fundamentally, the procedure of the anti-PEG IgG-specific ELISA published by Chen *et al.* was adapted in this work with slight modifications regarding the concentration range of the calibration.[22] First, the capabilities of the herein used ELISA method were investigated by determining the method's limit of detection (LOD) and limit of quantification (LOQ) in accordance with DIN 32645.[128] For this, ten blank samples (sample buffer) were analyzed according to the protocol described in chapter 4.5. Following that, the mean absorbance ($\bar{A}_{405nm}$) and standard deviation (σ) of these ten blank samples were used to calculate LOD (see equation 3.3.1) and LOQ (see equation 3.3.2).[128]

$$LOD = \bar{A}_{405nm} + 3.3 \cdot \sigma \qquad (3.3.1)$$

$$LOQ = \bar{A}_{405nm} + 10 \cdot \sigma \qquad (3.3.2)$$

As a result, LOD was determined to be an absorbance of $A_{LOD} = 0.42$ and LOQ was determined to be an absorbance of $A_{LOQ} = 0.65$. With this information, a calibration using a chimeric human anti-PEG IgG (c3.3-IgG) as standard compound was developed with concentrations of 2, 3, 4, 5, 6, 7 and 8 mg L^{-1}. These concentrations were chosen because the

absorbance of the standard with 2 mg L^{-1} was close to LOD ($A_{2\ mg/L} = 0.45 \pm 0.03$), and the absorbance of the standard with 8 mg L^{-1} was at a high absorbance of $A_{8\ mg/L} = 2.87 \pm 0.34$. The graph for a calibration curve of the ELISA used in this chapter is depicted in Figure 3.3.1.
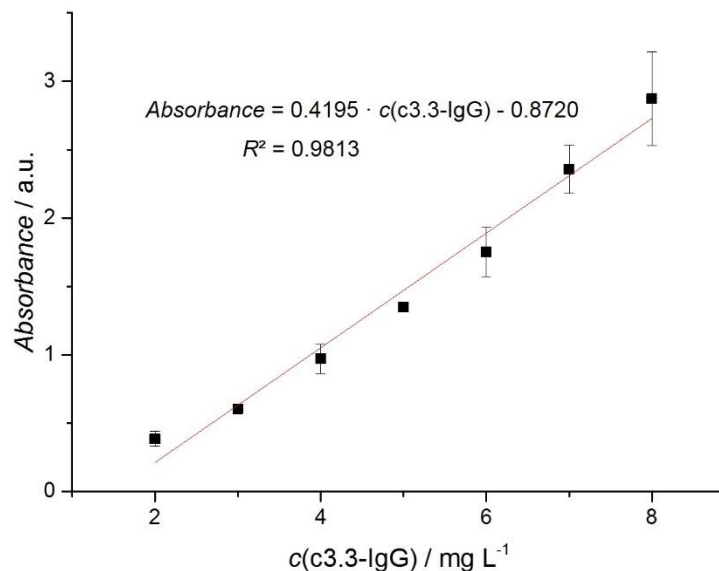
Figure 3.3.1: Calibration curve of the ELISA used in this chapter with c3.3-IgG as standard substance with corresponding linear equation and correlation coefficient (R^2). Mean and standard deviation for all standard samples were determined from triplicates.

The curve is linear in the concentration range between 2 - 8 mg L^{-1} with $R^2 > 0.98$ and, therefore, the concentration range is used for all ELISA calibration curves in the following. For each well plate used in an ELISA experiment, a separate calibration was performed based on the calibration curve shown above. Following that, the concentration of anti-PEG IgG within the normal plasma used in this chapter and the chapters above was analyzed *via* ELISA with an additional competition assay utilizing free PEG (M_w = 10,000 g mol^{-1}, terminal hydroxyl groups) in the solution (see chapter 2.4.2). Like this, the anti-PEG IgG was quantified in pooled plasma from multiple healthy donors (male and female donors, up to 65 years old, relatively high proportion of the age group below 30 years old). The resulting concentrations of anti-PEG IgG in normal plasma are depicted in Figure 3.3.2.
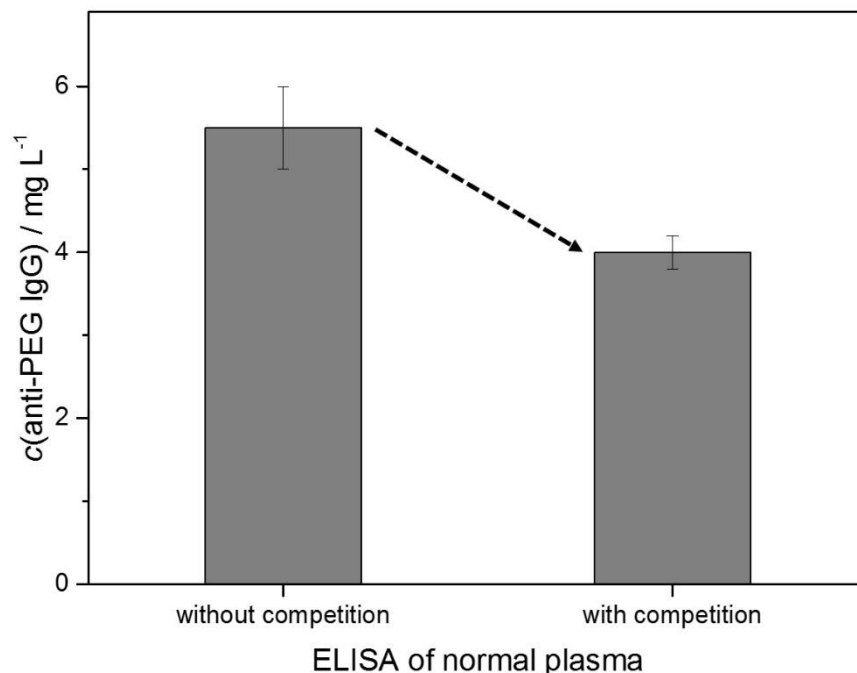
Figure 3.3.2: Concentration of c3.3-IgG in normal plasma *via* ELISA with and without competition using free $PEG_{10,000}$. The arrow indicates the concentration decrease (27%) in the competition assay as validation of specific interactions.

The concentration of anti-PEG IgG in normal plasma was determined to be 5.5 ± 0.5 mg L^{-1} which is in accordance with values found in the study by Chen at al.[22] discussed above, determining the mean concentration of anti-PEG IgG in the blood of Han Chinese blood donors to be between 5.0 and 7.5 mg L^{-1} among donors who were positive on anti-PEG IgG. Therefore, the herein reported value of 5.5 ± 0.5 mg L^{-1} in blood plasma from a supposedly relatively young donor group seems plausible, especially considering that this value includes the blood plasma from potentially anti-PEG IgG-negative donors. Furthermore, the concentration was significantly decreased by 27% in the competition assay to a concentration of 4.0 ± 0.2 mg L^{-1}. This means, that the interaction of the measured IgG was indeed specific to PEG and not solely an unspecific adsorption of any IgG on the well material.

Subsequently, the question arises if such anti-PEG IgG antibodies can be found in the corona of different nanocarriers (especially PEGylated vs. non-PEGylated) and if so, in what quantities they appear. For this, different nanocarriers were used in the course of this study (see Table 3.3.1).

Table 3.3.1: Nanocarriers used for analysis of interaction with anti-PEG IgG.

abbreviation	material	surfactant	hydrodynamic radii *via* multi-angle-DLS / nm	zeta potential / mV
PS-NPs-LUT	polystyrene	Lutensol	52 ± 5	-10 ± 1
PS-NPs-SDS	polystyrene	SDS	53 ± 5	-50 ± 3
PS-NPs-NH$_2$	polystyrene-NH$_2$	CTMA-Cl	48 ± 5	+49 ± 3
PS-NPs-NH$_2$-PEG	polystyrene-NH$_2$ covalently PEGylated	CTMA-Cl	62 ± 6	+7 ± 1
PS-NPs-PMEP	polystyrene	poly(methyl ethylene phosphate) (PMEP)	52 ± 5	-48 ± 1
HES-NCs	hydroxyethyl starch	SDS	112 ± 11	-11 ± 1
SiO$_2$-NCs-CTAC	silica	CTMA-Cl	171 ± 17	-10 ± 1
SiO$_2$-NCs-LUT	silica	Lutensol	87 ± 9	-10 ± 1

For nanocarriers containing PEG on their surface, Lutensol-stabilized polystyrene nanoparticles (PS-NPs-LUT), Lutensol-stabilized silica nanocapsules (SiO$_2$-NCs-LUT), covalently PEGylated amino-functionalized polystyrene nanoparticles (PS-NPs-NH$_2$-PEG) and poly(methyl ethylene phosphate)-stabilized polystyrene nanoparticles (PS-NPs-PMEP) were used. Lutensol is a PEG-hexadecyl ether with an ethyleneoxide length of about 50 units and PMEP is a polyphosphate with PEG-analogue structure (see Figure 3.3.3). PS-NPs-PMEP was produced by Dr. Kristin Bauer as previously published.[129]
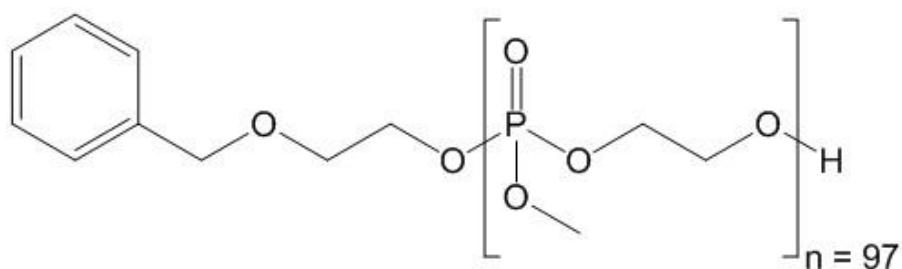
Figure 3.3.3: Chemical structure of PMEP.

The protein coronas of the nanocarriers listed in Table 3.3.1 were prepared according to the same procedure used in the previous chapters (see chapter 4.2.1). After the desorption of proteins from the nanocarriers' surface *via* incubation in an SDS-solution, the isolated protein solution was analyzed in a Pierce assay in order to determine the overall protein solution. However, since not all proteins might be desorbed by incubation in a solution of SDS, especially in case of an interaction with very high binding affinity, a separate assay was performed to determine the amount of proteins that remained on the nanocarriers' surfaces after isolation of the desorbed proteins. This analysis cannot be performed with a Pierce assay, as the presence of the nanocarriers may interfere with the assay's results. For this, an assay based on bicinchoninic acid (BCA) was performed with the nanocarriers after isolation of the corona and resuspension in water (see chapter 4.5), because this assay is independent on the presence of the herein used nanocarriers. The results of both assays (Pierce assay for the proteins detached from the corona and BCA assay for the proteins that remained on the surface of nanocarriers) are shown for six of the used nanocarriers in Figure 3.3.4.
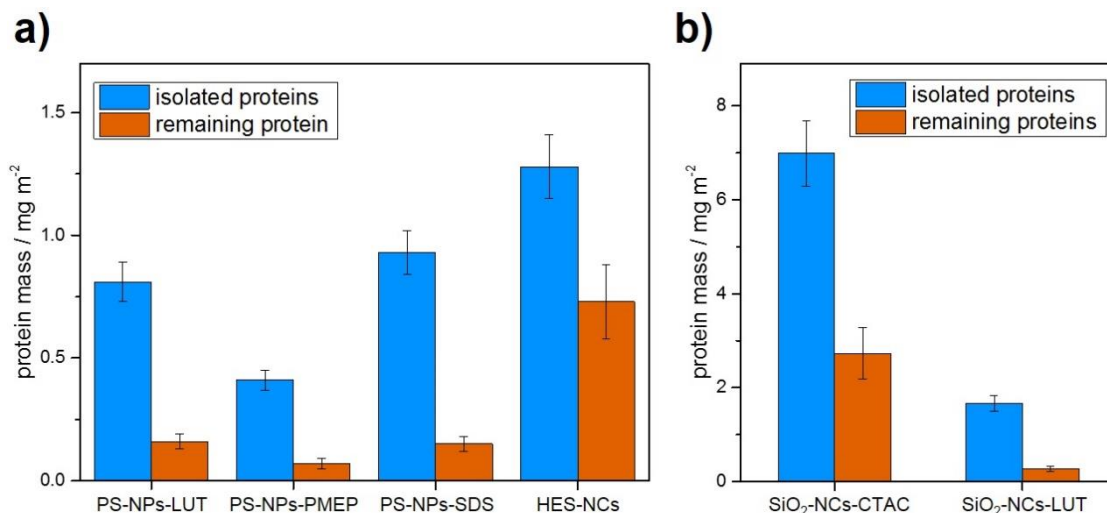
Figure 3.3.4: Protein mass of proteins isolated from the protein corona of different nanocarriers *via* Pierce assay (blue columns) and protein mass of proteins remaining on the surface of nanocarriers after isolation *via* BCA assay (orange column). In the left graph a) protein coronas of PS-NPs-LUT, PS-NPs-NH$_2$, PS-NPs-SDS and HES-NCs are shown, while in the right graph b) protein coronas of SiO$_2$-NCs-CTAC and SiO$_2$-NCs-LUT are shown.

Comparing the mass of proteins isolated from the nanocarriers with the protein mass that remained on their surface after isolation, it is seen that most proteins were detached by treatment with a solution of SDS at high temperature. However, significant amounts of proteins were detected remaining on the surface of the nanocarriers, especially in the case of HES-NCs and SiO$_2$-NCs-CTAC. In the case of HES-NCs, the used dye (Sulforhodamin 101; $\lambda_{Ex.} = 586$ nm, $\lambda_{Em.} = 605$ nm) might interfere with the measurement of the assay at $\lambda = 562$ nm, while in the case of SiO$_2$-NCs-CTAC severe aggregation occurred after incubation in plasma, so that not all proteins may have been removed *via* SDS-treatment. This should be considered in the analysis of the isolated corona proteins in the following, as it might be possible that anti-PEG IgG remains on the surface of nanocarriers and will not be detected in the ELISA – especially if it binds to PEG on the nanocarrier surface with very high binding affinity. In order to determine the concentration of anti-PEG IgG in the corona of all nanocarriers listed in Table 3.3.1, the proteins were isolated from the surface of each nanocarrier *via* desorption with a solution of SDS. Subsequently, the isolated proteins were diluted to reach the same total protein concentration $c_{proteins} = 279$ mg L^{-1} in each sample for comparability of the concentrations of anti-PEG IgG in the corona *via* ELISA. This concentration of total proteins was chosen, because this was the lowest concentration of total

proteins obtained from the eight nanocarriers without further dilution. With the total protein concentration normalized for all eight nanocarriers, the concentration of anti-PEG IgG was determined *via* ELISA (see Table 3.3.2 and Figure 3.3.5).
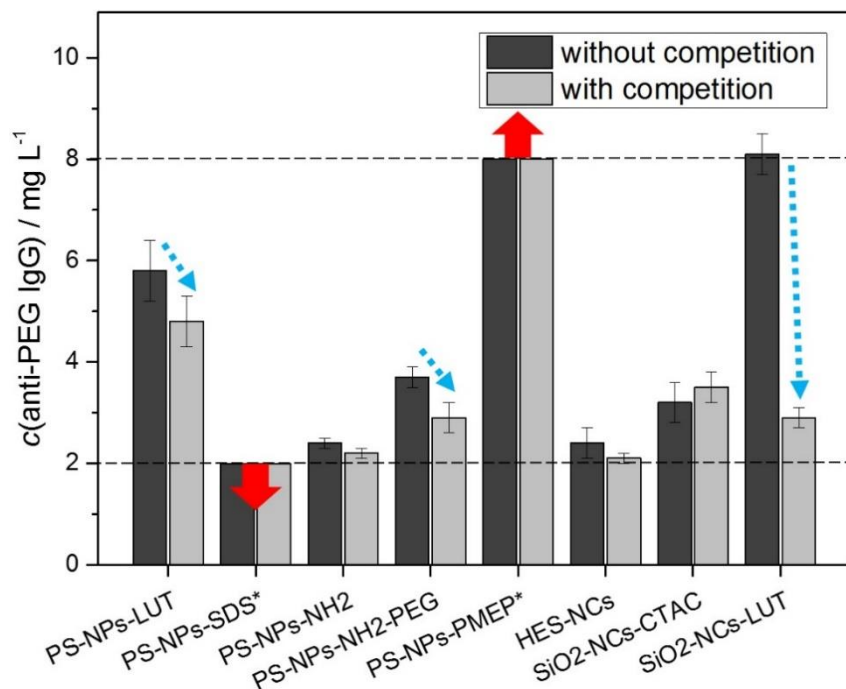
Table 3.3.2: Concentration of anti-PEG IgG from the isolated proteins of different nanocarriers with and without competition using free $PEG_{10,000}$ *via* ELISA.

Nanocarrier	c(anti-PEG IgG) without competition / mg L^{-1}	c(anti-PEG IgG) with competition / mg L^{-1}
PS-NPs-LUT	5.8 ± 0.6	4.8 ± 0.5
PS-NPs-SDS	<2	<2
PS-NPs-NH$_2$	2.4 ± 0.1	2.2 ± 0.1
PS-NPs-NH$_2$-PEG	3.7 ± 0.2	2.9 ± 0.3
PS-NPs-PMEP	>8	>8
HES-NCs	2.4 ± 0.3	2.1 ± 0.1
SiO$_2$-NCs-CTAC	3.2 ± 0.4	3.5 ± 0.3
SiO$_2$-NCs-LUT	8.1 ± 0.4	2.9 ± 0.2

It can be seen that the highest concentrations of anti-PEG IgG were found on the four nanocarriers with surfaces modified with PEG or PEG-based surfactants (PS-NPs-LUT, PS-NPs-NH$_2$-PEG, PS-NPs-PMEP and SiO$_2$-NCs-LUT). While the concentration of anti-PEG IgG isolated from PS-NPs-PMEP was above the highest concentration used for calibration (8 mg L^{-1}), no reduction could be observed in the competition assay. The other three nanocarriers containing PEG on their surface experienced significant reduction in anti-PEG IgG during the competition assay. This highlights the specificity of the interaction between IgG and PEG on the nanocarriers' surface. The proteins isolated from the surface of nanocarriers without PEG were close to LOD and in the case of PS-NPs-SDS even below LOD. Additionally, no significant decrease of IgG measured could be observed for those nanocarriers in the competition assay. Therefore, unspecific adsorption of IgG (including anti-PEG IgG) is observed as well, yet the concentration of anti-PEG IgG is lower for these nanocarriers as anticipated.

Figure 3.3.5: Concentration of anti-PEG IgG from the isolated proteins of different nanocarriers with and without competition using free $PEG_{10,000}$ *via* ELISA. Dashed horizontal lines mark the lowest concentration of the calibration at 2 mg L^{-1} and the highest concentration at 8 mg L^{-1} of anti-PEG IgG. The concentration of nanocarriers marked with "*" were outside of the calibration area and are marked with red arrows. Blue, dashed arrows indicate significant reduction during the competition assay for PS-NPs-LUT, PS-NPs-NH$_2$-PEG and SiO$_2$-NCs-LUT.

The question arises if all anti-PEG IgG molecules were detached from the surface and whether the concentration of anti-PEG IgG determined *via* ELISA will be different if the proteins are not isolated from the nanocarriers surface, but the whole nanoparticle with its protein corona is used for incubation. Therefore, the ELISA was repeated with PS-NPs-LUT including its protein corona, because these nanocarriers are well characterized and show significant amounts of anti-PEG IgG in their corona isolated using SDS (see Figure 3.3.5). However, in this ELISA experiment, the nanoparticles were incubated with the PEG-coated wells for three days instead of the one-hour long incubation of isolated proteins in order to allow re-organization of anti-PEG IgG from the PEG-chains of the NPs to the PEG-coating in the well. While the concentration of anti-PEG IgG in the isolated proteins of PS-NPs-LUT was $5.8 \pm 0.6 \text{ mg L}^{-1}$, incubation with the whole NPs (including the protein corona) resulted in a concentration below LOD

(c(anti-PEG IgG) < 2 mg L^{-1}). It is not plausible that the amount of anti-PEG IgG is higher after their isolation from the surface compared to the original amount of proteins attached to the NPs. This implies that even after three days of incubation, the antibodies did not significantly desorb from the PEG on the NPs and re-adsorb on the immobilized PEG on the bottom of the wells resulting from a strong binding. As a result, the concentrations of anti-PEG IgG could be even higher on the surface of all PEGylated nanocarriers, as it might not be possible detach them fully from the nanocarriers' PEG chains.

To put the amount of anti-PEG IgG into perspective, the amount of all immunoglobulins in plasma and in the protein corona of PS-NPs-LUT was compared with the amount of anti-PEG IgG in both. The respective protein concentrations of plasma and the isolated corona of PS-NPs-LUT are depicted in Figure 3.3.6. For the concentration of all immunoglobulins in plasma, the average Ig concentration in the used plasma of 16.4 ± 3.3 g L^{-1} is shown. For the concentration of all immunoglobulins of the isolated protein corona of PS-NPs-LUT, 8.4 ± 0.8 mg L^{-1} are shown, as the total protein concentration was set to be 279 mg L^{-1} and around 3% of all proteins were shown to be immunoglobulins (see Figure 3.2.6).
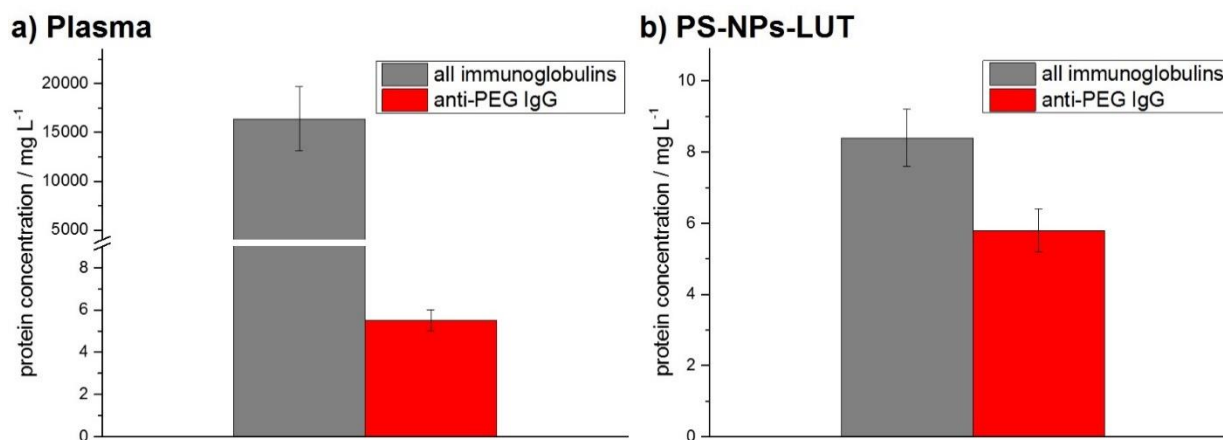
Figure 3.3.6: Protein concentration of all immunoglobulins and anti-PEG IgG in a) plasma and in b) the isolated protein corona of PS-NPs-LUT.

As a result of this comparison, it can be seen that only around 0.03% of all immunoglobulins in plasma are anti-PEG IgG, which correlated well with literature values,[22] while there is a significant enrichment of anti-PEG IgG in the corona of PS-NPs-LUT. In the corona of

PS-NPs-LUT, roughly 66% of all immunoglobulins can be attributed to anti-PEG IgG. It should be noted though, that the absolute amount of immunoglobulins in the protein corona of this nanocarrier is relatively low and it is unclear if all immunoglobulins were detached from the NPs by incubation in SDS. This indicated that while PEGylation can generally prevent most of the unspecific adsorption of immunoglobulins onto nanocarriers, the PEG-chains on the nanocarrier in this case promoted the specific adsorption of anti-PEG IgG.

3.3.3   Conclusion

In conclusion, anti-PEG IgG was quantified in the "normal plasma" used for most projects of this thesis and also in the protein corona of different nanocarriers in the course of this chapter. While anti-PEG IgG could be shown to be present in the corona of most nanocarriers used, a higher concentration of anti-PEG IgG was found in the corona of all nanocarriers stabilized by PEG or PEG-based molecules like Lutensol or PMEP. This stands in contrast to the general reduction of the unspecific adsorption of immunoglobulins on nanocarriers after PEGylation and can be attributed to specific interactions between anti-PEG IgG and the PEG-chains on the nanocarriers. It is unclear whether all molecules of anti-PEG IgG are detached from the nanocarriers' surface by incubation with SDS as significant amounts of proteins remain on the nanocarriers. Therefore, the amount of anti-PEG IgG on each nanocarrier could be higher than measured after protein isolation. Yet, offering the isolated proteins from the corona for one hour yields a higher measured concentration of anti-PEG IgG than offering the whole nanoparticle with its protein corona for three days, indicating a strong binding of the antibody to PEG-chains preventing re-organization. The amount of other anti-PEG antibodies, such as anti-PEG IgM, in the protein corona could be of further interest as well. It has been reported, that multiple injections of PEGylated liposomes induce advances blood clearance (the so-called "ABC phenomenon"), and the question arises if multiple injections of PEGylated nanocarriers lead to a similarly increased concentration of anti-PEG antibodies in blood. In the hypothetical case of a promoted production of anti-PEG antibodies due to the PEGylation of nanocarriers, the consequences of multiple injections during therapy utilizing PEGylated nanocarriers on the protein corona are of utmost importance. It remains to be seen what influence the presence of anti-PEG antibodies in the protein corona may have on the behavior of nanocarriers.

4.   Experimental Part

4.1   Materials

All proteins and chemicals used in experiments for this work were used without further purification. Blood was taken from ten healthy donors at the transfusion center of the university medical center of the Johannes Gutenberg-University Mainz after obtaining their informed consent in accordance with the declaration of Helsinki and after physical examination. Sodium citrate was added to the blood in order to prevent clotting. The citrate-containing blood was centrifuged in order to exclude cellular blood components in the pellet and the supernatant (blood plasma) was pooled, aliquoted and stored at -80 °C. Freshly thawed plasma was centrifuged at 20,000 g for one hour and filtered through Millex-GS 220 nm filters (Merck Millipore, Billerica, USA) before experiments.

All herein used polystyrene NPs were synthesized by Katja Klein (MPI-P) using the miniemulsion (co)polymerization method with styrene, comonomers (in the case of carboxylic nanoparticles: acrylic acid or in the case of amino-functionalized nanoparticles: 2-aminoethyl methacrylate hydrochloride (AEMH)) and Lutensol AT50 (a poly(ethylene oxide)-hexadecyl ether with an ethyleneoxide length of about 50 units) as surfactant as previously published.[130] In brief, a mixture of styrene, the respective comonomer, initiator 2,20-azobis(2-methylbutyronitrile) (V59, Wako Chemicals), hydrophobe (hexadecane) and N-(2,6-diisopropylphenyl)-perylene-3,4-dicarboximide (PMI, BASF) were added to the aqueous phase containing Lutensol AT50. After 1 h of pre-emulsification, the mixture was sonicated (Branson Sonifier (1/2" tip, 6.5 mm diameter) for 2 min at 450 W and 90% amplitude) in an ice-cooled bath. The copolymerization was carried out at 72 °C at 1000 rpm. The resulting NPs were washed five times *via* centrifugation and resuspension in Milli-Q water. Minimal amounts of surfactant remained in the nanoparticle dispersion for preventing agglomeration of the nanomaterials. The used nanoparticles were filtered through Millex-SV 5 µm filters (Merck Millipore, Billerica, USA) before use in order to remove aggregates or potential impurities like dust.

The used hydroxyethyl starch based NCs were synthesized by Katja Klein (MPI-P) using the inverse miniemulsion polymerization method with hydroxyethyl starch (HES, $M_w = 200000$ g mol^{-1}, Fresenius Kabi), the oil-soluble surfactant poly((ethylene-co-butylene)-b-(ethylene oxide)),P(E/B-b-EO), the water-soluble surfactant sodium dodecyl sulfate (SDS), 2,4-Toluene diisocyanate (TDI) and cyclohexane as previously published.[131] In brief, P(E/B-b-EO) was dissolved in cyclohexane and added to an aqueous solution of HES. After 1 h of pre-emulsification, the mixture was sonicated (Branson Sonifier (1/2" tip, 6.5 mm diameter) for 3 min at 450 W and 90% amplitude, 30 s pulse, 20 s pause) in an ice-cooled bath. Afterwards, a clear solution consisting of cyclohexane, P(E/B-b-EO), and TDI was added dropwise to the previously prepared mixture and stirred for 20 h at 25 °C. The resulting NCs were washed twice *via* centrifugation and resuspension in cyclohexane. To transfer the NCs from cyclohexane to water, the dispersion was mixed with an aqueous solution of SDS. The NCs were washed once again and dialyzed for 24 h (14.000 molecular weight cut off) against water.

Silica nanocapsules (SiO$_2$-NCs) were synthesized by Shuai Jiang using an inverse miniemulsion polymerization method as previously published.[132,133] In brief, tetraethoxysilane was mixed with hexadecane and olive oil to form the oil phase. In the second step, 30 mL of an aqueous solution of cetyltrimethylammonium chloride (CTMA-Cl) was poured into the oil mixture under stirring. After a pre-emulsification step by stirring at 1000 rpm for 1 h, the obtained emulsion was sonicated by using a Branson 450 W sonifier with a 1/2'' tip at 70% amplitude for 180 s (30 s of sonication, 10 s of pause) with ice cooling. The resulting miniemulsion was stirred at 1000 rpm for 12 h at room temperature to obtain an aqueous dispersion of SiO$_2$-NCs-CTMA-Cl. SiO$_2$-NCs-LUT were prepared by replacing the templating surfactant CTMA-Cl by the nonionic surfactant Lutensol AT50. Specifically, 35 mg of Lutensol AT50 were added to 2 mL of SiO$_2$-NCs-CTMA-Cl dispersion. The dispersion was stirred at 1000 rpm for 2 h and then dialyzed against water with a dialysis tube with molecular weight cut off of 1000 g mol^{-1}. In this case, CTMA-Cl ($M_w = 320$ g mol^{-1}) could diffuse through the dialysis membrane into the aqueous dialysis medium while Lutensol AT50 ($M_w = 2460$ g mol^{-1}) was kept inside.

A summary of proteins and chemicals used in this work with their respective supplier is listed in Table 4.1. Parts of the experimental part (chapter 4; especially chapter 4.4) were published in the journal *Advanced Science*.[52]

Table 4.1: Summary of proteins and chemicals used in this work with their respective supplier

Protein or chemical substance	Supplier
2,2′-Azino-bis(3-ethylbenzthiazoline-6-sulfonic Acid) (ABTS) (product no. 194434)	Merck (Darmstadt, Germany)
3-[(3-Cholamidopropyl)dimethylammonio]-1-propanesulfonate (CHAPS) (product no. 220201)	Merck (Darmstadt, Germany)
Anti-Human IgG (Fc specific) − Peroxidase antibody (product no. A0170)	Sigma Aldrich (St. Louis, USA)
Apolipoprotein J (Clusterin) (product no. RD172034100-S)	BioVendor (Brno, Czech Republic)
Bovine Serum Albumin (BSA) (product no. 11920)	SERVA Electrophoresis GmbH (Heidelberg, Germany)
Chimeric human anti-PEG IgG (clone no. c3.3‑IgG)	IBMS Academia Sinica (Taipei, Taiwan)
Coomassie Brilliant Blue G-250	SERVA Electrophoresis GmbH (Heidelberg, Germany)
Dulbecco's phosphate buffered saline (PBS)	Thermo Fisher Scientific (Waltham, USA)
Human serum albumin (HSA) (product no. A3782)	Sigma Aldrich (St. Louis, USA)
Immunoglobulin A (IgA) (product no. I4036)	Sigma Aldrich (St. Louis, USA)
Immunoglobulin G (IgG) (product no. I4506)	Sigma Aldrich (St. Louis, USA)
Immunoglobulin M (IgM) (product no. I8260)	Sigma Aldrich (St. Louis, USA)
Ionic detergent compatibility reagent (product no. 22663)	Thermo Fisher Scientific (Waltham, USA)

Lutensol® AT50 (poly(ethylene glycol)-hexadecyl ether)	BASF SE (Ludwigshafen am Rhein, Germany)
Milli-Q water	Merck Millipore (Burlington, USA)
poly(ethylene glycol) (average Mn = 10,000) (product no. 92897)	Sigma Aldrich (St. Louis, USA)
poly(ethylene glycol) diamine (average Mn = 10,000) (product no. 752460)	Sigma Aldrich (St. Louis, USA)
SeeBlue Plus2 Pre-Stained Standard	Thermo Fisher Scientific (Waltham, USA)
Skim milk powder	VWR International (Radnor, USA)
Sodium dodecyl sulfate (SDS) (product no. 39574)	SERVA Electrophoresis GmbH (Heidelberg, Germany)
Styrene	Merck Millipore (Darmstadt, Germany)

4.2   Methods and instrumentation

In the following (chapter 4.2), general descriptions of the methods and instruments that were used are discussed with applicability for all chapters of this thesis. Afterwards (see chapters 4.3 to 4.5), chapter-specific methods and details (e.g. used concentrations) are described.

4.2.1 Protein corona preparation

An aqueous nanoparticle (or nanocapsule) suspension (0.05 m² of surface area in a total volume of 300 µL) was mixed in an Eppendorf-tube with 1 mL of plasma. After 1 h of mild shaking at 37 °C, the sample was centrifuged for 1 h at 20,000 g and 4 °C. The supernatant was discarded and the pellet was resuspended in 1 mL of PBS. The suspension was centrifuged again for 1 h at 20,000 g and 4 °C. These washing steps were repeated three times. Before the last washing step, the suspension was transferred into a new Eppendorf-tube. The resulting pellet contained nanocarriers with proteins in their respective corona.

4.2.2 Sodium dodecyl sulfate polyacrylamide gel electrophoresis (SDS-PAGE)

After the last washing step of the corona preparation (see chapter 4.2.1), the pellet was suspended in 100 µL of a 62.5 mM Tris · HCl solution containing 2 % (w/v) of SDS. The suspension was incubated at 95 °C for 5 minutes and centrifuged for 1 h at 20,000 g and 4 °C. The protein concentration of each sample was determined using a Pierce 660 nm Assay Kit by ThermoFisher (Waltham, USA) with bovine serum albumin (BSA) as standard reagent as described by the manufacturer. A volume of 26 µL of samples containing proteins were mixed with 4 µL of reducing agent and 10 µL of sample buffer. Freshly thawed plasma or pure protein solutions were used as reference samples. After 1 h at 100 V, the electrophoresis was stopped. Staining was performed using a SilverQuest staining Kit (Invitrogen; Carlsbad, USA) as described by the manufacturer or a ready-to-use Coomassie Brilliant Blue (SimplyBlue SafeStain) staining solution for two hours and destaining in ultrapure water over night.

4.2.3 Zeta potential

Zeta potential measurements were performed using a Nano Z Zetasizer (Malvern Instruments GmbH, Herrenberg, Germany). For samples of nanocarriers including their respective protein corona, the pellet was resuspended in 1 mL of water after the last washing step of the protein corona preparation (see chapter 4.2.1). 20 µL of each sample (pure proteins, pure nanocarrier suspension or nanocarriers with protein corona) were diluted with 1 mL of a 1 mM KCl solution and measured instantly at 25 °C after two minutes of equilibration. Each measurement was repeated in triplicate and mean values as well as standard deviations were calculated.

4.2.4 Isothermal titration calorimetry (ITC)

ITC measurements were performed using a NanoITC Low Volume (TA Instruments, Eschborn, Germany) with an effective cell volume of 170 µL. During each experiment 50 µL of a solution of proteins were titrated into 300 µL of an aqueous suspension of nanocarriers. Additionally, the same amount of protein solution was titrated into 300 µL of ultrapure water for determining the dilution heat for reference. The number of injections was set to 25 for each measurement (25 x 2 µL) with a spacing of 250 s between every injection. The integrated heats of dilution were subtracted from the integrated heats of every adsorption measurement. The normalized heats were fitted according to an independent binding model to obtain the association constant (K_a), the reaction enthalpy (ΔH), the entropy (ΔS), the *Gibbs* free energy (ΔG) and the reaction stoichiometry (*n*). Each measurement was carried out in triplicate and the mean value as well as standard deviation for each parameter were calculated. Data evaluation of the ITC measurements was performed using the Nano Analyze Data Analysis Software from TA Instruments. The molecular concentration of nanocarriers was determined from the solid content by assuming particles with spherical morphology and applying the respective radius *via* DLS, the material density and in the case of HES-NCs the shell thickness of the capsules.

4.2.5 Dynamic light scattering (DLS)

DLS measurements were performed using an instrument from ALV (Langen, Germany) consisting of an electronically controlled goniometer and an ALV-5000 multiple τ full-digital correlator with 320 channels with a measurement range between 10^{-7} s and 10^{3} s. A helium-neon laser (Type 1145 P) from JDS Uniphase (Milpitas, USA) of 632.8 nm wavelength and 25 mV output power was used as source of light. Before measurements, samples were filtered into quartz cuvettes for light scattering from Hellma (Müllheim, Germany) with an inner radius of 9 mm. Millex-SV filters (Merck Millipore, Billerica, USA) with 5 µm pore size were used. Prior to use, the quartz cuvettes were cleaned with acetone using a Thurmond apparatus.[134]

4.2.6 Nano Differential Scanning Fluorimetry (nanoDSF)

NanoDSF measurements were performed using a NanoDSF Prometheus NT.48 device with standard capillaries (NanoTemper Technologies, München, Germany). The protein concentration in each sample containing proteins was 1.0 g L^{-1}. Analysis and online monitoring of the nanoDSF measurement was performed using the PR.Controll Data Analysis Software (v1.12.3) from NanoTemper Technologies. Fluorescence of each sample was analyzed at a wavelength of 350 nm and 330 nm. The temperature was increased from 20.0 °C to 95.0 °C at a rate of 0.5 °C min^{-1}.

4.2.7 Liquid chromatography - mass spectrometry (LC-MS)

All LC-MS measurements were performed by Dr. Johanna Simon (MPI-P). LC-MS analysis of protein samples was carried out as described previously.[48,52] Briefly, a nanoACQUITY UPLC system coupled with a Synapt G2-Si mass spectrometer (Waters Corporation) was used. A nanoACQUITY system equipped with a C_{18} analytical reversed-phase column (1.7 μm, 75 μm x 150 mm, Waters Corporation) and a C_{18} nanoACQUITY Trap Column (5 μm, 180 μm x 20 mm, Waters Corporation) were used to separate the tryptic-digested peptides originating from 25 μg total protein. Peptide separation was done with a mobile phase A consisting of 0.1% (v/v) formic acid in water and a mobile phase B consisting of acetonitrile with 0.1% (v/v) formic acid at a flow rate of 0.3 μL min^{-1}, using a gradient of 2 - 40% mobile phase B for 70 min. 150 fmol μL^{-1} Glu-Fibrinopeptide was infused at a flow rate of 0.5 μL min^{-1} as a reference compound. Data-independent acquisition (MSE) experiments were done on the Synapt G2-Si in resolution mode. Electrospray Ionization (ESI) was carried out in positive ion mode using a NanoLockSpray source. Data acquisition was performed in a range of m/z 50-2000 Da with one second scan time and ramped trap collision energy from 20 to 40 V with a total acquisition time of 90 min. All samples were analyzed in two technical replicates. Data were acquired and processed using MassLynx 4.1 and Progenesis QI for proteomics v2.0 software. Data were lock mass corrected after acquisition. As noise reduction thresholds for low energy, high energy and peptide intensity, 120, 25 and 750 counts were used. The protein false discovery rate was set at 4% in database searches. The generated peptide masses were compared to a reviewed human protein sequence database

downloaded from Uniprot. As search criteria, one missed cleavage, maximum protein mass 600 kDa, fixed carbamidomethyl modification for cysteine and variable oxidation for methionine were applied. A peptide required at least two assigned fragments and a protein required at least two assigned peptides and five assigned fragments in order to be identified. Quantitative data were generated based on the TOP3/Hi3 approach, providing the amount of each protein in fmol. The protein corona was prepared as described above.

4.2.8 Transmission electron microscopy (TEM)

TEM micrographs depicted in this dissertation were taken by Christoph Sieber (MPIP). TEM micrographs were taken on a FEI Tecnai F20 transmission electron microscope operated at 200 kV using a 2k CCD (charge-coupled device) camera from Gatan (Type: Ultrascan 1000).

4.3   Interactions of isolated immunoglobulins with differently charged polymer nanoparticles

In the following (chapter 4.3), methods and details regarding experiments of chapter 3.1 specifically are discussed.

4.3.1 Sodium dodecyl sulfate polyacrylamide gel electrophoresis (SDS-PAGE)

For a general procedure regarding SDS-PAGE, see chapter 4.2.2. Staining was performed using a ready to use Coomassie Brilliant Blue (SimplyBlue SafeStain) staining solution for two hours and destaining in ultrapure water over night. In the case of non-reducing SDS-PAGE, the 4 µL of reducing agent in the procedure described above were replaced by 4µL of ultrapure water.

4.3.2 Isothermal titration calorimetry (ITC)

During each experiment, 50 µL of the respective immunoglobulin (c(IgG) = 10 g L^{-1} (6.7 · 10^{-2} mM), c(IgA) = 1.1 g L^{-1} (6.9 · 10^{-3} mM) and c(IgM) = 0.1 g L^{-1} (1.0 · 10^{-4} mM) in PBS) were titrated into 300 µL of an aqueous suspension of the respective nanocarriers. For titrations with IgG: c(nanocarriers) = 19 g L^{-1}, for titrations with IgA: c(nanocarriers) = 1.9 g L^{-1}, for titrations with IgM: c(nanocarriers) = 6.0 g L^{-1}. Additionally, the same amount of immunoglobulin solution was titrated into 300 µL of ultrapure water for determining the dilution heat for reference. The number of injections was set to 25 for each measurement (25 x 2 µL) with a spacing of 250 s between every injection. Each measurement was carried out at 15 °C. For a general procedure regarding ITC-measurements, regard chapter 4.2.4.

4.3.3 Nano Differential Scanning Fluorimetry (nanoDSF)

NanoDSF measurements of immunoglobulin solutions with or without presence of nanocarriers were performed using a NanoDSF Prometheus NT.48 device with standard capillaries (NanoTemper Technologies, München, Germany). The immunoglobulin concentration in each sample containing immunoglobulins was 1.0 g L^{-1} in PBS. Further information concerning the general procedure for nanoDSF measurements can be found in chapter 4.2.6.

4.3.4 Surface charge mapping of immunoglobulins

Crystal structures of IgG and IgA-F$_c$ were downloaded from www.rcsb.org (PDB ID (IgG): 1IGT; PDB ID (IgA-F$_c$): 1OW0). The crystal structure of the IgM F$_c$-domain (PDB ID (IgM-F$_c$): 1O0V) was generated *via* homology modeling with the SWISS-MODEL server (http://swissmodel.expasy.org/) using the template with the highest quality (1o0v.1.B). The IgM-F$_c$ model was calculated based on the target-template alignment *via* energy minimization using the fully-integrated protein structure prediction program PRIME (Schrödinger LLC, New York, NY) in a similar fashion to the recent publication by Hiramoto *et al*.[135] Images of the crystal structures

depicting surface charge mapping were created utilizing the software "Molecular Operating Environment" (MOE 2019.01) by Dr. Seah Ling Kuan (MPI-P). The energy of the 3D structures was minimized applying the MMFF94x force field before plotting the surface map. Red areas in the graphics represent negatively charged patches, while blue areas represent positively charged patches and white areas are of neutral charge.

4.4   The influence of varied immunoglobulin concentrations in blood plasma on the protein corona

In the following (chapter 4.4), methods and details regarding experiments of chapter 3.2 specifically are discussed.

4.4.1 Protein corona preparation

For preparation of the protein corona using IgG-enriched plasma, 200 µL of freshly thawed and centrifuged plasma were diluted with 800 µL of PBS, resulting in 1 mL of plasma (diluted to 20 vol%). 6 mg of IgG were dissolved in 1 mL of 20%-diluted plasma, resulting in IgG-enriched plasma. Nanocarriers were incubated with 66 µL of an aqueous clusterin solution (20 mg L^{-1} in PBS) for 10 minutes at 37°C before addition of IgG-enriched plasma for precoating nanocarriers with clusterin. For the preparation of the protein corona using IgA- or IgM-enriched plasma, 100 µL of freshly thawed and centrifuged plasma were diluted with 900 µL of IgA- or IgM-solution respectively (c(IgA) = 1.1 g L^{-1}, c(IgM) = 0.8 g L^{-1}), resulting in 1 mL of IgA- or IgM-enriched plasma (diluted to 10 vol%). For each sample, an aqueous nanoparticle suspension (0.05 m² of surface area in a total volume of 300 µL) was mixed in an Eppendorf-tube with 1 mL of the respective Ig-enriched plasma. The following preparation steps for the protein corona are as described in chapter 4.2.1.

4.4.2 Isothermal titration calorimetry (ITC)

During each experiment 50 µL of the respective plasma were titrated into 300 µL of an aqueous suspension of PS-NPs ($c = 5.3 \cdot 10^{-5}$ mM) or 300 µL of an aqueous suspension of HES-NCs ($c = 8.2 \cdot 10^{-7}$ mM) respectively. Additionally, the same amount of plasma solution was titrated into 300 µL of ultrapure water for determining the dilution heat for reference. The number of injections was set to 25 for each measurement (25 x 2 µL) with a spacing of 250 s between every injection. Each measurement was carried out at 15 °C. For a general procedure regarding ITC-measurements, see chapter 4.2.4.

4.4.3 Cell culture

All cell culture experiments were performed by Jorge Pereira (MPI-P). The murine macrophage cell line RAW264.7, human HeLa and THP-1 cell lines were maintained in RPMI-1640 medium supplemented with 10% fetal calf serum (FCS) and 100 U mL^{-1} penicillin (all from Gibco, Germany) at 37 °C with 5% CO_2 in an incubator.

4.4.4 THP-1 Macrophage differentiation

THP-1 macrophage differentiation was performed by Jorge Pereira (MPI-P). The human monocyte cell line THP-1 was differentiated into macrophages prior the experiments with the nanocarriers for 5 days. On day 0 the cells were stimulated with 100 ng mL^{-1} of phorbol 12-myristate 13-acetate (PMA) (Sigma-Aldrich, Germany) and seeded at a density of 150 000 cells per well in 24-well plates. After 2 days, the medium was changed to fresh RPMI without PMA and the cells rested for the following 3 days before the experiment.

4.4.5 Cell Blocking experiments with antibodies

All cell blocking experiments with antibodies were performed by Jorge Pereira (MPI-P). For the cell blocking experiments, purified anti-CD64, CD16 and/or CD32 (BioLegend, USA) were added to the cells at 5 µg mL^{-1} in fresh serum-free medium for 30 minutes at 37 °C before the respective samples. After the incubation, the nanoparticles were added to the wells and the cells incubated according to the time-points described below. No washing step was performed after the incubation with the antibodies.

4.4.6 Cell uptake experiments and flow cytometry measurements

All cell uptake experiments and flow cytometry measurements were performed by Jorge Pereira (MPI-P). For the cell uptake experiments, cells were seeded at a density of 150,000 cells per well in 24-well plates. The cells were incubated in fresh serum-free medium with the nanocarrier dispersions added at a concentration of 75 µg mL^{-1} to the cells for 2 h (RAW 264.7 and THP-1) or 16 h (HeLa cells). For flow cytometry experiments, adherent cells were washed with PBS and detached from the culture vessel with 2.5% trypsin (Gibco, Germany) and measurements were performed on the Attune Nxt cytometer (Invitrogen, Germany) with a 488 nm laser for excitation of BODIPY and a 561 nm laser for excitation of Sulforhodamine. The viability of the cells was measured by staining with the viability dye Zombie Aqua (BioLegend, USA) according to the manufacturer's instruction, prior the flow cytometry measurements. A 405 nm laser was used for the excitation of the Zombia Aqua dye.

4.4.7 Sodium dodecyl sulfate polyacrylamide gel electrophoresis (SDS-PAGE)

For a general procedure regarding SDS-PAGE, see chapter 4.2.2. Staining was performed using a SilverQuest staining Kit (Invitrogen; Carlsbad, USA) as described by the manufacturer.

4.4.8 Depletion of IgG from citrate plasma *via* high-performance liquid chromatography (HPLC)

An HPLC system by Agilent Technologies (1200 series, Santa Clara, USA) with an UV/VIS-detector by Soma optics (S-3702, Tokyo, Japan) was used for the separation of IgG from citrate plasma. A ToyoScreen AF-rProtein A HC-650F column (1 mL; Tosoh Bioscience, Griesheim, Germany) was used for fractionation with 10mM Tris · HCl (pH = 7.4) as running buffer. The flow rate was set to be 0.5 mL min^{-1}; the pressure within the system was monitored during the whole experiment and did not exceed three bar. Human citrate plasma was freshly thawed, centrifuged for 30 min at 4 °C and 20,000 g, diluted to a final concentration of 33 % (v/v) with running buffer and filtered through Millex-LCR (450 nm, Merck Millipore, Billerica, USA) filters. The system was purged with running buffer for 30 min before loading 0.5 mL of plasma (c = 33% (v/v)) onto the column. The flow-through containing IgG-depleted plasma was collected between 60 to 300 s after the injection of plasma. Roughly 10 min after the flow-through was collected, 2 mL of 0.2 M citric acid were injected in order to detach IgG bound to the column material. Between 60 s and 240 s after the injection of citric acid, the fraction containing separated IgG was collected.

4.4.9 Salt exchange of IgG-depleted plasma

The IgG-depleted plasma obtained after elution *via* HPLC (see chapter 4.3.5) was desalted using a PD-10 desalting column from GE Healthcare (Chicago, USA) in order to remove the Tris · HCl buffer used in the plasma fractionation process (see chapter 4.3.5). 2.5 mL of IgG-depleted plasma were loaded onto the desalting column and the "gravity protocol" was followed as described by the manufacturer with Milli-Q water as elution medium. In brief, the column storage solution was discarded and the column was washed for four times with Milli-Q water before use. Afterwards, 2.5 mL of IgG-depleted plasma were added to the column and allowed to enter the bed. The flow-through was discarded. Eight fractions were collected (with a volume of 1 mL each) and the presence of proteins in each fraction was analyzed *via* Pierce 660 nm

protein assay (Thermo Scientific, Rockford, USA) according to the instructions by the manufacturer with BSA as protein standard. Fractions no. 3 to 6 contained proteins and were combined. 4 mL of (salt-free) IgG-depleted plasma were mixed with 444 µL of 10x phosphate buffered saline (PBS) in order to restore a more physiological salt environment for the plasma proteins.

4.5   Anti-PEG immunoglobulin G in the protein corona

In the following (chapter 4.5), methods and details regarding experiments of chapter 3.3 specifically are discussed. The concentration of anti-PEG immunoglobulin G in plasma and proteins from the protein corona of different nanocarriers was analyzed *via* Enzyme-linked immunosorbent assay (ELISA). Chimeric human anti-PEG IgG (clone no. c3.3 IgG) was purchased from IBMS Academia Sinica (Taipei, Taiwan) and used as a standard for calibration without further purification. Fundamentally, the procedure published by Chen *et al*. was followed.[22] For standard solutions, the stock solution of chimeric human anti-PEG IgG of $c = 220\,\mu g\,mL^{-1}$ ($1.47 \cdot 10^{-3}\,mM$) was diluted with 2 % (w/v) skim milk in PBS to final concentrations of 8, 7, 6, 5, 4, 3, 2 and 0 µg mL^{-1}. 50 µL of poly(ethylene glycol) diamine (10 mg L^{-1} in 0.1 M NaHCO$_3$/Na$_2$CO$_3$) were added in each well of a Maxisorp 96-well plate (Thermo Fisher Scientific, Waltham, USA) and incubated at 4 °C over night. After discarding of the wells' content, 200 µL of 5 % (w/v) skim milk in PBS were added to each well and incubated for 2 h at room temperature. The content of the wells was then discarded and each well was washed with 100 µL of PBS. In wells where no competition took place, 50 µL of 2 % (w/v) skim milk in PBS were added, while in wells where a competition experiment took place, 50 µL of poly(ethylene glycol) (5 g L^{-1} in 2 % (w/v) skim milk in PBS) were added. The wells were incubated for 30 min at room temperature. For each sample (including standards), 60 µL of sample were diluted with 120 µL of 2 % (w/v) skim milk in PBS (33%-dilution). 50µL of these 33%-diluted samples were added in the respective well (with or without PEG for competition) and incubated for 1 h at room temperature. The content of the wells was discarded and each well was washed twice with 100 µL of 0.1 % (w/v) CHAPS in PBS and then washed once with 100 µL of pure PBS. Afterwards, 50 µL of anti-human IgG - peroxidase antibody (0.25 mg L^{-1} in 2 % (w/v) skim milk in PBS, Fc-specific) were

added to each well and incubated for 1 h at room temperature. The content of wells was discarded and each well was washed four times with 100 µL 0.1 % (w/v) CHAPS in PBS and once with 100 µL PBS. After the last washing step, 100 µL of ABTS solution were added to each well and incubated for 30 min in the dark at room temperature. The absorbance was measured at $\lambda = 405$ nm. For the measurement of normal citrate plasma, 600 µL of plasma were diluted with 400 µL of 5 % (w/v) skim milk in PBS (60% dilution). For the determination of the method's limit of detection (LOD) and limit of quantification (LOQ), ten blank samples (2 % (w/v) skim milk in PBS) were measuered. LOD and LOQ were calculated in accordance with DIN 32645. For the measurement of proteins on the surface of nanocarriers, the protein corona for each NC was prepared according to chapter 4.2.1. After the last washing step, the pellet was suspended in 100 µL of a 62.5 mM Tris · HCl solution containing 2 % (w/v) of SDS. The suspension was incubated at 95 °C for 5 minutes and was centrifuged for 1 h at 20,000 g and 4 °C. The protein concentration of each sample was determined using a Pierce 660 nm Assay Kit by ThermoFisher (Waltham, USA) with bovine serum albumin (BSA) as standard reagent as described by the manufacturer. The concentration of proteins attached to the nanocarriers' surface after detachment with SDS was determined using a bicinchoninic acid (BCA) assay kit by ThermoFisher (Waltham, USA) with bovine serum albumin (BSA) as standard reagent as described by the manufacturer. Each protein corona sample was diluted with 2 % (w/v) skim milk in PBS in order to achieve similar (total) protein concentration (279 µg mL^{-1}) before measurement as samples *via* ELISA. Each sample was measured in triplicate, mean and standard deviation were calculated.

5.   **Summary and Outlook**

In this work, the interactions between nanocarriers and blood proteins with special regard to immunoglobulins were studied thoroughly. Binding mechanisms and the consequences of nanoparticle-immunoglobulin interactions on the physicochemical properties of both, nanocarriers and immunoglobulins, were investigated. Subsequently, the influence of specific and unspecific binding of different immunoglobulins to different nanocarriers in blood plasma was illuminated. Furthermore, the effect of varied, physiologically relevant immunoglobulin concentrations in blood plasma on the composition of the protein corona was investigated in detail. As PEGylation is a common method of extending the circulation time of nanocarriers, PEG-binding IgG was quantified in the corona of different PEGylated and non-PEGylated nanocarriers in order to investigate if PEG on the surface of nanocarriers leads to promoted binding of these anti-PEG IgG antibodies.

First, the influence of different immunoglobulins isolated from blood serum in the protein corona of differently charged polystyrene nanoparticles was investigated. While all immunoglobulins were present on the nanoparticles' surface, immunoglobulins influenced the physico-chemical properties of nanoparticles upon interaction and *vice versa*. The surface charge of nanoparticles was influenced by adsorption of immunoglobulins and in some cases aggregation processes were induced. This was especially the case for interactions between IgG and nanoparticles with differently charged functional groups. Therefore, nanoparticles with neutral surface charge exhibited less unfavorable interaction with immunoglobulins. While IgA and IgM expressed mostly weak interactions with nanoparticles, IgG underwent stronger hydrophobic interactions with unfunctionalized polystyrene nanoparticles and more hydrophilic interactions with carboxylic or amino-functionalized nanoparticles. Only for the adsorption of IgM on carboxylic nanoparticles, strong electrostatic interactions were observed, which did not result in dominant bridging and aggregation processes. Adsorption of IgG on charged nanoparticles resulted in significant aggregation. All Igs appeared to be denatured on the surface of polystyrene nanoparticles with the possible consequence of (unwanted) reactions of the immune system. From this it can be concluded, that unfavorable NP-Ig interactions can be reduced by designing

nanocarriers with (close to) neutral surface charge. As hydrophobic interactions play an important role in NP-Ig interactions, forming nanocarriers of more hydrophilic materials should further minimize these interactions.

After the interactions between nanocarriers and Igs have been characterized by investigating isolated proteins, the influence of these NP-Ig interactions on the protein corona in whole blood plasma was studied. For this, the protein corona composition of different nanocarriers was compared after incubation in normal blood plasma and blood plasma of varied, physiologically relevant immunoglobulin concentrations. Therefore, the pooled plasma was modified by adding commercially available IgG, IgA or IgM from human serum or by decreasing the IgG concentration *via* fractionation by HPLC.

In all four cases, a significant alteration of the protein corona was observed compared to the normal plasma. In the cases where one Ig class was enriched in the plasma, the corresponding Ig fractions were also enriched in the protein corona while decreasing the amount of other proteins, such as clusterin. Upon doubling the concentration of IgG in plasma, the fraction of IgG in the protein corona of different nanocarriers was elevated roughly by a factor of 40. This promoted adsorption of IgG in IgG-enriched plasma was further analyzed and resulted in a promoted uptake in human and murine macrophages *via* F_c-receptor mediated endocytosis, as supported by F_c-blocking experiments. In ITC experiments, it was observed that the binding parameters of proteins in normal and IgG-enriched plasma differed significantly and in case of IgG-enriched plasma were more similar to the binding parameters of isolated IgG on the nanocarriers. Thus, the mechanism of interaction of the proteins overall differed comparing both plasmas. The IgG-enrichment-effect on the protein corona in IgG-enriched plasma could be prevented successfully by pre-coating of nanocarriers with the protein clusterin, which additionally reduced cellular internalization.

A similar enrichment of IgA- or IgM-fractions in the protein corona of different nanocarriers was observed after incubation in IgA- or IgM-enriched plasma. Completely removing IgG from the pooled plasma also resulted in an altered protein corona composition. This could be due to a change of protein-protein interactions or a possible change of other proteins' structure after the isolation process of IgG from pooled plasma.

Therefore, studies on the protein corona in pooled blood plasma from healthy donors did not generally correlate with the protein corona in the blood of individuals, particularly in the case of diseases altering immunoglobulin concentrations in blood. However, the influence of the individual blood composition on the biological fate of nanocarriers could be reduced by pre-coating the nanocarriers with clusterin or potentially other stealth proteins with high binding affinities. This suggests the engineering of nanocarriers with body-own materials, such as specific blood components, to be a powerful method in order to achieve universally applicable nanomedicines. Using this general method, more control over the protein corona formation process could be gained and, therefore, could pave the way to more successful translation of nanocarriers into precision medicine. Further studies are needed to minimize the influence of individual factors on the protein corona of nanocarriers in order to guarantee their universally safe use in medicine.

After investigating unspecific interactions between different nanocarriers and Igs, specific antibody-antigen interactions were investigated. One specific interaction which could occur between nanocarriers and Igs could be between PEG-binding Igs and PEG-chains on the surface of nanocarriers. Therefore, anti-PEG IgG was quantified in blood plasma and in the protein corona of different (PEGylated and non-PEGylated) nanocarriers *via* enzyme-linked immunosorbent assay (ELISA) and confirmed by a competition assay. A key question was whether or not the presence of PEG-chains on the surface nanocarriers ultimately leads to specific interactions with anti-PEG IgG.

The concentration of anti-PEG IgG in normal plasma was determined to be 5.5 ± 0.5 mg L^{-1} which corresponds to roughly 0.03% of all immunoglobulins in the blood proteome. Comparing PEGylated and non-PEGylated nanocarriers, a higher concentration of anti-PEG IgG was found in the corona of all nanocarriers stabilized by PEG or PEG-based molecules like Lutensol. Considering that the overall concentration of all immunoglobulins was relatively low on some of these nanocarriers (e.g. roughly 3% of all proteins in the corona of PS-NPs stabilized by Lutensol), the amount of anti-PEG binding IgG on these nanoparticles was relatively high (around 66% of all immunoglobulins in the corona of Lutensol-stabilized PS-NPs).

This stands in contrast to the general reduction of the unspecific Ig adsorption on nanocarriers after PEGylation and can be attributed to specific interactions between anti-PEG IgG and the PEG-chains on the nanocarriers. Additionally, not all molecules of anti-PEG IgG were detached from the nanocarriers' surface by incubation with SDS as significant amounts of proteins remained on the nanocarriers. Therefore, the amount of anti-PEG IgG on each nanocarrier could be higher than measured after protein isolation. Yet, offering the isolated proteins from the corona yielded a higher measured concentration of anti-PEG IgG than offering the whole nanoparticle with its protein corona for three days. This means that the binding of anti-PEG IgG to PEG-chains is so strong, that they cannot be detached from each other with complete certainty.

The amount of other anti-PEG antibodies, such as anti-PEG IgM, in the protein corona could be of further interest as well, as these are also produced by the organism as a result of using products containing PEG. Furthermore, it remains to be seen what influence the presence of anti-PEG antibodies may have on the behavior of nanocarriers in vitro and in vivo. Furthermore, the continuous use of nanocarriers, which utilize PEG or PEG-based materials, could induce the production of more anti-PEG IgG in blood resulting in a possible increase of these antibodies in the corona. This means that, ultimately, it is unclear if the use of PEGylated nanocarriers in biomedical applications is viable in general and further research is needed to understand the influence of these specific nanocarrier-protein interactions on the fate of the nanocarriers. The use of materials other than PEG for stabilization of nanocarriers, which induce a similar stealth effect in the protein corona could be a way to circumvent this obstacle.

In conclusion, the importance and mechanism of the interactions between nanocarriers and immunoglobulins were elucidated. New insights on the relevance of individual immunoglobulin levels in blood plasma on the entire protein corona, including stealth proteins, was gained including different interactions of nanocarriers with cells of the immune system. Furthermore, pre-coating of nanocarriers with the stealth protein clusterin was shown to be a powerful method to reduce the influence of the individual blood composition on the biological fate of nanocarriers. The knowledge gained in this work could pave the way to gain control over the behavior of nanocarriers in biological media and help to reduce unwanted activation of immune responses upon their administration.

Bibliography

1. Lin, W., Introduction: Nanoparticles in Medicine. *Chem. Rev.*, **2015**, *115*(19), 10407–10409.

2. Caracciolo, G., Farokhzad, O., and Mahmoudi, M., Biological Identity of Nanoparticles In Vivo: Clinical Implications of the Protein Corona. *Trends Biotechnol.*, **2017**, *35*(3), 257-264.

3. Lynch, I. and Dawson, K., Protein-nanoparticle interactions. *Nano Today*, **2008**, *3*(1-2), 40-47.

4. Lynch, I., Salvati, A., and Dawson, K., Protein-nanoparticle interactions: What does the cell see? *Nat. Nanotechnol.*, **2009**, *4*, 546-547.

5. Cedervall, T., Lynch, I., Lindman, S., Berggård, T., Thulin, E., Nilsson, H., Dawson, K.A., and Linse, S., Understanding the nanoparticle–protein corona using methods to quantify exchange rates and affinities of proteins for nanoparticles. *Proceedings of the National Academy of Sciences*, **2007**, *104*(7), 2050.

6. Owens, D.E. and Peppas, N.A., Opsonization, biodistribution, and pharmacokinetics of polymeric nanoparticles. *International Journal of Pharmaceutics*, **2006**, *307*(1), 93-102.

7. Lundqvist, M., Stigler, J., Elia, G., Lynch, I., Cedervall, T., and Dawson, K., Nanoparticle size and surface properties determine the protein corona with possible implications for biological impacts. *Proc. Natl. Acad. Sci. U.S.A.*, **2008**, *105*(38), 14265-14270.

8. Müller, J., Bauer, K.N., Prozeller, D., Simon, J., Mailänder, V., Wurm, F.R., Winzen, S., and Landfester, K., Coating nanoparticles with tunable surfactants facilitates control over the protein corona. *Biomaterials*, **2017**, *115*, 1-8.

9. Winzen, S., Schoettler, S., Baier, G., Rosenauer, C., Mailänder, V., Landfester, K., and Mohr, K., Complementary analysis of the hard and soft protein corona: sample preparation critically effects corona composition. *Nanoscale*, **2015**, *7*, 2992-3001.

10. Schöttler, S., Becker, G., Winzen, S., Steinbach, T., Mohr, K., Landfester, K., Mailänder, V., and Wurm, F.R., Protein adsorption is required for stealth effect of poly(ethylene glycol)- and poly(phosphoester)-coated nanocarriers. *Nat Nano*, **2016**, *11*(4), 372-377.

11. Ritz, S., Schöttler, S., Kotman, N., Baier, G., Musyanovych, A., Kuharev, J., Landfester, K., Schild, H., Jahn, O., Tenzer, S., and Mailänder, V., Protein Corona of Nanoparticles: Distinct Proteins Regulate the Cellular Uptake. *Biomacromolecules*, **2015**, *16*(4), 1311-1321.

12.   Schöttler, S., Landfester, K., and Mailänder, V., Controlling the Stealth Effect of Nanocarriers through Understanding the Protein Corona. *Angew.Chem.Int. Ed.*, **2016**, *55*, 8806-8815.

13.   French, M.A.H., Immunoglobulins in Health and Disease. **1986**, *DOI: 10.1007/978-94-009-4169-4*.

14.   Treuel, L., Docter, D., Maskos, M., and Stauber, R.H., Protein corona – from molecular adsorption to physiological complexity. *Beilstein Journal of Nanotechnology*, **2015**, *6*, 857-873.

15.   Müller, L., Simon, J., Rosenauer, C., Mailänder, V., Morsbach, S., and Landfester, K., The Transferability from Animal Models to Humans: Challenges Regarding Aggregation and Protein Corona Formation of Nanoparticles. *Biomacromolecules*, **2018**, *19*(2), 374-385.

16.   Corbo, C., Molinaro, R., Tabatabaei, M., Farokhzad, O.C., and Mahmoudi, M., Personalized protein corona on nanoparticles and its clinical implications. *Biomater. Sci.*, **2017**, *5*, 378-387.

17.   Schöttler, S., Klein, K., Landfester, K., and Mailänder, V., Protein source and choice of anticoagulant decisively affect nanoparticle protein corona and cellular uptake. *Nanoscale*, **2016**, *8*, 5526-5536.

18.   Upton, J., Immunodeficiencies with hypergammaglobulinemia: a review. *LymphoSign Journal*, **2014**, *2*(2), 57-73.

19.   D. Howard, M., Jay, M., Dziubla, T., and Lu, X., *PEGylation of Nanocarrier Drug Delivery Systems: State of the Art*. Vol. 4. 2008. 133-148.

20.   Kang, B., Okwieka, P., Schöttler, S., Winzen, S., Langhanki, J., Mohr, K., Opatz, T., Mailänder, V., Landfester, K., and Wurm, F., Carbohydrate-Based Nanocarriers Exhibiting Specific Cell Targeting with Minimum Influence from the Protein Corona. *Angew. Chem. Int. Ed.*, **2015**, *54*(25), 7436-7440.

21.   Hershfield, M.S., Ganson, N.J., Kelly, S.J., Scarlett, E.L., Jaggers, D.A., Sundy, J.S.J.A.R., and Therapy, Induced and pre-existing anti-polyethylene glycol antibody in a trial of every 3-week dosing of pegloticase for refractory gout, including in organ transplant recipients. **2014**, *16*(2), R63.

22.   Chen, B.-M., Su, Y.-C., Chang, C.-J., Burnouf, P.-A., Chuang, K.-H., Chen, C.-H., Cheng, T.-L., Chen, Y.-T., Wu, J.-Y., and Roffler, S.R., Measurement of Pre-Existing IgG and IgM Antibodies against Polyethylene Glycol in Healthy Individuals. *Analytical Chemistry*, **2016**, *88*(21), 10661-10666.

23.   Richter, A.W. and Åkerblom, E., Polyethylene Glycol Reactive Antibodies in Man: Titer Distribution in Allergic Patients Treated with Monomethoxy Polyethylene Glycol Modified Allergens or Placebo, and in Healthy Blood Donors. *International Archives of Allergy and Immunology*, **1984**, *74*(1), 36-39.

24.   Cheng, T.-L., Wu, P.-Y., Wu, M.-F., Chern, J.-W., and Roffler, S.R., Accelerated Clearance of Polyethylene Glycol-Modified Proteins by Anti-Polyethylene Glycol IgM. *Bioconjugate Chemistry*, **1999**, *10*(3), 520-528.

25.   Wang, X., Ishida, T., and Kiwada, H., Anti-PEG IgM elicited by injection of liposomes is involved in the enhanced blood clearance of a subsequent dose of PEGylated liposomes. *Journal of Controlled Release*, **2007**, *119*(2), 236-244.

26.   Suzuki, T., Ichihara, M., Hyodo, K., Yamamoto, E., Ishida, T., Kiwada, H., Ishihara, H., and Kikuchi, H., Accelerated blood clearance of PEGylated liposomes containing doxorubicin upon repeated administration to dogs. *International Journal of Pharmaceutics*, **2012**, *436*(1), 636-643.

27.   Berg, J.M., Tymoczko, J.L., and Stryer, L., *Biochemistry, Sixth edition*. 2007, Munich: Elsevier.

28.   Everett, D.H., Basic principles of colloid science. *Royal Society of Chemistry*, **1988**.

29.   Atkins, P.W. and de Paula, J., *Physikalische Chemie*. 2006, Weinheim: Wiley-VCH.

30.   Martin, E.A., Concise medical dictionary. *Oxford University Press*, **2010**.

31.   Anderson, N.L. and Anderson, N.G., The Human Plasma Proteome. *History, Character, and Diagnostic Prospects*, **2002**, *1*(11), 845-867.

32.   Peters, T., All about Albumin: Biochemistry, Genetics, and Medical Applications. *Academic Press, San Diego, CA* **1996**.

33.   Gonzalez-Quintela, A., Alende, R., Gude, F., Campos, J., Rey, J., Meijide, L.M., Fernandez-Merino, C., and Vidal, C., Serum levels of immunoglobulins (IgG, IgA, IgM) in a general adult population and their relationship with alcohol consumption, smoking and common metabolic abnormalities. *Clinical & Experimental Immunology*, **2008**, *151*(1), 42-50.

34.   Sigma Aldrich, https://www.sigmaaldrich.com/content/dam/sigma-aldrich/docs/Sigma/General_Information/hupoaqua.pdf (accessed 22.05.2019).

35.   Haab, B.B., Geierstanger, B.H., Michailidis, G., Vitzthum, F., Forrester, S., Okon, R., Saviranta, P., Brinker, A., Sorette, M., Perlee, L., Suresh, S., Drwal, G., Adkins, J.N., and Omenn, G.S., Immunoassay and antibody microarray analysis of the HUPO Plasma Proteome Project reference specimens: Systematic variation between sample types and calibration of mass spectrometry data. *PROTEOMICS*, **2005**, *5*(13), 3278-3291.

36.   Tu, C., Rudnick, P.A., Martinez, M.Y., Cheek, K.L., Stein, S.E., Slebos, R.J.C., and Liebler, D.C., Depletion of Abundant Plasma Proteins and Limitations of Plasma Proteomics. *Journal of Proteome Research*, **2010**, *9*(10), 4982-4991.

37.   Matsumura, Y. and Kataoka, K., Preclinical and clinical studies of anticancer agent-incorporating polymer micelles. *Cancer Science*, **2009**, *100*(4), 572-579.

38.   Landfester, K., Bechthold, N., Tiarks, F., and Antonietti, M., Formulation and Stability Mechanisms of Polymerizable Miniemulsions. *Macromolecules*, **1999**, *32*(16), 5222-5228.

39.   Vogler, E., Protein adsorption in three dimensions. *Biomaterials*, **2012**, *33*, 1201-1237.

40.   Treuel, L. and Nienhaus, G., Towards a molecular understanding of nanoparticle-protein interactions. *Biophys Rev*, **2012**, *4*, 137-147.

41.   Nel, A.E., Mädler, L., Velegol, D., Xia, T., Hoek, E.M.V., Somasundaran, P., Klaessig, F., Castranova, V., and Thompson, M., Understanding biophysicochemical interactions at the nano–bio interface. *Nature Materials*, **2009**, *8*, 543.

42.   Docter, D., Strieth, S., Westmeier, D., and Hayden, O., No king without a crown - impact of the nanomaterial-protein corona on nanobiomedicine. *Nanomedicine (Lond.)*, **2015**, *10*(3), 503-519.

43.   Monopoli, M.P., Walczyk, D., Campbell, A., Elia, G., Lynch, I., Baldelli Bombelli, F., and Dawson, K.A., Physical−Chemical Aspects of Protein Corona: Relevance to in Vitro and in Vivo Biological Impacts of Nanoparticles. *Journal of the American Chemical Society*, **2011**, *133*(8), 2525-2534.

44.   Vroman, L., Effect of Adsorbed Proteins on the Wettability of Hydrophilic and Hydrophobic Solids. *Nature*, **1962**, *196*, 476-477.

45.   Tenzer, S., Docter, D., Rosfa, S., Wlodarski, A., Kuharev, J., Rekik, A., Knauer, S.K., Bantz, C., Nawroth, T., Bier, C., Sirirattanapan, J., Mann, W., Treuel, L., Zellner, R., Maskos, M., Schild, H., and Stauber, R.H., Nanoparticle Size Is a Critical Physicochemical Determinant of the Human Blood Plasma Corona: A Comprehensive Quantitative Proteomic Analysis. *ACS Nano*, **2011**, *5*(9), 7155-7167.

46.   Simon, J., Wolf, T., Klein, K., Landfester, K., Wurm, F.R., and Mailänder, V., Hydrophilicity Regulates the Stealth Properties of Polyphosphoester-Coated Nanocarriers. **2018**, *57*(19), 5548-5553.

47.   Vogler, E.A., Interfacial Chemistry in Biomaterials Science. *In: Berg J, editor. Wettability. Marcel Dekker; New York*, **1993**, 184-250.

48.   Müller, J., Prozeller, D., Ghazaryan, A., Kokkinopoulou, M., Mailänder, V., Morsbach, S., and Landfester, K., Beyond the protein corona – lipids matter for biological response of nanocarriers. *Acta Biomater.*, **2018**, *71*, 420-431.

49.   Krishnan, A., Sturgeon, J., Siedlecki, C.A., and Vogler, E.A., Scaled interfacial activity of proteins at the liquid–vapor interface. **2004**, *68A*(3), 544-557.

50.   Claesson, P.M., Blomberg, E., Fröberg, J.C., Nylander, T., and Arnebrant, T., Protein interactions at solid surfaces. *Advances in Colloid and Interface Science*, **1995**, *57*, 161-227.

51.   Horbett, T.A., *Protein Adsorption on Biomaterials*, in *Biomaterials: Interfacial Phenomena and Applications*. 1982, AMERICAN CHEMICAL SOCIETY. p. 233-244.

52.   Prozeller, D., Pereira, J., Simon, J., Mailänder, V., Morsbach, S., and Landfester, K., Prevention of Dominant IgG Adsorption on Nanocarriers in IgG-Enriched Blood Plasma by Clusterin Precoating. *Advanced Science*, **2019**, *6*(10), 1802199.

53.   Huang, R. and Lau, B.L.T., Biomolecule–nanoparticle interactions: Elucidation of the thermodynamics by isothermal titration calorimetry. *Biochimica et Biophysica Acta (BBA) - General Subjects*, **2016**, *1860*(5), 945-956.

54.   Freyer, M.W. and Lewis, E.A., *Isothermal Titration Calorimetry: Experimental Design, Data Analysis, and Probing Macromolecule/Ligand Binding and Kinetic Interactions*, in *Methods in Cell Biology*. 2008, Academic Press. p. 79-113.

55.   Lewis, E.A. and Murphy, K.P., *Isothermal Titration Calorimetry*, in *Protein-Ligand Interactions: Methods and Applications*, G. Ulrich Nienhaus, Editor. 2005, Humana Press: Totowa, NJ. p. 1-15.

56.   Velázquez-Campoy, A., Ohtaka, H., Nezami, A., Muzammil, S., and Freire, E., Isothermal Titration Calorimetry. **2004**, *23*(1), 17.8.1-17.8.24.

57.   Freire, E., Mayorga, O.L., and Straume, M., Isothermal titration calorimetry. *Anal. Chem.*, **1990**, *62*(18), 950A-959A.

58.   Kabiri, M. and Unsworth, L.D., Application of Isothermal Titration Calorimetry for Characterizing Thermodynamic Parameters of Biomolecular Interactions: Peptide Self-Assembly and Protein Adsorption Case Studies. *Biomacromolecules*, **2014**, *15*(10), 3463-3473.

59.   Christensen, J.J., Izatt, R.M., Hansen, L.D., and Partridge, J.A., Entropy Titration. A Calorimetric Method for the Determination of ΔG, ΔH, and ΔS from a Single Thermometric Titration1a,b. *The Journal of Physical Chemistry*, **1966**, *70*(6), 2003-2010.

60.   Cliff, M.J. and Ladbury, J.E., A survey of the year 2002 literature on applications of isothermal titration calorimetry. **2003**, *16*(6), 383-391.

61.   O'Brien, R. and Haq, I., *Applications of Biocalorimetry: Binding, Stability and Enzyme Kinetics*, in *Biocalorimetry 2*. p. 1-34.

62.   Spink, C. and Wadso, I., Calorimetry as an analytical tool in biochemistry and biology. *Methods Biochem. Anal.*, **1976**, *23*, 1-159.

63.   Chiad, K., Stelzig, S.H., Gropeanu, R., Weil, T., Klapper, M., and Müllen, K., Isothermal Titration Calorimetry: A Powerful Technique To Quantify Interactions in Polymer Hybrid Systems. *Macromolecules*, **2009**, *42*(19), 7545-7552.

64.   Henzler, K., Haupt, B., Lauterbach, K., Wittemann, A., Borisov, O., and Ballauff, M., Adsorption of β-Lactoglobulin on Spherical Polyelectrolyte Brushes: Direct Proof of Counterion Release by Isothermal Titration Calorimetry. *Journal of the American Chemical Society*, **2010**, *132*(9), 3159-3163.

65.   Becker, A.L., Welsch, N., Schneider, C., and Ballauff, M., Adsorption of RNase A on Cationic Polyelectrolyte Brushes: A Study by Isothermal Titration Calorimetry. *Biomacromolecules*, **2011**, *12*(11), 3936-3944.

66.   Welsch, N., Becker, A.L., Dzubiella, J., and Ballauff, M., Core–shell microgels as "smart" carriers for enzymes. *Soft Matter*, **2012**, *8*(5), 1428-1436.

67.   Yigit, C., Welsch, N., Ballauff, M., and Dzubiella, J., Protein Sorption to Charged Microgels: Characterizing Binding Isotherms and Driving Forces. *Langmuir*, **2012**, *28*(40), 14373-14385.

68.   Vilanova, O., Mittag, J.J., Kelly, P.M., Milani, S., Dawson, K.A., Rädler, J.O., and Franzese, G., Understanding the Kinetics of Protein-Nanoparticle Corona Formation. *ACS nano*, **2016**, *10*(12), 10842-10850.

69.   Lindman, S., Lynch, I., Thulin, E., Nilsson, H., Dawson, K.A., and Linse, S., Systematic Investigation of the Thermodynamics of HSA Adsorption to N-iso-Propylacrylamide/N-tert-Butylacrylamide Copolymer Nanoparticles. Effects of Particle Size and Hydrophobicity. *Nano Lett*, **2007**, *7*, 914-920.

70.   De, M., You, C.-C., Srivastava, S., and Rotello, V.M., Biomimetic Interactions of Proteins with Functionalized Nanoparticles: A Thermodynamic Study. *Journal of the American Chemical Society*, **2007**, *129*(35), 10747-10753.

71.   Chen, K., Xu, Y., Rana, S., Miranda, O.R., Dubin, P.L., Rotello, V.M., Sun, L., and Guo, X., Electrostatic Selectivity in Protein–Nanoparticle Interactions. *Biomacromolecules*, **2011**, *12*(7), 2552-2561.

72.   Houtman, J.C.D., Brown, P.H., Bowden, B., Yamaguchi, H., Appella, E., Samelson, L.E., and Schuck, P., Studying multisite binary and ternary protein interactions by global analysis of isothermal titration calorimetry data in SEDPHAT: Application to adaptor protein complexes in cell signaling. **2007**, *16*(1), 30-42.

73.   Welsch, N., Lu, Y., Dzubiella, J., and Ballauff, M., Adsorption of proteins to functional polymeric nanoparticles. *Polymer*, **2013**, *54*(12), 2835-2849.

74. Draczkowski, P., Matosiuk, D., and Jozwiak, K., Isothermal titration calorimetry in membrane protein research. *Journal of Pharmaceutical and Biomedical Analysis*, **2014**, *87*, 313-325.

75. Rajarathnam, K. and Rösgen, J., Isothermal titration calorimetry of membrane proteins — Progress and challenges. *Biochimica et Biophysica Acta (BBA) - Biomembranes*, **2014**, *1838*(1, Part A), 69-77.

76. Pilloni, M., Nicolas, J., Marsaud, V., Bouchemal, K., Frongia, F., Scano, A., Ennas, G., and Dubernet, C., PEGylation and preliminary biocompatibility evaluation of magnetite–silica nanocomposites obtained by high energy ball milling. *International Journal of Pharmaceutics*, **2010**, *401*(1), 103-112.

77. Mandal, S., Hossain, M., Devi, P.S., Kumar, G.S., and Chaudhuri, K., Interaction of carbon nanoparticles to serum albumin: elucidation of the extent of perturbation of serum albumin conformations and thermodynamical parameters. *Journal of Hazardous Materials*, **2013**, *248-249*, 238-245.

78. Chakraborty, S., Joshi, P., Shanker, V., Ansari, Z.A., Singh, S.P., and Chakrabarti, P., Contrasting Effect of Gold Nanoparticles and Nanorods with Different Surface Modifications on the Structure and Activity of Bovine Serum Albumin. *Langmuir*, **2011**, *27*(12), 7722-7731.

79. Weber, C., Simon, J., Mailänder, V., Morsbach, S., and Landfester, K., Preservation of the soft protein corona in distinct flow allows identification of weakly bound proteins. *Acta Biomaterialia*, **2018**, *76*, 217-224.

80. Müller, J., Simon, J., Rohne, P., Koch-Brandt, C., Mailänder, V., Morsbach, S., and Landfester, K., Denaturation via Surfactants Changes Composition of Protein Corona. *Biomacromolecules*, **2018**, *19*(7), 2657-2664.

81. Winzen, S., Schwabacher, J.C., Müller, J., Landfester, K., and Mohr, K., Small Surfactant Concentration Differences Influence Adsorption of Human Serum Albumin on Polystyrene Nanoparticles. *Biomacromolecules*, **2016**, *17*(11), 3845-3851.

82. Zhang, X., Zhang, J., Zhang, F., and Yu, S., Probing the binding affinity of plasma proteins adsorbed on Au nanoparticles. *Nanoscale*, **2017**, *9*(14), 4787-4792.

83. Wang, X., Matei, E., Gronenborn, A.M., Ramström, O., and Yan, M., Direct Measurement of Glyconanoparticles and Lectin Interactions by Isothermal Titration Calorimetry. *Analytical Chemistry*, **2012**, *84*(10), 4248-4252.

84. Reynolds, M., Marradi, M., Imberty, A., Penadés, S., and Pérez, S., Multivalent Gold Glycoclusters: High Affinity Molecular Recognition by Bacterial Lectin PA-IL. *Chemistry – A European Journal*, **2012**, *18*(14), 4264-4273.

85.   Li, X., Chen, M., Yang, W., Zhou, Z., Liu, L., and Zhang, Q., Interaction of bovine serum albumin with self-assembled nanoparticles of 6-O-cholesterol modified chitosan. *Colloids and Surfaces B: Biointerfaces*, **2012**, *92*, 136-141.

86.   Liu, S., Han, Y., Qiao, R., Zeng, J., Jia, Q., Wang, Y., and Gao, M., Investigations on the Interactions between Plasma Proteins and Magnetic Iron Oxide Nanoparticles with Different Surface Modifications. *The Journal of Physical Chemistry C*, **2010**, *114*(49), 21270-21276.

87.   Rabbani, G., Khan, M.J., Ahmad, A., Maskat, M.Y., and Khan, R.H., Effect of copper oxide nanoparticles on the conformation and activity of β-galactosidase. *Colloids and surfaces. B, Biointerfaces*, **2014**, *123*, 96-105.

88.   Chatterjee, T., Chakraborti, S., Joshi, P., Singh, S.P., Gupta, V., and Chakrabarti, P., The effect of zinc oxide nanoparticles on the structure of the periplasmic domain of the Vibrio cholerae ToxR protein. *The FEBS Journal*, **2010**, *277*(20), 4184-4194.

89.   Chakraborti, S., Joshi, P., Chakravarty, D., Shanker, V., Ansari, Z.A., Singh, S.P., and Chakrabarti, P., Interaction of Polyethyleneimine-Functionalized ZnO Nanoparticles with Bovine Serum Albumin. *Langmuir*, **2012**, *28*(30), 11142-11152.

90.   Morsbach, S., Gonella, G., Mailänder, V., Wegner, S., Wu, S., Weidner, T., Berger, R., Koynov, K., Vollmer, D., Encinas, N., Kuan, S.L., Bereau, T., Kremer, K., Weil, T., Bonn, M., Butt, H.-J., and Landfester, K., Engineering Proteins at Interfaces: From Complementary Characterization to Material Surfaces with Designed Functions. **2018**, *57*(39), 12626-12648.

91.   Saptarshi, S.R., Duschl, A., and Lopata, A.L.J.J.o.N., Interaction of nanoparticles with proteins: relation to bio-reactivity of the nanoparticle. **2013**, *11*(1), 26.

92.   Brown, W.E. and Wold, F., Alkyl isocyanates as active-site-specific reagents for serine protease. Identification of the active-site serine as the site of reaction. *Biochemistry*, **1973**, *12*(5), 835-840.

93.   Schärtl, W., Light scattering from polymer solutions and nanoparticle dispersions. *Springer: Berlin*, **2007**.

94.   Arndt, K.-F. and Müller, G., Polymercharakterisierung. *Hanser: München*, **1996**.

95.   Kratochvil, P., Classical light scattering from polymer solutions. *Elsevier: Amsterdam*, **1987**.

96.   Rausch, K., Reuter, A., Fischer, K., and Schmidt, M., Evaluation of Nanoparticle Aggregation in Human Blood Serum. *Biomacromolecules*, **2010**, *11*(11), 2836-2839.

97.   Gustafson, H.H., Holt-Casper, D., Grainger, D.W., and Ghandehari, H., Nanoparticle Uptake: The Phagocyte Problem. *Nano Today*, **2015**, *10*(4), 487-510.

98.   Prin, C., Bene, M.C., Gobert, B., Montagne, P., and Faure, G.C., Isoelectric restriction of human immunoglobulin isotypes. *Biochimica et Biophysica Acta (BBA) - General Subjects*, **1995**, *1243*(2), 287-289.

99.   Fallatah, H.I. and Akbar, H.O., Elevated serum immunoglobulin G levels in patients with chronic liver disease in comparison to patients with autoimmune hepatitis. *Libyan J Med*, **2010**, *5*, 4857 - DOI: 10.3402/ljm.v5i0.4857.

100.   Julkunen, I., Hovi, T., Seppälä, I., and Mäkelä, O., Immunoglobulin G subclass antibody responses in influenza A and parainfluenza type 1 virus infections. *Clin. Exp. Immunol.*, **1985**, *60*, 130-138.

101.   Kyle, R.A. and Rajkumar, S.V., Criteria for diagnosis, staging, risk stratification and response assessment of multiple myeloma. *Leukemia*, **2009**, *23*, 3-9.

102.   Müller, L.K., Simon, J., Schöttler, S., Landfester, K., Mailänder, V., and Mohr, K., Pre-coating with protein fractions inhibits nanocarrier aggregation in human blood plasma. *RCS Adv.*, **2016**, *6*, 96495-96509.

103.   Loos, C., Syrovets, T., Musyanovych, A., Mailänder, V., Landfester, K., Nienhaus, G.U., and Simmet, T., Functionalized polystyrene nanoparticles as a platform for studying bio–nano interactions. *Beilstein J Nanotechnol*, **2014**, *5*, 2403-2412.

104.   Vermeer, A.W.P., Bremer, M.G.E.G., and Norde, W., Structural changes of IgG induced by heat treatment and by adsorption onto a hydrophobic Teflon surface studied by circular dichroism spectroscopy. *Biochim. Biophys. Acta.*, **1998**, *1425*, 1 - 12.

105.   Vermeer, A.W.P. and Norde, W., The thermal stability of immunoglobulin: unfolding and aggregation of a multi-domain protein. *Biophys J.*, **2000**, *78*(1), 394-404.

106.   Hirsh, S.L., McKenzie, D.R., Nosworthy, N.J., Denman, J.A., Sezerman, O.U., and Bilek, M.M.M., The Vroman effect: Competitive protein exchange with dynamic multilayer protein aggregates. *Colloids Surf B Biointerfaces*, **2013**, *103*(1), 395-404.

107.   Casals, E., Pfaller, T., Duschl, A., Oostingh, G.J., and Puntes, V., Time Evolution of the Nanoparticle Protein Corona. *ACS Nano*, **2010**, *4*(7), 3623-3632.

108.   Tenzer, S., Docter, D., Kuharev, J., Musyanovych, A., Fetz, V., Hecht, R., Schlenk, F., Fischer, D., Kiouptsi, K., Reinhardt, C., Landfester, K., H. Schild, Maskos, M., Knauer, S.K., and Stauber, R.H., Rapid formation of plasma protein corona critically affects nanoparticle pathophysiology. *Nat. Nanotechnol.*, **2013**, *8*, 772-781.

109.   Benech, P.D., Sastry, K., Iyer, R.R., Eichbaum, Q.G., Raveh, D.P., and Ezekowitz, R.A., Definition of interferon gamma-response elements in a novel human Fc gamma receptor

gene (Fc gamma RIb) and characterization of the gene structure. *J. Exp. Med.*, **1992**, *215*(7), 1115-1123.

110.   van Schie, R.C.A.A. and Wilson, M.E., Evaluation of Human FcγRIIA (CD32) and FcγRIIIB (CD16) Polymorphisms in Caucasians and African-Americans Using Salivary DNA. *Clin. Diagn. Lab. Immunol.*, **2000**, *7*(4), 676-681.

111.   Kalsi, J., Delacroix, D.L., and Hodgson, H.J., IgA in alcoholic cirrhosis. *Clinical and experimental immunology*, **1983**, *52*(3), 499-504.

112.   Manjula, S., Aroor, A.R., Raja, A., Rao, S.N., and Rao, A., Serum immunoglobulins in brain tumours. *Acta Neurochirurgica*, **1992**, *115*(3), 103-105.

113.   Martin, D.M., Vroon, D.H., and Nasrallah, S.M., Value of serum immunoglobulins in the diagnosis of liver disease. *Liver*, **1984**, *4*(3), 214-218.

114.   Vasti, C., Bonnet, L.V., Galiano, M.R., Rojas, R., and Giacomelli, C.E., Relevance of protein–protein interactions on the biological identity of nanoparticles. *Colloids and Surfaces B: Biointerfaces*, **2018**, *166*, 330-338.

115.   McCusker, C., Upton, J., and Warrington, R., Primary immunodeficiency. *Allergy, asthma, and clinical immunology : official journal of the Canadian Society of Allergy and Clinical Immunology*, **2018**, *14*(Suppl 2), 61-61.

116.   Boyle, J.M. and Buckley, R.H., Population Prevalence of Diagnosed Primary Immunodeficiency Diseases in the United States. *Journal of Clinical Immunology*, **2007**, *27*(5), 497-502.

117.   Choe, W., Durgannavar, T.A., and Chung, S.J., Fc-Binding Ligands of Immunoglobulin G: An Overview of High Affinity Proteins and Peptides. *Materials (Basel, Switzerland)*, **2016**, *9*(12), 994.

118.   Harris, J.M. and Chess, R.B., Effect of pegylation on pharmaceuticals. *Nature Reviews Drug Discovery*, **2003**, *2*, 214.

119.   Fukuda, A., Tahara, K., Hane, Y., Matsui, T., Sasaoka, S., Hatahira, H., Motooka, Y., Hasegawa, S., Naganuma, M., Abe, J., Nakao, S., Takeuchi, H., and Nakamura, M., Comparison of the adverse event profiles of conventional and liposomal formulations of doxorubicin using the FDA adverse event reporting system. *PLOS ONE*, **2017**, *12*(9), e0185654.

120.   Banerjee, S.S., Aher, N., Patil, R., and Khandare, J., Poly(ethylene glycol)-Prodrug Conjugates: Concept, Design, and Applications. *Journal of Drug Delivery*, **2012**, *2012*, 17.

121.   Alconcel, S.N.S., Baas, A.S., and Maynard, H.D., FDA-approved poly(ethylene glycol)–protein conjugate drugs. *Polymer Chemistry*, **2011**, *2*(7), 1442-1448.

122. Swierczewska, M., Lee, K.C., and Lee, S., What is the future of PEGylated therapies? *Expert Opinion on Emerging Drugs*, **2015**, *20*(4), 531-536.

123. Ishida, T. and Kiwada, H., Accelerated blood clearance (ABC) phenomenon upon repeated injection of PEGylated liposomes. *International Journal of Pharmaceutics*, **2008**, *354*(1), 56-62.

124. Ishida, T., Ichihara, M., Wang, X., and Kiwada, H., Spleen plays an important role in the induction of accelerated blood clearance of PEGylated liposomes. *Journal of Controlled Release*, **2006**, *115*(3), 243-250.

125. Hara, E., Makino, A., Kurihara, K., Yamamoto, F., Ozeki, E., and Kimura, S., Pharmacokinetic change of nanoparticulate formulation "Lactosome" on multiple administrations. *International Immunopharmacology*, **2012**, *14*(3), 261-266.

126. Abu Lila, A.S., Kiwada, H., and Ishida, T., The accelerated blood clearance (ABC) phenomenon: Clinical challenge and approaches to manage. *Journal of Controlled Release*, **2013**, *172*(1), 38-47.

127. Ganson, N.J., Povsic, T.J., Sullenger, B.A., Alexander, J.H., Zelenkofske, S.L., Sailstad, J.M., Rusconi, C.P., and Hershfield, M.S., Pre-existing anti–polyethylene glycol antibody linked to first-exposure allergic reactions to pegnivacogin, a PEGylated RNA aptamer. *Journal of Allergy and Clinical Immunology*, **2016**, *137*(5), 1610-1613.e7.

128. DIN 32465:2008, Chemische Analytik - Nachweis-, Erfassungs- und Bestimmungsgrenze unter Wiederholbedingungen - Begriffe, Verfahren, Auswertung

129. Bauer, K.N., Liu, L., Wagner, M., Andrienko, D., and Wurm, F.R., Mechanistic study on the hydrolytic degradation of polyphosphates. *European Polymer Journal*, **2018**, *108*, 286-294.

130. Holzapfel, V., Musyanovych, A., Landfester, K., Lorenz, M.R., and Mailänder, V., Preparation of Fluorescent Carboxyl and Amino Functionalized Polystyrene Particles by Miniemulsion Polymerization as Markers for Cells. *Macromolecular Chemistry and Physics*, **2005**, *206*(24), 2440-2449.

131. Baier, G., Musyanovych, A., Dass, M., Theisinger, S., and Landfester, K., Cross-Linked Starch Capsules Containing dsDNA Prepared in Inverse Miniemulsion as "Nanoreactors" for Polymerase Chain Reaction. *Biomacromolecules*, **2010**, *11*(4), 960-968.

132. Jiang, S., Lv, L., Li, Q., Wang, J., Landfester, K., and Crespy, D., Tailoring nanoarchitectonics to control the release profile of payloads. *Nanoscale*, **2016**, *8*(22), 11511-11517.

133.   Jiang, S., Ma, B.C., Reinholz, J., Li, Q., Wang, J., Zhang, K.A.I., Landfester, K., and Crespy, D., Efficient Nanofibrous Membranes for Antibacterial Wound Dressing and UV Protection. *ACS Applied Materials & Interfaces*, **2016**, *8*(44), 29915-29922.

134.   Thurmond, C., Control of Dust in Solutions for Turbidimetry. *J. Polym. Sci.*, **1952**, *8*(6), 607-609.

135.   Hiramoto, E., Tsutsumi, A., Suzuki, R., Matsuoka, S., Arai, S., Kikkawa, M., and Miyazaki, T., The IgM pentamer is an asymmetric pentagon with an open groove that binds the AIM protein. *Science Advances*, **2018**, *4*(10), eaau1199.

Appendix
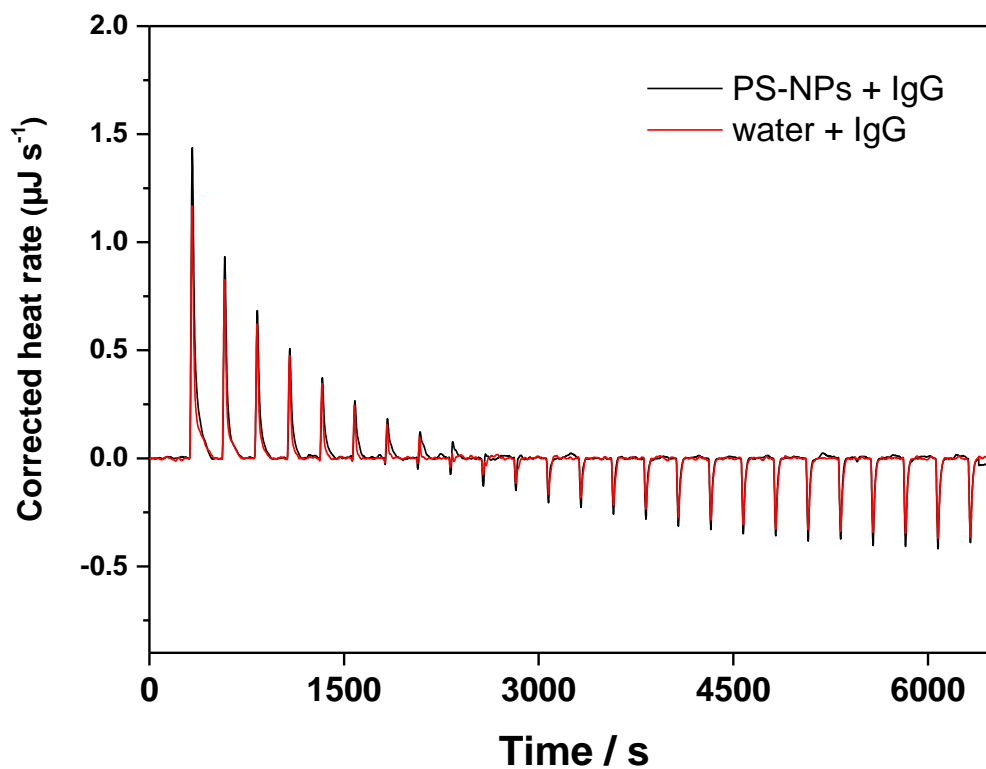
Figure A1: ITC raw heat rates of the titration of PS-NPs with IgG. The signal of the titration of IgG into a suspension of PS-NPs is shown in black, while the signal of the titration of IgG into water (heat of dilution) is shown in red. In the graphs shown in Figure 3 of the main manuscript, the heat of dilution was subtracted from the original signal.
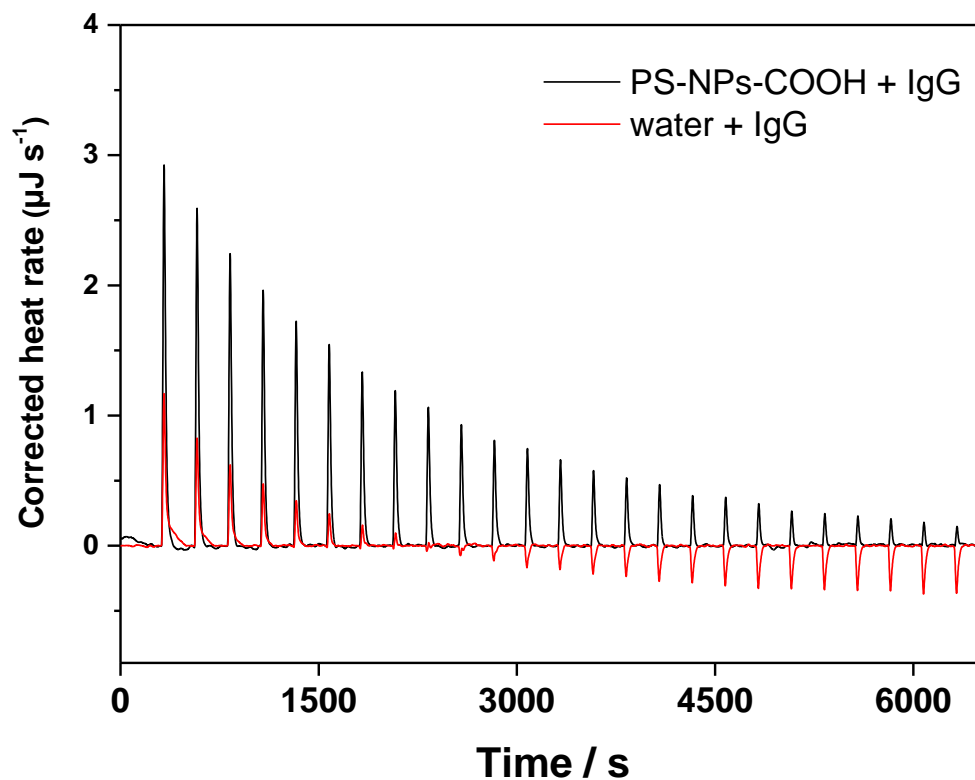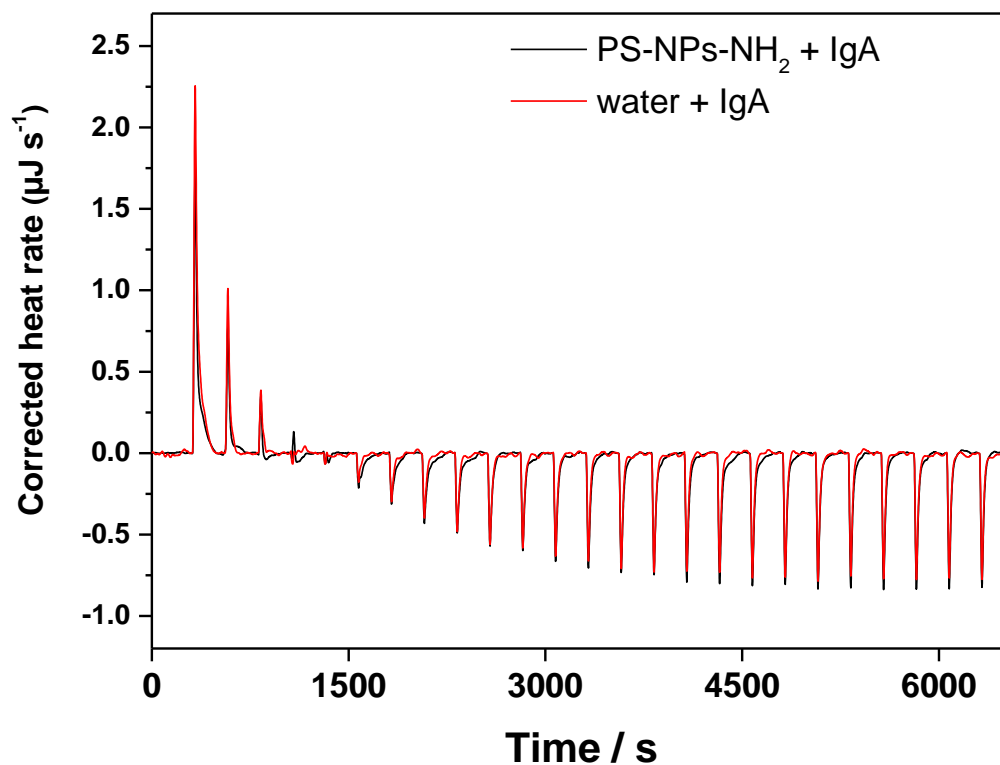
Figure A2: ITC raw heat rates of the titration of PS-NPs-COOH with IgG. The signal of the titration of IgG into a suspension of PS-NPs-COOH is shown in black, while the signal of the titration of IgG into water (heat of dilution) is shown in red. In the graphs shown in Figure 3 of the main manuscript, the heat of dilution was subtracted from the original signal.
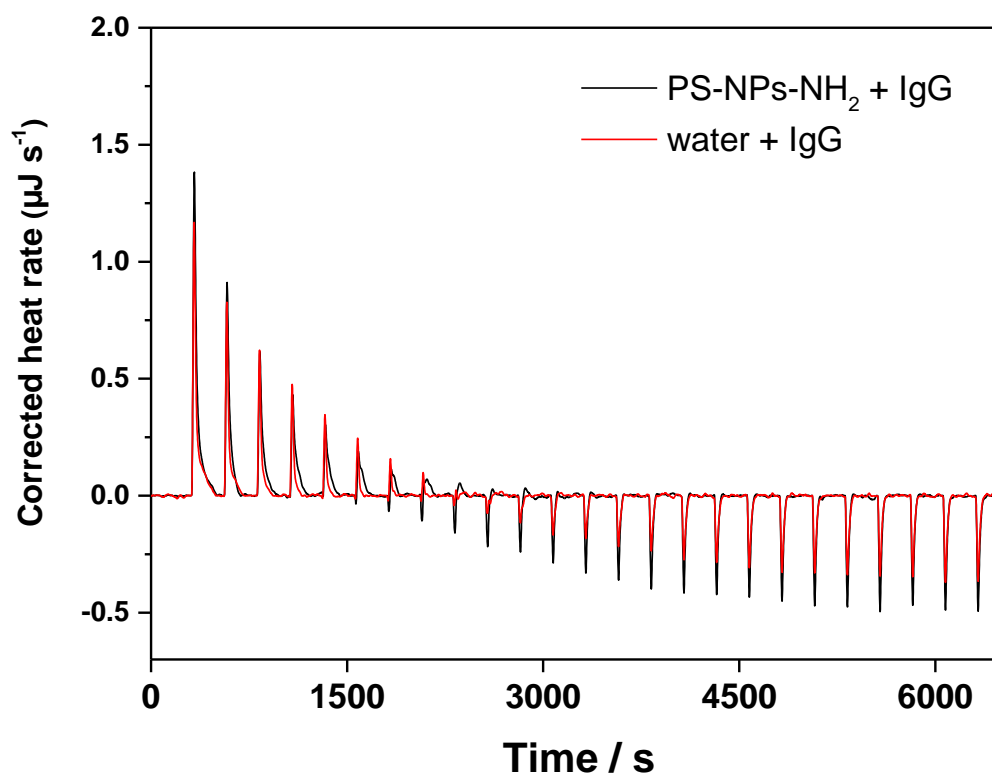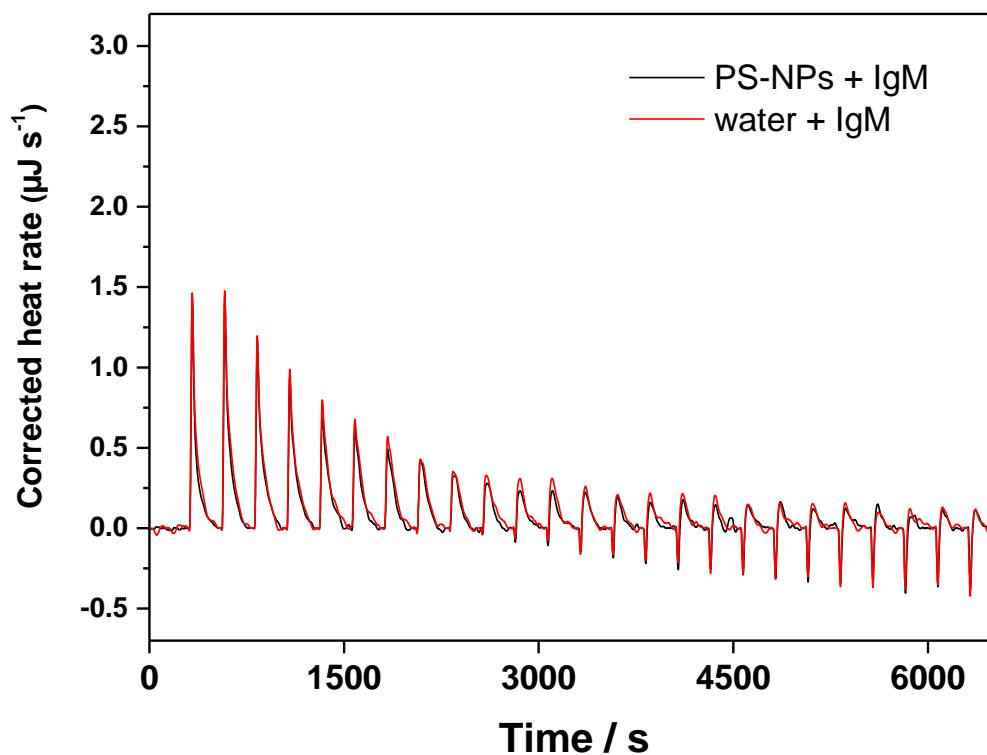
Figure A3: ITC raw heat rates of the titration of PS-NPs-NH$_2$ with IgG. The signal of the titration of IgG into a suspension of PS-NPs-NH$_2$ is shown in black, while the signal of the titration of IgG into water (heat of dilution) is shown in red. In the graphs shown in Figure 3 of the main manuscript, the heat of dilution was subtracted from the original signal.
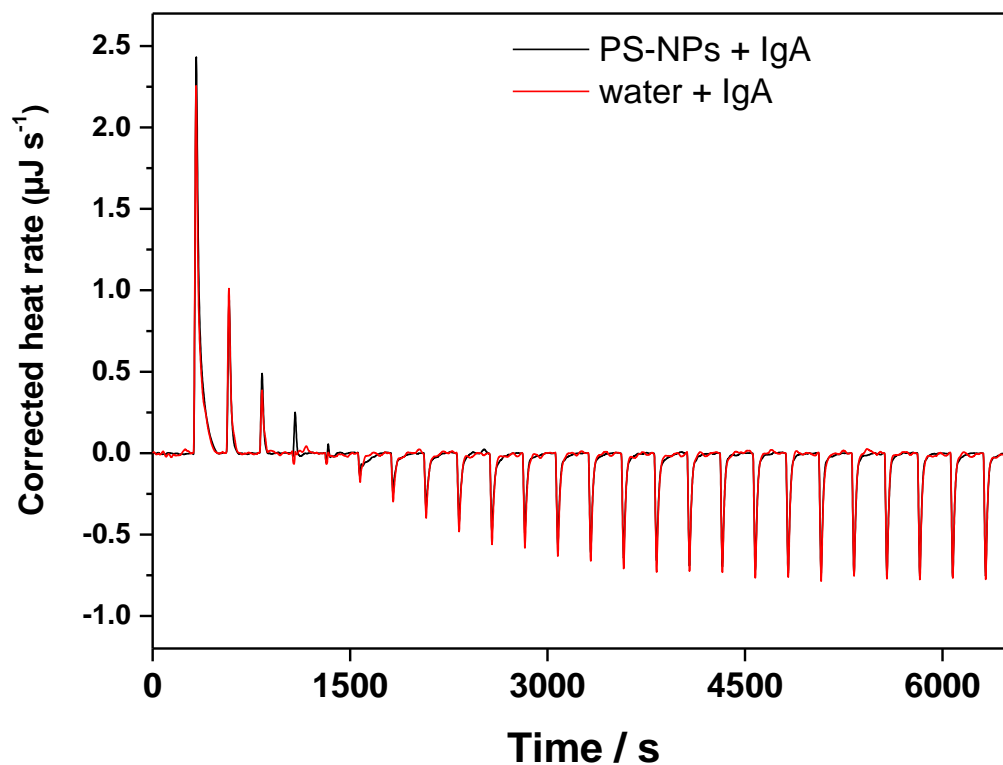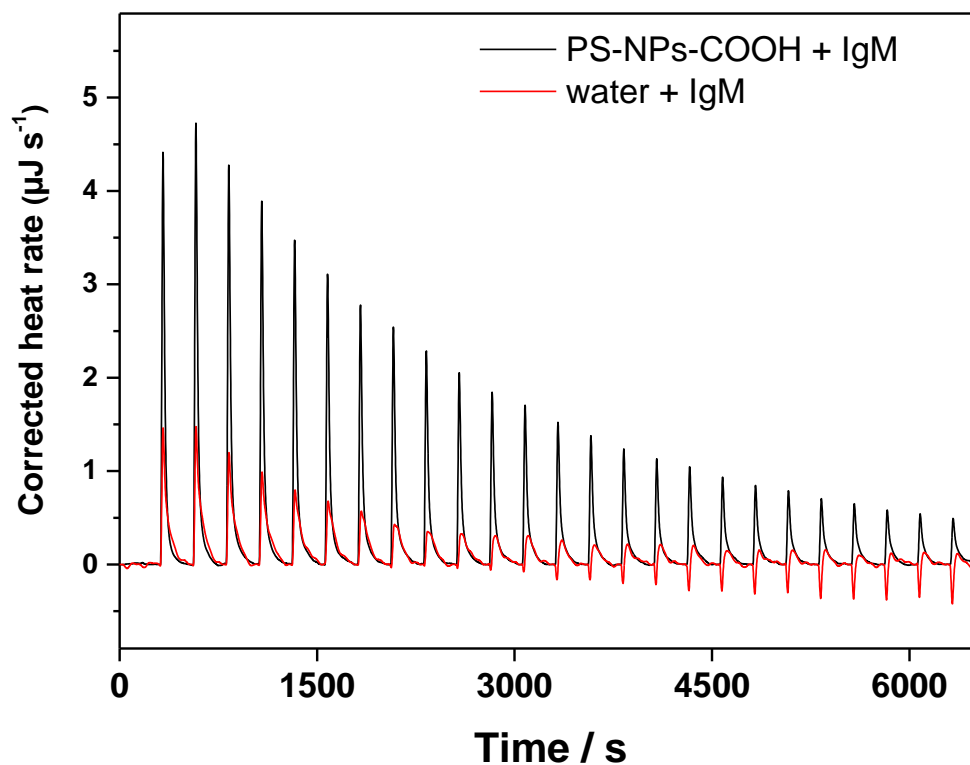
Figure A4: ITC raw heat rates of the titration of PS-NPs with IgA. The signal of the titration of IgA into a suspension of PS-NPs is shown in black, while the signal of the titration of IgA into water (heat of dilution) is shown in red. In the graphs shown in Figure 3 of the main manuscript, the heat of dilution was subtracted from the original signal.
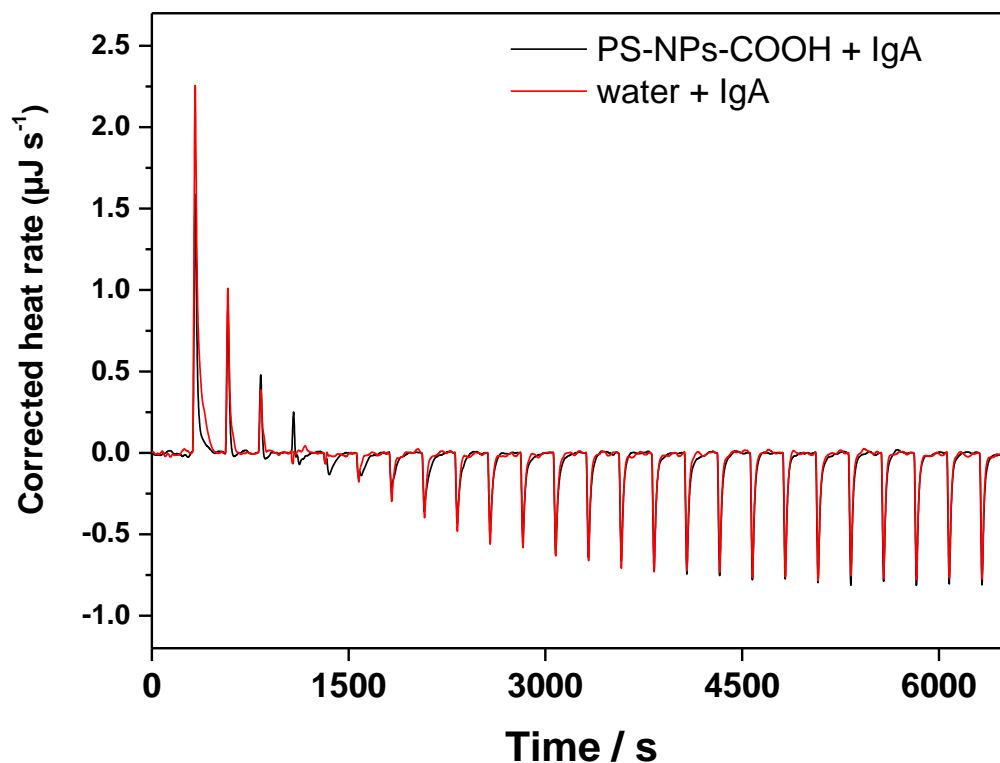
Figure A5: ITC raw heat rates of the titration of PS-NPs-COOH with IgA. The signal of the titration of IgA into a suspension of PS-NPs-COOH is shown in black, while the signal of the titration of IgA into water (heat of dilution) is shown in red. In the graphs shown in Figure 3 of the main manuscript, the heat of dilution was subtracted from the original signal.
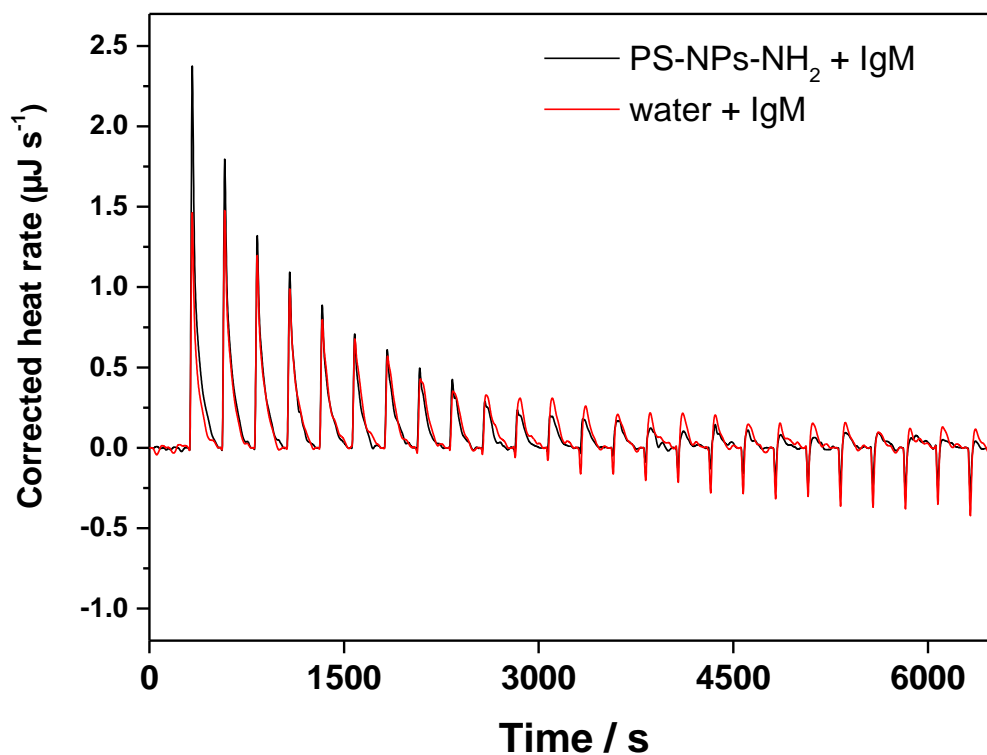
Figure A6: ITC raw heat rates of the titration of PS-NPs-NH$_2$ with IgA. The signal of the titration of IgA into a suspension of PS-NPs-NH$_2$ is shown in black, while the signal of the titration of IgA into water (heat of dilution) is shown in red. In the graphs shown in Figure 3 of the main manuscript, the heat of dilution was subtracted from the original signal.

Figure A7: ITC raw heat rates of the titration of PS-NPs with IgM. The signal of the titration of

IgM into a suspension of PS-NPs is shown in black, while the signal of the titration of IgM into

water (heat of dilution) is shown in red. In the graphs shown in Figure 3 of the main manuscript,

the heat of dilution was subtracted from the original signal.

Figure A8: ITC raw heat rates of the titration of PS-NPs-COOH with IgM. The signal of the titration of IgM into a suspension of PS-NPs-COOH is shown in black, while the signal of the titration of IgM into water (heat of dilution) is shown in red. In the graphs shown in Figure 3 of the main manuscript, the heat of dilution was subtracted from the original signal.

Figure A9: ITC raw heat rates of the titration of PS-NPs-NH₂ with IgM. The signal of the titration of IgM into a suspension of PS-NPs-NH₂ is shown in black, while the signal of the titration of IgM into water (heat of dilution) is shown in red. In the graphs shown in Figure 3 of the main manuscript, the heat of dilution was subtracted from the original signal.
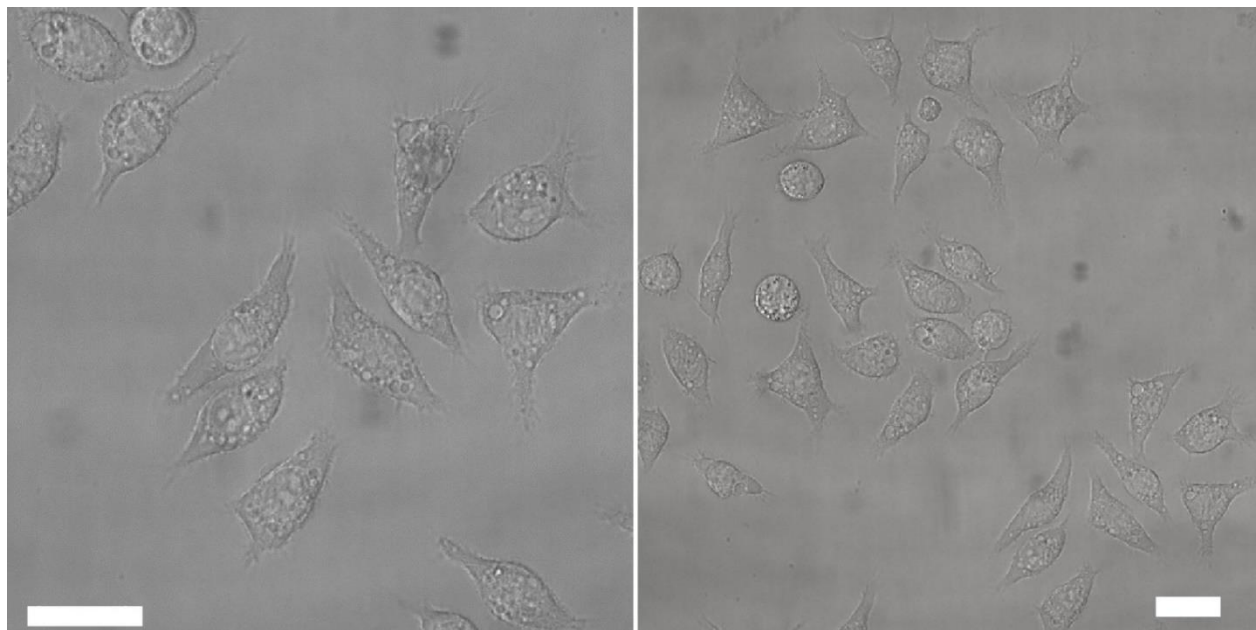
Figure A10: Additional cLSM pictures of RAW 264.7 cells without nanocarriers (negative control). The scale bar corresponds to a length of 20 µm. Published by Wiley-VCH.[52]
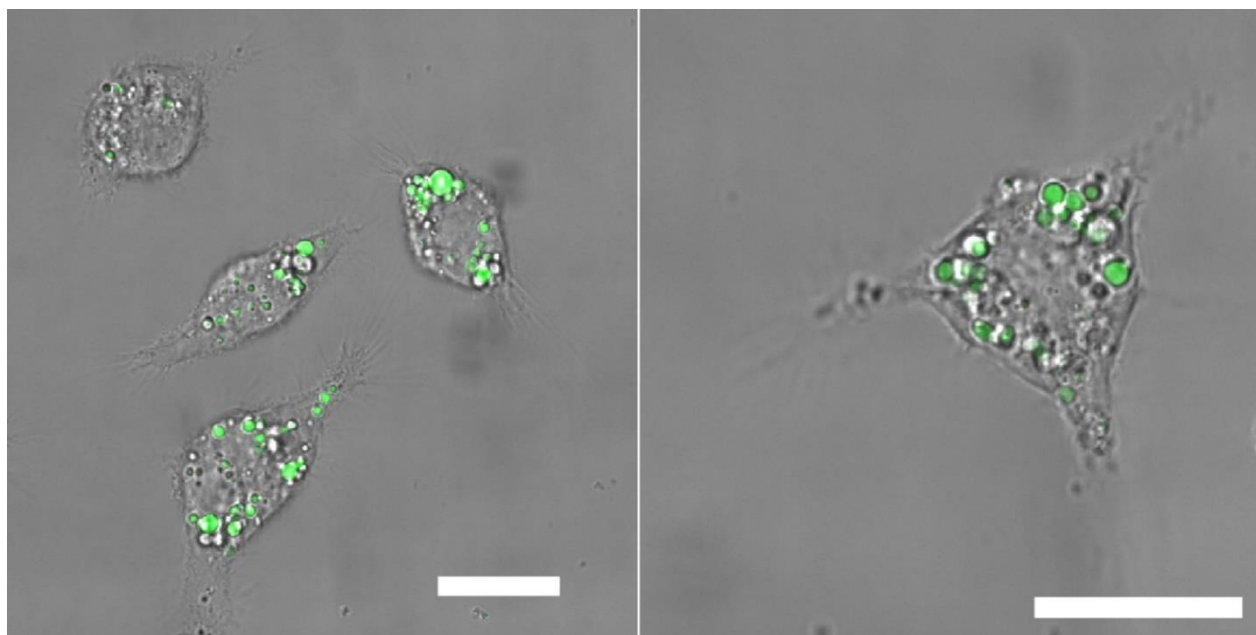
Figure A11: Additional cLSM pictures of PS-NPs in RAW 264.7 cells. Exemplary cLSM pictures of PS-NPs without protein corona in RAW 264.7 cells were chosen to distinguish cellular uptake from cell membrane decoration. The scale bar corresponds to a length of 20 µm. Published by Wiley-VCH.[52]
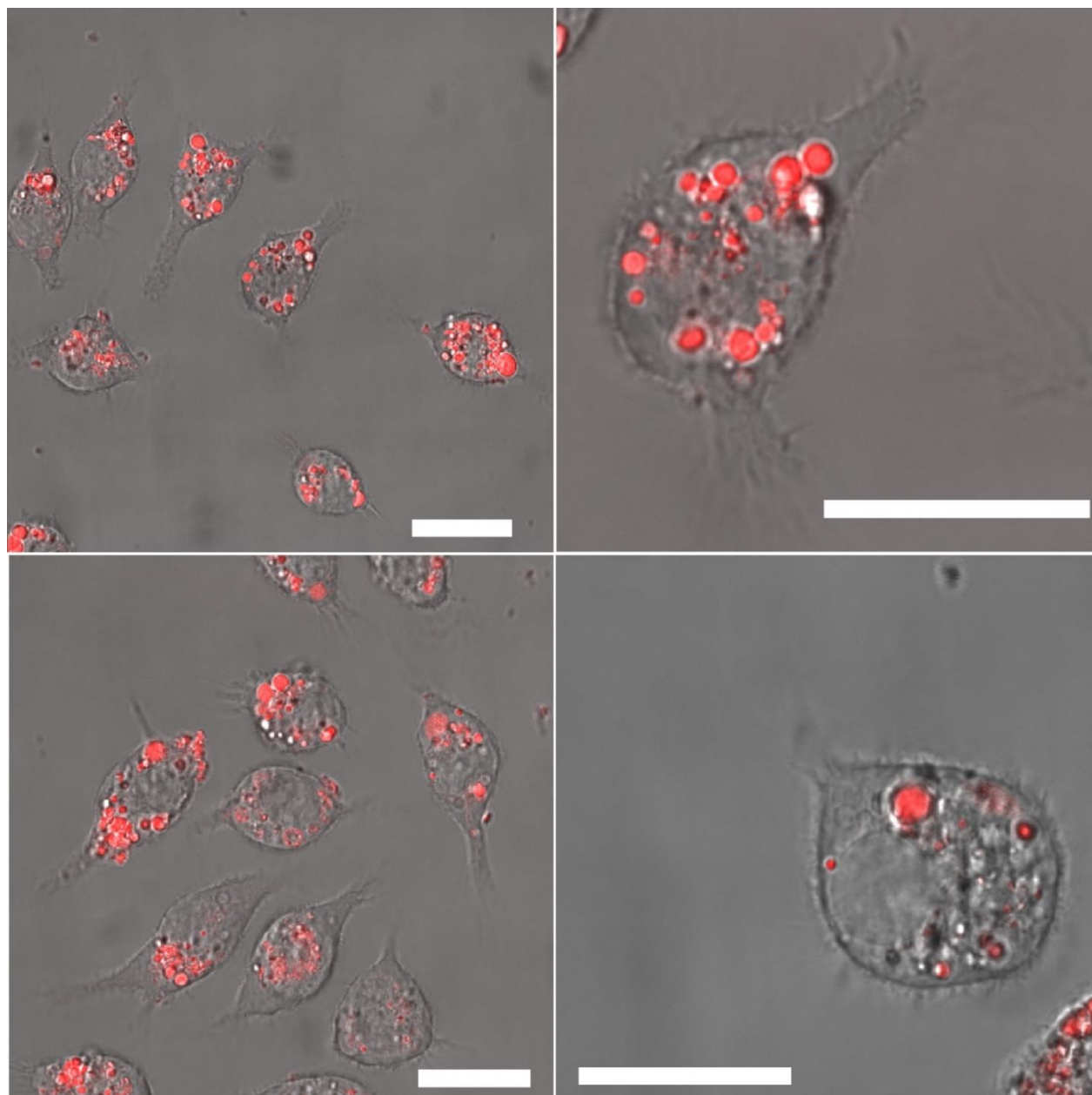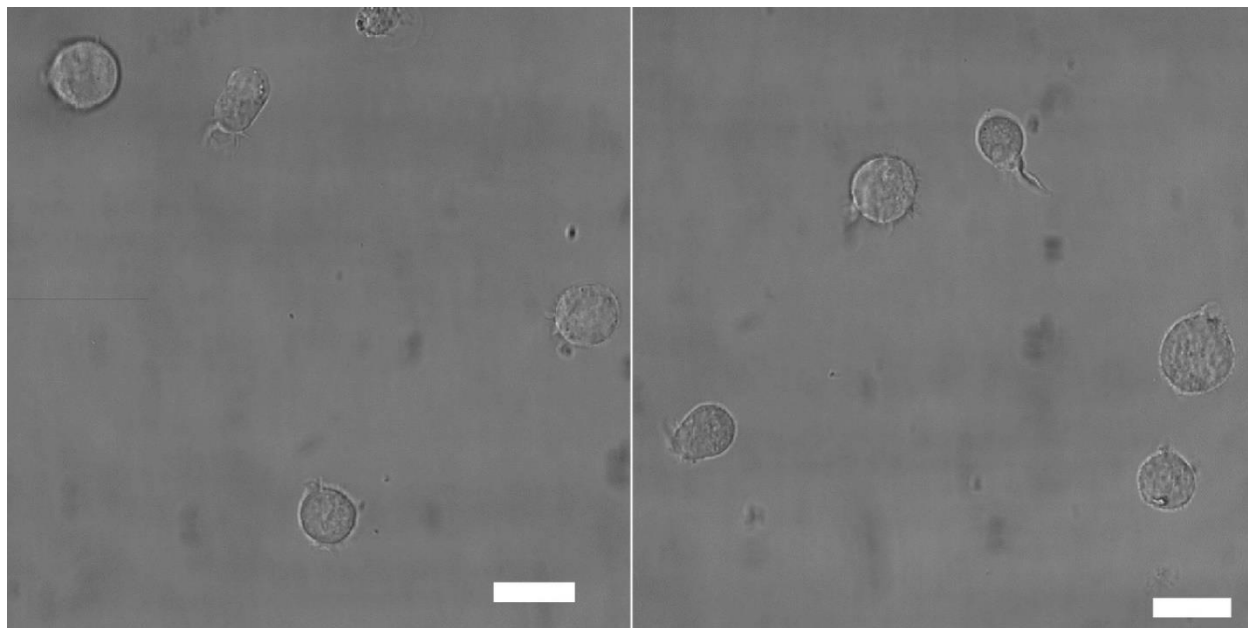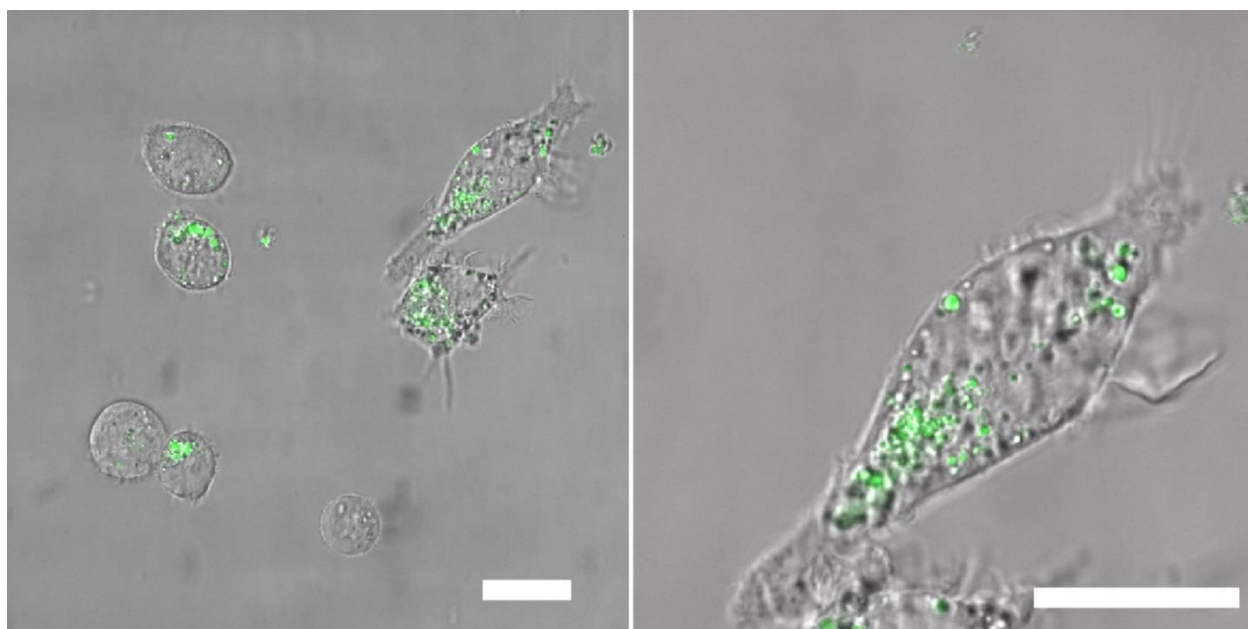
Figure A12: Additional cLSM pictures of HES-NCS in RAW 264.7 cells. Exemplary cLSM pictures of HES-NCs without protein corona in RAW 264.7 cells were chosen to distinguish cellular uptake from cell membrane decoration. The scale bar corresponds to a length of 20 μm. Published by Wiley-VCH.[52]

Figure A13: Additional cLSM pictures of THP-1 cells without nanocarriers (negative control). The scale bar corresponds to a length of 20 μm. Published by Wiley-VCH.[52]

Figure A14: Additional cLSM pictures of PS-NPs in THP-1 cells. Exemplary cLSM pictures of PS-NPs without protein corona in THP-1 cells were chosen to distinguish cellular uptake from cell membrane decoration. The scale bar corresponds to a length of 20 μm. Published by Wiley-VCH.[52]
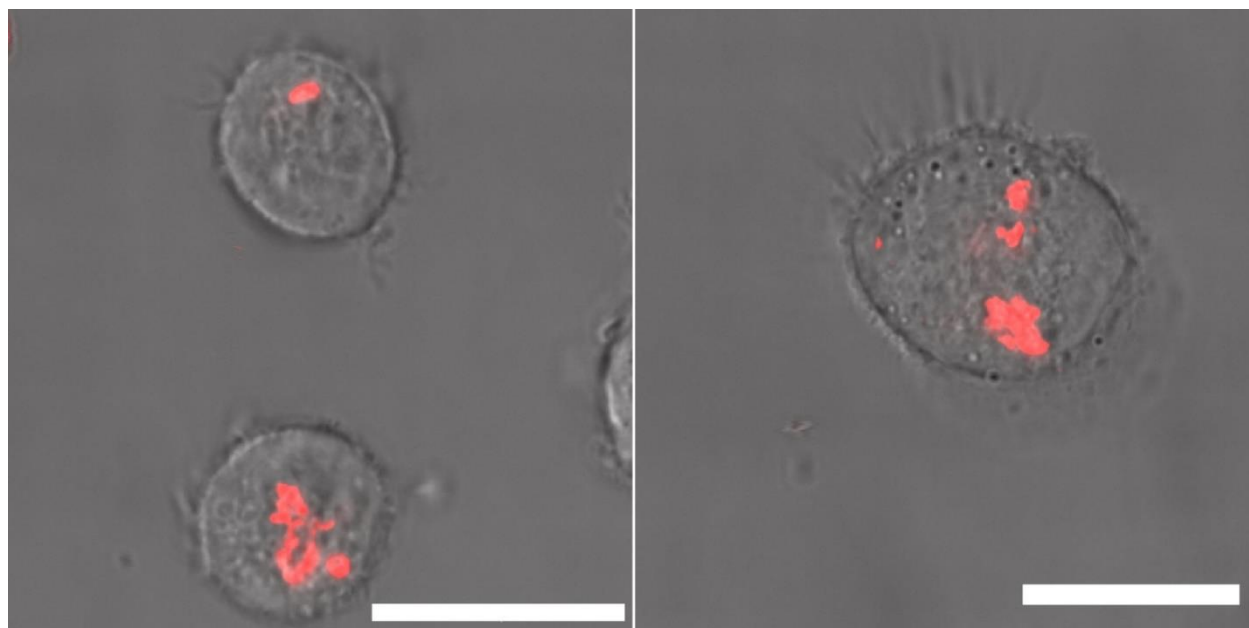
Figure A15: Additional cLSM pictures of HES-NCs in THP-1 cells. Exemplary cLSM pictures of HES-NCs without protein corona in THP-1 cells were chosen to distinguish cellular uptake from cell membrane decoration. The scale bar corresponds to a length of 20 µm. Published by Wiley-VCH.[52]
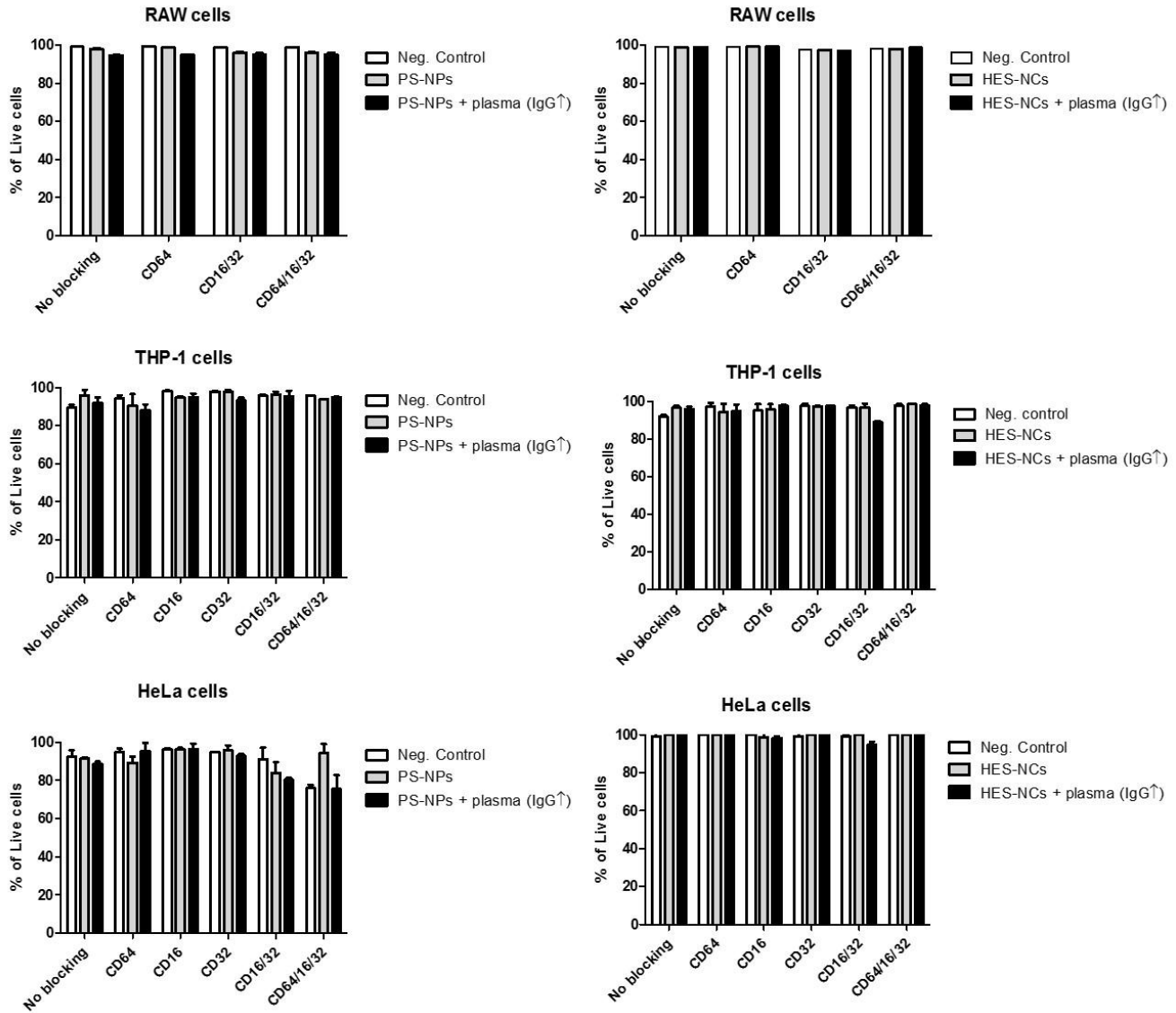
Figure A16: Cell viability tests *via* Zombie Aqua viability kits. Published by Wiley-VCH.[52]